

A NEW PRODUCTION METHODOLOGY FOR VACUUM INFUSION  
PROCESS OF ADVANCED COMPOSITE STRUCTURES

A THESIS SUBMITTED TO  
THE GRADUATE SCHOOL OF NATURAL AND APPLIED SCIENCES  
OF  
MIDDLE EAST TECHNICAL UNIVERSITY

BY

MOHSEN POORZEINOLABEDIN

IN PARTIAL FULFILLMENT OF THE REQUIREMENTS  
FOR  
THE DEGREE OF DOCTOR OF PHILOSOPHY  
IN  
MECHANICAL ENGINEERING

SEPTEMBER 2017



**A NEW PRODUCTION METHODOLOGY FOR VACUUM INFUSION  
PROCESS OF ADVANCED COMPOSITE STRUCTURES**

Submitted by **MOHSEN POORZEINOLABEDIN** in partial fulfillment of the requirements for the degree of **Doctor of Philosophy in Mechanical Engineering Department, Middle East Technical University** by,

Prof. Dr. Gülbin Dural Ünver  
Dean, Graduate School of **Natural and Applied Sciences**

Prof. Dr. M. A. Sahir Arıkan  
Head of Department, **Mechanical Engineering**

Prof. Dr. Kemal Levend Parnas  
Supervisor, **Mechanical Engineering Dept., METU**

**Examining Committee Members:**

Prof. Dr. Haluk Darendeliler  
Mechanical Engineering Dept., METU

Prof. Dr. Kemal Levend Parnas  
Mechanical Engineering Dept., METU

Assoc. Prof. Dr. Demirkan Çöker  
Aerospace Engineering Dept., METU

Prof. Dr. Müfit Gülgeç  
Mechatronics Engineering Dept., Çankaya University

Prof. Dr. Can Çoğun  
Mechatronics Engineering Dept., Çankaya University

**Date:** 26.09.2017

**I hereby declare that all information in this document has been obtained and presented in accordance with academic rules and ethical conduct. I also declare that, as required by these rules and conduct, I have fully cited and referenced all material and results that are not original to this work.**

Name, Last name: Mohsen Poorzeinolabedin

Signature :

## **ABSTRACT**

### **A NEW PRODUCTION METHODOLOGY FOR VACUUM INFUSION PROCESS OF ADVANCED COMPOSITE STRUCTURES**

Poorzeinolabedin, Mohsen  
PhD, Department of Mechanical Engineering  
Supervisor: Prof. Dr. Kemal Levend Parnas

September 2017, 120 pages

Vacuum Infusion Process (VIP) is one of the Liquid Composite Molding (LCM) methods which are widely used in out-of-autoclave processes especially for the manufacturing of large scale composite parts in aerospace, automotive, wind energy and marine industries. In order to simulate the infusion process, the permeability of preforms is an essential parameter. Absence of any standard is a challenge for the determination of in-plane permeabilities of a preform. The first objective of this study is to develop an approach to estimate the principle permeability from a single rectilinear infusion. The presented method for permeability measurement is able to obtain preform permeability in three different directions, simultaneously and allows the calculation of the principle permeability. The repeatability of results and unusual resin filling patterns are the main challenges of this approach. It is due to the heterogeneous nature of fabrics, nesting the layers during the molding and the process over-dependency on the labor skill. Although, the simulation of the process can overcome some of the process challenges to some extent, it may not be helpful for the undesirable filling scenarios. Therefore, a real-time resin flow control may guarantee a near-perfect filling process. Another objective of this study is the resin flow control in real time. The specific resin flow control approach named here as Electromagnetically Induced Preform Resting (EIPR) introduces a new creative upper flexible mold for resting the preform to increase the permeability of preforms locally in a real time manner. This process is demonstrated experimentally and numerically. The results show the reliability and efficiency of the presented method.

Keywords: Permeability, resin infusion, resin flow control, EIPR, numerical methods



## ÖZ

### İLERİ KOMPOZİT YAPILARDA VAKUMLU İNFÜZYON SÜRECİ İÇİN YENİ BİR ÜRETİM METODOLOJİSİ

Poorzeinolabedin, Mohsen  
PhD, Makina Mühendisliği Bölümü  
Tez Danışmanı : Prof. Dr. Kemal Levend Parnas

Eylül 2017, 120 sayfa

Vakum İnfüzyon Prosesi (VİP), özellikle havacılık, otomotiv, rüzgar enerjisi ve gemicilik sanayilerindeki büyük ölçekli kompozit parçaların üretimi için otoklav dışı işlemlerde yaygın olarak kullanılan Sıvı Kompozit Döküm (LCM) bazlı üretim yöntemlerinden biridir. İnfüzyon işlemini doğru şekilde simüle etmek için preformun geçirgenliği önemli bir parametredir. Herhangi bir standardın olmaması nedeniyle, bir preformun düzlemsel geçirgenliğinin doğru olarak belirlenmesi oldukça zordur. Bu çalışmanın ilk hedefi, tek bir doğrusal infüzyon kullanarak asal geçirgenliklerin hesaplanması için bir yaklaşım geliştirmektir. Geçirgenlik ölçümü için sunulan bu yöntemle göre, önce üç farklı yön için aynı anda preform geçirgenliği elde edilmekte ve bu değerler kullanılarak asal geçirgenlikler belirlenmektedir. Sonuçların tekrarlanabilirliği ve alışılmışın dışındaki reçine dolum biçimleri bu sürecin uygulamalarında karşılaşılan temel zorluklardır. Bu durumun nedenleri arasında; kumaşların heterojen yapısının neden olduğu sorunları, infüzyon sırasında katmanların üstüste binmesini ve süreç kalitesinin el becerisine bağımlılığını saymak mümkündür. Her ne kadar infüzyon sürecinin bilgisayarla simülasyonu sayesinde bazı zorlukların bir ölçüde üstesinden gelinmesi mümkün olsa da, istenmeyen infüzyon durumlarının tahmin edilmesi için bazen bu yaklaşım bile çözüm olamayabilmektedir. Bu nedenle mükemmel yakın dolum işlemini garantilemek için gerçek zamanlı bir reçine akış kontrolü gereklidir. Bu tezin bir diğer amacı, reçine akış kontrolünün gerçek zamanlı olarak yapılmasıdır. Elektromanyetik Endükleme ile Preformun Rahatlatılması (EIPR) olarak adlandırılan bu özel reçine akış kontrol yaklaşımı ile, yeni ve yaratıcı bir üst esnek kalıp kullanarak, preformun geçirgenliğinin lokal ve gerçek zamanlı olarak artırılacağı gösterilmiştir. Bu işlem deneysel ve sayısal olarak gösterilmiştir. Sonuçlar bu çalışmada sunulan yöntemin güvenilirliğini ve etkinliğini göstermektedir.

Anahtar kelimeler: Geçirgenlik, reçine infüzyonu, reçine akış kontrolü, EIPR, sayısal yöntemler

*To:*

*my parents,*

*my brother*

*and specially my wife*

*who always supported me*

## ACKNOWLEDGEMENTS

I would like to give my sincere gratitude to my supervisor, Prof. Dr. Kemal Levend Parnas, for his gentleness, his appreciated and treasured advices. The constant individual attention I have received from him throughout this experience has been rewarding academically as well as personally.

I also appreciate Assoc. Prof. Dr. Demirkan Çöker, Prof. Dr. Haluk Darendeliler and Assoc. Prof. Dr. Merve Erdal for their kindly guidance in the different stages of the thesis study.

I moreover thank Leopard Composite Engineering and Consulting Services Ltd. for providing the necessary environment and conditions for experimental part of the study.

The Author is delighted to thank TÜBİTAK (The Scientific and Technological Research Council of Turkey) for supporting this thesis under the graduate scholarship program for international students (Grant No: 2215).



## TABLE OF CONTENTS

|   |      |
|---|------|
| ABSTRACT .....  | v    |
| ÖZ .....  | vii  |
| ACKNOWLEDGEMENTS .....                                      | ix   |
| TABLE OF CONTENTS .....                                     | xi   |
| LIST OF TABLES .....  | xv   |
| LIST OF FIGURES .....                                       | xvii |
| LIST OF SYMBOLS .....                                       | xxi  |
| CHAPTERS .....  | 1    |
| 1. INTRODUCTION .....                                       | 1    |
| 1.1 Liquid composite molding .....                          | 1    |
| 1.2 Literature review .....                                 | 3    |
| 1.3 Objectives of research .....                            | 9    |
| 1.4 Scope of this dissertation .....                        | 10   |
| 2. CALCULATION OF IN-PLANE PRINCIPLE PERMEABILITIES .....   | 11   |
| 2.1 Introduction .....                                      | 11   |
| 2.2 Analytical determination of in-plane permeability ..... | 14   |
| 2.3 Principle permeability calculation methodology .....    | 19   |
| 2.4 Permeability measurement experiment .....               | 20   |
| 2.4.1 Test set-up .....                                     | 20   |
| 2.4.2 Elastomer silicone vacuum bag.....                    | 21   |
| 2.4.3 Permeability calculation.....                         | 22   |

|  |           |
|--|-----------|
| 2.5 Results and discussion.....  | 24        |
| 2.6 Summary .....  | 29        |
| <b>3. FLOW CORRECTION CONTROL WITH ELECTROMAGNETICALLY<br/>INDUCED PREFORM RESTING PROCESS .....</b>                           | <b>31</b> |
| 3.1 Introduction .....   | 31        |
| 3.2 EIPR process for resin flow controlling.....   | 33        |
| 3.2.1 Embedded element and array .....   | 35        |
| 3.3 Control methodology design .....   | 37        |
| 3.4 Experimental set-up.....   | 39        |
| 3.4.1 Preparation of upper flexible mold.....  | 41        |
| 3.4.2 Flow front monitoring .....  | 41        |
| 3.4.3 Automated gantry system.....   | 42        |
| 3.5 Experimental validation .....  | 43        |
| 3.5.1 Preform configurations.....  | 43        |
| 3.5.2 Test fluid .....   | 44        |
| 3.5.3 Experimental Procedure .....   | 44        |
| 3.6 Results and discussion.....  | 45        |
| 3.7 Summary .....  | 50        |
| <b>4. CHARACTERIZATION AND MODELING OF IN-PLANE PERMEABILITY<br/>IN ELECTROMAGNETICALLY INDUCED PREFORM RESTING PROCESS ..</b> | <b>53</b> |
| 4.1 Introduction .....   | 54        |
| 4.2 EIPR process.....  | 56        |
| 4.3 Permeability measurement method .....  | 57        |
| 4.4 Design of experiment .....   | 58        |
| 4.5 Experiments.....   | 58        |
| 4.5.1 Set-up .....   | 58        |

|  |   |    |
|--|---|----|
| 4.5.2  | Material .....  | 59 |
| 4.5.3  | Permeability characterization for EIPR process .....                              | 60 |
| 4.5.4  | Permeability measurements .....   | 64 |
| 4.5.5  | Test procedure.....   | 65 |
| 4.6  | Results and discussion .....  | 65 |
| 4.6.1  | Permeability and filling time.....  | 65 |
| 4.6.2  | Response surface analysis and regression model for EIPR process permeability..... | 69 |
| 4.6.3  | 3D Surface and 2D contour plots for preform permeability of EIPR process.....     | 74 |
| 4.6.4  | Optimization.....   | 78 |
| 4.7  | Summary .....   | 78 |
| 5. MODELING AND EVALUATION OF ELECTROMAGNETICALLY INDUCED PREFORM RESTING (EIPR) PROCESS ..... |   | 81 |
| 5.1  | Introduction .....  | 81 |
| 5.1.1  | EIPR process .....  | 82 |
| 5.1.2  | Resin flow simulation .....   | 84 |
| 5.1.3  | Material characterization.....  | 84 |
| 5.2  | Experimental characterization of materials.....                                   | 87 |
| 5.2.1  | Material .....  | 87 |
| 5.2.2  | Permeability measurement for EIPR preforms .....                                  | 88 |
| 5.2.3  | Fabric compressibility .....  | 90 |
| 5.3  | EIPR process simulation .....   | 92 |
| 5.4  | Validation.....   | 93 |
| 5.4.1  | Permeability of preform with/without EIPR process.....                            | 94 |
| 5.4.2  | Experimental procedure .....  | 94 |

|                                    |     |
|------------------------------------|-----|
| 5.5 Results and discussion.....    | 95  |
| 5.6 Summary .....                  | 103 |
| 6. CONCLUSION AND FUTURE WORK..... | 105 |
| 6.1 Conclusions .....              | 105 |
| 6.2 Future works.....              | 109 |
| REFERENCES.....                    | 111 |
| VITA .....                         | 119 |

## LIST OF TABLES

### TABLES

|  |     |
|--|-----|
| Table 2.1. Permeabilities of zone sequences and their codes .....  | 24  |
| Table 2.2. Permeability of the reinforcements at different orientation .....                                 | 27  |
| Table 3.1 Material permeability under controlled and non-controlled .....                                    | 44  |
| Table 4.1. Actual and coded levels of parameters in this study .....   | 66  |
| Table 4.2. Permeability and filling time for the preforms without EIPR process (VARTM).....                  | 66  |
| Table 4.3. Experimental design and corresponding response .....  | 70  |
| Table 4.4. Analysis of variance for transformed response.....  | 71  |
| Table 4.5. Model summary for transformed response .....  | 73  |
| Table 5.1. Fabric compressibility (P is pressure and Vf is fiber volume of fraction). 92                     |     |
| Table 5.2. Effective and principle permeability and Ellipse orientation of materials in both processes ..... | 94  |
| Table 5.3. Filling time of simulations and experiments with/without the EIPR.....                            | 103 |



## LIST OF FIGURES

### FIGURES

|   |    |
|---|----|
| Figure 1.1. Schematic of resin flow controlling in VARTM by using localized induction heating [2]. .....                          | 6  |
| Figure 1.2. Cross-sectional schematic of the VIPR process workstation [18].....   | 8  |
| Figure 2.1. Schematic of the experiment lay-up .....  | 15 |
| Figure 2.2. Flow front elliptic pattern, $K_1, K_2$ and $\beta$ are principle permeabilities and angle of flow elliptic [43]..... | 20 |
| Figure 2.3. Typical experiment mold.....  | 21 |
| Figure 2.4. Race-tracking and its elimination by a elastomer vacuum bag .....   | 22 |
| Figure 2.5. Directions of each segments layers in the reinforcement roll [17].....  | 22 |
| Figure 2.6. Placement of fabrics on the transparent mold .....  | 23 |
| Figure 2.7. Flow front position as a function of time.....  | 25 |
| Figure 2.8. Effect of placement on filling time .....   | 25 |
| Figure 2.9. Flow front position vs. time for the first zone in P3.....  | 26 |
| Figure 2.10. Permeability of the second zone with $0^\circ$ for P3 test.....  | 26 |
| Figure 2.11. Permeability of the third zone with $90^\circ$ for P3.....   | 27 |
| Figure 2.12. Permeability for $0^\circ, 45^\circ$ and $90^\circ$ orientations .....   | 28 |
| Figure 2.13. Elliptic pattern of permeability for preform used .....  | 29 |
| Figure 3.1. Schematics of EIPR process .....  | 34 |
| Figure 3.2. Amplitude and frequency of EIPR process .....   | 35 |
| Figure 3.3. Element shape.....  | 35 |
| Figure 3.4. Hysteresis loops of soft and hard ferromagnetic material [106] .....  | 36 |
| Figure 3.5. Geometry of the mold for the case studies and distance of flow front for each section from inlet line. ....           | 38 |
| Figure 3.6. Control flowchart used in case studies .....  | 38 |
| Figure 3.7. Case studies for infusion where a high permeability preform stiffened with low permeability one.....                  | 40 |

|  |    |
|--|----|
| Figure 3.8. Special reusable vacuum bag with embedded elements .....   | 41 |
| Figure 3.9. 2D automated gantry system with electromagnet.....   | 43 |
| Figure 3.10. Filling process before (a) and after (b, c) frames of filling process.....  | 46 |
| Figure 3.11. Case 1: (a) Effect of EIPR process preventing dry spot formation, (b) Formation of a dry spot for no-controlled process .....             | 48 |
| Figure 3.12. Case 2: (a) Effect of the EIPR process preventing dry spot formation, (b) Formation of a dry spot for no-controlled process .....         | 49 |
| Figure 3.13. Case 3: (a) Effect of EIPR process on flow front preventing dry spot formation, (b) Formation of dry spot for no-controlled process ..... | 50 |
| Figure 4.1. Schematic of EIPR process.....   | 57 |
| Figure 4.2. Upper flexible mold with two embedded FM elements for permeability measurement.....  | 59 |
| Figure 4.3. E-Glass samples: a) Twill b) Multiaxial c) Mat .....   | 60 |
| Figure 4.4. Element shapes: a) circle b) square.....   | 61 |
| Figure 4.5. Flow front patterns for 2 different elements of a) circular shape b) square shape.....   | 61 |
| Figure 4.6. Case studies of element distance from gate line .....  | 62 |
| Figure 4.7. Effect of element position on the filling time compared with un-controlled process.....  | 63 |
| Figure 4.8. Amplitude of EIPR process .....  | 64 |
| Figure 4.9. Flow front progression through (a) Mat (b) Multiaxial (c) Twill .....  | 68 |
| Figure 4.10. Effectiveness of terms in form of Pareto chart for permeability .....   | 72 |
| Figure 4.11. Residual plots for permeability. (a) Normal probability (b) versus fits (c) histogram (d) versus order.....                               | 74 |
| Figure 4.12. (a) 3D surface and (b) 2D contour plot for mat preform on permeability.....   | 75 |
| Figure 4.13. (a) 3D surface and (b) 2D contour plot for multiaxial on permeability.....  | 76 |
| Figure 4.14. (a) 3D surface and (b) 2D contour plot for twill on permeability.....   | 77 |
| Figure 4.15. Mean effects plot of frequency, amplitude and material on preform permeability fitted mean.....   | 78 |
| Figure 5.1. EIPR process and its components .....  | 83 |
| Figure 5.2. Fabric samples, twill (left), mat (right).....   | 88 |
| Figure 5.3. Schematic of experiment for characterization of in-plane permeabilities .....  | 90 |
| Figure 5.4. Test set-up for measuring compressibility of preforms .....  | 90 |

|  |     |
|--|-----|
| Figure 5.5. Pressure response of twill preform .....   | 91  |
| Figure 5.6. Pressure response of mat .....   | 91  |
| Figure 5.7. Geometry of plates in case studies (a) case 1 (b) case 2.....  | 93  |
| Figure 5.8. Filling pattern for case 1 (a) simulation, experiments at (b) 300s and (c) 550s .....  | 96  |
| Figure 5.9. Flow front of case 1 (a) at 445s of VARTM process for simulationm (b) experiment, (c) dry spot in simulation and (d) dry spot in experiment..... | 98  |
| Figure 5.10. Filling pattern of case 2 for simulation (a) and experiments at (b) 357s and (c) 459s for EIPR process.....                                     | 100 |
| Figure 5.11. Flow front of case 2 (a) at 304s of VARTM process for simulation, (b) experiment, (c) predicted dry spot in simulation and (d) experiment.....  | 102 |
| Figure 6.1. Suggested upper flexible elastomer mold with mixed metal (Iron Oxide) powder.....  | 109 |



## LIST OF SYMBOLS

| <i>Symbol</i>   | Explanation                   | <i>Symbol</i> | Explanation            |
|-----------------|-------------------------------|---------------|------------------------|
| $Q$             | flowrate per unit width       | $l$           | Length of preform      |
| $K_{xx}$        | permeability                  | $w$           | Width of preform       |
| $\mu$           | Viscosity                     | $h$           | Thickness of preform   |
| $p$             | Pressure                      | $X_i$         | Significant parameters |
| $L$ or $x_{ff}$ | flow front position           | $\varepsilon$ | Error term             |
| $\varphi$       | porosity of the preform       | $\beta_0$     | Constant coefficients  |
| $v_f$           | fiber volume fraction.        | $\beta_i$     | linear                 |
| $K_{xx1}$       | permeability of first section | $\beta_{ii}$  | quadratic              |
| $K_{xx2}$       | permeability of first section | $\beta_{ij}$  | interaction            |
| $K_{xx3}$       | permeability of first section | $P_{atm}$     | atmospheric pressure   |
| $K_1, K_2$      | Principle permeabilities      | $P_{vac}$     | vacuum pressure        |
| $\beta$         | angle of flow elliptic        | $P_{resin}$   | Resin pressure         |
| $m_f$           | total mass of fabric          | $P_{com}$     | compaction pressure    |



# CHAPTER 1

## INTRODUCTION

### 1.1 Liquid composite molding

Advanced composite materials are used in various industrial applications i.e. aircraft structures, turbine blades, automotive, boat hull and containers. One of the keys to increasing the acceptance of composite materials in fabricating structures is to find ways to improve their mechanical and strength characteristics while employing cost-effective and efficient methods of fabrication.

Low cost, high-quality, and non-autoclave-based composite fabrication technologies have encouraged greater and more competitive use of composites in recent years. The most well-known alternative to autoclave-based methods includes Liquid Composite Molding (LCM) processes, which provides the ability to produce complex and large-scale structures with sufficiently high fiber-volume fraction. In LCM processes resin injects or infuses into the closed mold which includes reinforcement preforms to saturate them completely[1,2]. LCM is divided into two main branches. The first one is Resin Transfer Molding (RTM) and the second main branch is Vacuum Assisted Resin Transfer Molding (VARTM).

An important feature of the RTM is its two heavy solid molds. The fabric layers are placed on the top of the bottom mold and compressed by the top mold. And then resin is injected into the closed mold. High surface quality of the both sides of the produced parts, high volume fraction, tight thickness tolerance and low filling time are the most important advantages of the RTM process. However, tooling cost and invisible filling are the main drawbacks of this process. The tooling cost is still an effective factor for manufacturing large and complex structures. To deal with this problem, the upper rigid mold in RTM process is substituted with flexible vacuum

bags in the VARTM process. The VARTM process has numerous similarity to the RTM process in which resin infuses into the mold that is very different with RTM one. In this process one of the solid molds is replaced with a thin flexible bag that is called vacuum bag. Though the current VARTM process can greatly reduce equipment costs, it is in a very early phase and contains some challenges that limit applications of this process. The cost effectiveness of this process makes this very suitable for the large composite structures. Though, compaction of the preform and infusion of resin by atmospheric pressure and only one high surface quality limit this process. Much of the advancement in recent years in LCM has been creating variants of these processes to overcome their challenges. The Seemann's Composite Resin Infusion Molding Process (SCRIMP) is a variant of the VARTM process which increase the mold filling by placement of a Distribution Media (DM) over the preforms. Thus, the use of DM decreases the fill time because the resin first flows through the DM and then saturates the preform through the thickness direction. However, this process might lead to formation of voids and dry spots.

Filling time is a critical step of these processes that often leads to defects in fabricating parts. Indeed, unsaturated zones may appear if specifications like inlet and outlet of mold, injection pressure and permeability of preform are not well defined. A basic challenge in the filling step is the proper saturation of preforms, thereby eliminating the dry spots and voids. To deal with this challenge, a variation of permeability within the preform is one of the leading factors in the formation of dry spots and voids [3]. This variation in the first-place due to uncertainty in the preform pore structure, which is not a predictable parameter, and secondly due to heterogeneous preforms or stacking sequence of laminates [4]. It is also manifested itself in the particle filled resin infusion because of filtration by the fibrous reinforcements and so altering permeability during the filling step [5]. Another demonstration of the spatial permeability variability in complex shaped parts is race-tracking whereby the resin preferentially flows through high permeability channels formed at the edges of preform, at the edges of solid inserts, or at the preform mold interfaces within the mold. As a result of these variation in permeability from part to part infusion, obtaining complete saturation of preform without dry spots and voids in the filling step of vacuum infusion process in a constant manner is a critical

challenge [6]. Interlocking of the reinforcement layers that is known as nesting is another problem that occurs in LCM processing. Increasing numbers of layer in composite molding part that increase the fiber volume fraction (FVF) and stiffness intensify the nesting of preform [7,8]. The permeability of reinforcement is one of the important parameters governing the mold filling. So, a complete characterization of preform properties is necessary in this respect to understand the filling process clearly thereby finding a way to improve filling process. The lack of standardization of permeability measurement and exist of a significant scatter between the permeability values for the same materials under the same measurement condition are the main challenges of this feature measurement.

Other limitations of VARTM process include the poor surface finish on the bagging side; time involved in the process preparation, higher labor skills for the bagging stage, fabrication of high performance composite parts with high temperature matrix and low process repeatability. Some of these challenges are solvable with speeding the flow (for example by using DM in SCRIMP) or process optimization, however these solutions are off-line and are done before the process.

Hence, it is desirable to study on a reliable and repeatable method to measure the permeability of preforms and an on-line control system which prevent dry spot formation and manipulate the flow front deviation during the process.

## **1.2 Literature review**

A wide variety of numerical and experimental approaches have been established to calculate the in-plane permeability of preforms. Carman [9] presented a method to calculate the permeability of a single scale porous media by taking into account geometrical parameters of it. This method is not well adopted to obtain the permeability of dual scale fabric reinforcement. Thus more complex analytical methods have been applied to find the permeability of the fibrous reinforcement by researchers [10–14].

Sharma and et al. [15] summarized the permeability measurement methods into radial and rectilinear approaches for constant pressure and constant velocity. They also have done another classification based on the saturated and unsaturated flow in

the preform. They explained the available experimental and analytical approaches to calculate the principle permeabilities. To calculate these parameters of preform, in radial method there are some difficulties like complex data acquisition and flow front tracking. For the rectilinear one, at least three experiments need to obtain the principle permeabilities. However, non-repeatability of the current measurement approaches for the conducted test lead researchers to reduce the experiment numbers.

Fratta and et al. [16] presented a strategy to calculate the principle permeability based on injection along only two directions. This method relies on measurement of the flow front angle along with the effective permeability. Results show that the permeability of preforms can be accurately obtained with a reduced number of rectilinear experiments and, thus, with a considerable saving of time and material samples.

The lack of standardization of permeability measurement approach prevents researchers from comparing the permeability values of preforms from different approaches. Some studies have been conducted to create a standard method [17–19]. However, there was a significant scatter between all participants. So, finding a way to calculate the permeability of the preforms and their principle values are necessary.

In literature, there are many numerical and experimental studies associated with filling problems in VARTM process and flow manipulation. Hank. et al. [20] has studied flow modeling and simulation of resin flow through the preform to finding optimize location of vents and gates for minimum filling time and dry spots in complex and large geometries. Their results agreed well with experimental results. Ali Gokce et al. [21] have investigated a model to find the optimum injection gate location that fulfills two objectives: First, finding gate locations to obtain the minimum filling time and secondly finding an auxiliary gate location to minimize the dry spots and voids. They studied three different geometries for each case.

F. Sanchez et al. [22] have defined a process performance index based on the gate distance and growing time for liquid composite modeling process. Their index has allowed consideration of resin flow and curing issues in the process design optimization. The effectiveness of the approach was illustrated through many cases which involve race-tracking, different permeability area, etc. Also, other researchers

have focused on numerical models to find best location of gates and vents in order to achieve certain objectives such as finding minimum filling time, pressure, dry spots and voids [23–25].

An offline or passive control system, that gets database from the numerical flow simulation, can reduce the time and cost, and improve the part quality against trial-and-error methods, but the applications of these methods are limited by the assumption of ideal preform placement. However, VARTM processes have inherent permeability variations within the preform because of variability in preform architectures and stacking and other disturbance like race-tracking due to operator skill and placement of preform etc. Therefore, to compensate for these unknown disturbances, a real-time flow control for enhancing and correcting the resin flow is required during the infusion step [26].

For real-time controlling of resin infusion, Jeffrey et al. [27] used sensors and actuators during infusion to counteract the disturbances. In that study, a coupled mold filling simulation was used with a control methodology to identify the flow disturbances. The flow is corrected to successfully complete the mold filling process without dry spots and voids. However, their approach is not automatic and contains creation of software tools to finding fixed sensor locations, so some disturbances may occur in another area away from the fixed sensors.

Ryosuke Matsuzaki et al. [28,29] proposed an active flow control scheme by predicting flow pattern using numerical simulation and taking corrective action using dielectric heating at a specific targeted location to decrease the resin viscosity. In this study for monitoring full field of resin flow/temperature and actuating resin a thin multifunctional interdigital electrode array film was used.

R. J. Johnson et al. [4] have explored an innovative method to enhance the resin flow in VARTM by using localized induction heating. They developed a numerical model based on coupled resin flow and heat transfer phenomena. Their method using grayscale camera for monitoring resin flow to identify the low permeability regions within the preform and compensate the permeability variation of preform by locally reducing the viscosity of infused resin and reducing voids as Figure 1.1. Flow progression through changing viscosity is a serious challenge as it is required

detailed and exact resin properties. However, the viscosity of the thermoset resins is low to start with and just a limited control can be accomplished. Furthermore, heating the thermoset resin could initiate or accelerate the cure process thus increasing the viscosity and prematurely curing the composite part.

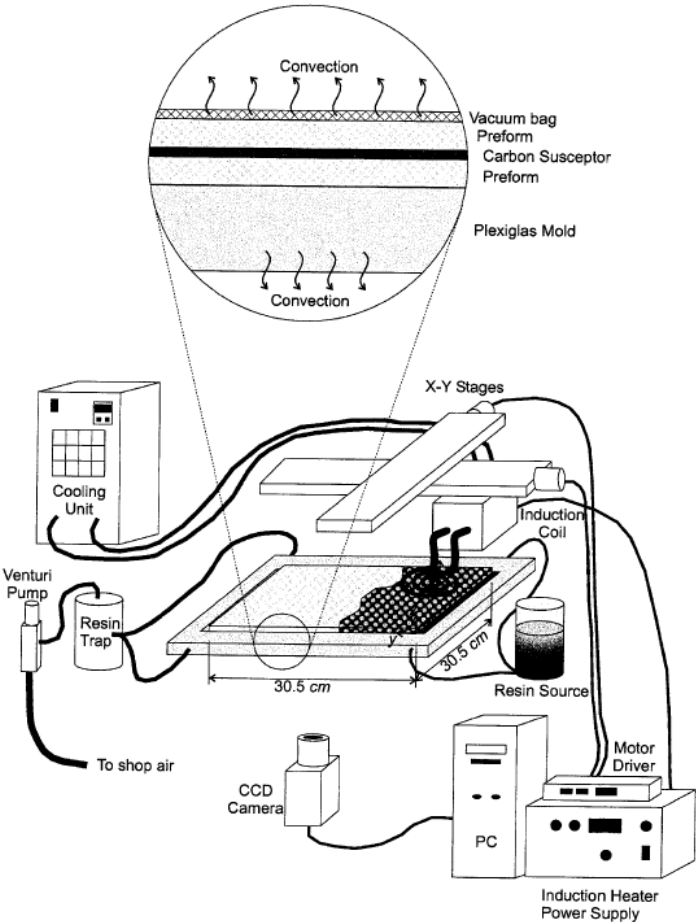


Figure 1.1. Schematic of resin flow controlling in VARTM by using localized induction heating [2].

Justin B. et al. [6] designed a port injection that utilizes a closed loop control system of ports and sensors built in the mold. Numerical simulation of this process showed complete infusion can consistently be achieved, even for large variation in permeability of preforms. Results showed this system is capable correctly delivering resin to low permeability areas usually unfilled via the standard VARTM process.

Dhiren M. et al. [28] proposed a new active control system that is capable of monitoring the resin flow, recognize the deviations from the expected or ideal flow pattern through the image analysis and making suitable correction decisions in real time through the computer controlling injection gates. Their control algorithm is based on the calculation of distance between the centroid of an unfilled area and the vent. Then the gate with minimum value of this distance was selected for the next step. Their system is validated using a numerical simulation and infusion experiments. However, for preforms with low permeability like plain woven, their approach is not helpful because the resin flow is mainly driven by capillary pressure and control action is impossible.

Ajit et al. [29] to improve the process controllability of VARTM developed multiple segments injection line that each of them operate separately. They designed two closed-loop control strategies for real-time flow front modifying and preventing the void formation. Inherent limitation in the resin driven at one atmosphere in the VARTM process makes the sequential injection of limited use.

The VIPR (Vacuum Induced Perform Relaxation) [30] and the Flow Flooding Chamber (FFC) [31] are variations of traditional VARTM. These processes start with a standard VARTM process and a rigid chamber is placed on the top of the vacuum bag to relax the preforms. The main difference between the VIPR and the FFC processes is that in VIPR process, a second vacuum chamber is placed over a local area of the vacuum bag to relax the preform instead of the entire surface of a part [27]. Their workstation is schematically shown in Figure 1.2. Advani et al. have presented a numerical model to identify the variation of permeability [6] and explained the filling process within this relaxation approach. They have extended their study [30] by relating this approach for real-time resin flow correcting with two flow controller designs. The first one, a simple closed loop controller, is based on a maximum distance between the vent and flow front in the direction of each gate. For calculating the distance an image processing algorithm was exploited. The latter one, the adaptive controller design was based on an adaptive flow control design for addressing a more complex mold geometry. They also studied the mechanical properties of the composites that were manufactured by this method to evaluate if their relaxation method has an adverse effect on the composite characteristics. Their

results showed that this process did not compromise mechanical properties of the resulting structure [31].

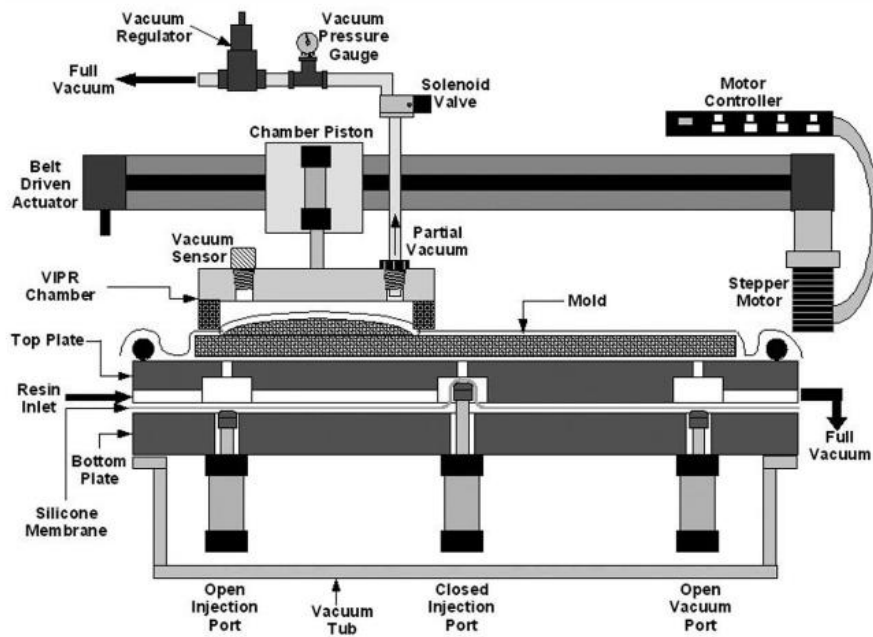


Figure 1.2. Cross-sectional schematic of the VIPR process workstation [18].

Justin B. Alms [24] worked on an injection port-based method that integrated with a VIPR chamber for increasing permeability temporarily. By this approach you can apply different vacuum pressure in the chamber and relax the compaction of preform. The goal of this approach was controlling the flow behavior and decrease the filling time.

Beside these challenges to control the resin flow, to control of the resin flow front and permeability of preform efficiently in real-time, the current vacuum bags are not appropriate. They are mostly oversized in significant terms and have numerous folds (overlapping) due to cutting of 2D sheets and then covering 3D preforms with them. Therefore, this would often lead to bridging and or bulging which can cause consistent infusions, dry spots and leave resin rich bag fold lines on the molded composite parts. Also, these bags are not reusable and thus end up in the dump after each mold run. Furthermore, properly installing these bags have some other disadvantage like higher labor cost, unsatisfactory durability, sealing, leaks and

bleeds off vacuum during filling and post filling, time consuming due to duplicating every step each time, especially for very large structures such as boat hulls [32].

Considering the problems and deficiencies inherent in the current vacuum bags, there exists a need for a new generation of vacuum bags that reusable for use in VARTM which would eliminate the non-repeatability seen in the current process, reduce the void content, improve the surface quality of the part. Also, this new generation of vacuum bags can be appropriate to real-time flow control and accomplishing the results of finite element simulations in a repeatable manner.

Silicone rubber is an elastomer that widely used in industry, and currently there are multiple formulations of it in the market. Platinum-based silicone rubbers cure quickly and have many merits, such as almost nil shrinkage (not more than 0.1%), high chemical resistance to aggressive components of some types of resins, good tear strength, high degree of precision in reproduction, high dimensional stability over time and non-deformability, high resistance to high temperatures and aging, excellent non-stick effect and good grade (environmental, odorless and nontoxic) [32].

The advantages of this material make it a candidate for a new application in composite manufacturing processes and it is highly suitable for fabricating new flexible molds.

### **1.3 Objectives of research**

Most of the researches in the recent decades are leaning to develop and overcome the drawbacks of the LCM processes to extend composite materials in any structural parts. There are some developments in this respect however they are not enough. Some new inventing variations of these processes are presented in the literature to automate and eliminate the VARTM process challenges. Still finding a novel idea to improve the VARTM in repeatability and reliability is necessary.

The first aim of this thesis is to develop an approach to understand and measure the permeability of preform in a reliable way so that increases the repeatability of the measured values in the same conditions. The second aim is to study an approach for resin flow control and increase the permeability locally in real time manner. Further the goal of this thesis characterization the presented method and extract a model for

permeability of the preforms which undergoes this process. This study needs a new upper flexible mold that provides the aims of this research due to inability of the current vacuum bags to achieve goals of this dissertation. Also, to carry the permeability measurement and flow manipulation a flow front sensing approach is necessary. And the last major objective of the study evaluates the filling of the mold under this process numerically. In this study, PAM RTM package is conducted for simulation.

#### **1.4 Scope of this dissertation**

This thesis focuses on the permeability measurement and permeability control in real time. For permeability measurement, a new approach is presented to calculate the principle permeabilities of reinforcement preforms in a single rectilinear method where reduces the experiment number and increase the reliability of the measurement test this that is presented in chapter 2. This chapter presents an analytical and experimental approach to calculate the different preform direction permeability in just one experiment. In chapter 3, the Electromagnetically Induced Preform Resting (EIPR) process is described. This chapter introduces how the EIPR process manipulates resin flow in real time by this system that includes an electromagnetic source, a new version of vacuum bag, an automated gantry system and an image processing unit. The EIPR process effect on permeability is characterized in chapter 4. This chapter studies the permeability of the preform as a function of the presented system parameters and provides a mode for the EIPR process permeability. In chapter 5, the EIPR process is considered numerically by equivalent permeability of the preform. Lastly in chapter 6, all conclusions and futures of this study are presented.

## CHAPTER 2

### CALCULATION OF IN-PLANE PRINCIPLE PERMEABILITIES

Accurate and reliable measurement of preform permeability is a very important factor that has a critical role in flow modeling of resin in the composite manufacturing process. This chapter presents a new approach to determine multiple-component permeability in a single rectilinear experiment in VARTM process. This approach is applied to predict the principle in-plane permeabilities in a single experiment. Fabrics in  $0^\circ$ ,  $45^\circ$  and  $90^\circ$  orientations are used for this purpose in this study. It is based on the tracking of the resin flow front during the infusion with respect to time. An analytical approach is developed to find the permeability for each orientation (or material), sequentially. After finding the permeability of each component, permeability of each component is employed to calculate the principle permeabilities. A validation study is conducted for all possible permutations of fabric orientations. Results show the efficiency of the presented method to estimate the in-plane principle permeability in a single experiment.

#### 2.1 Introduction

Liquid composite molding (LCM) methods are common processes for manufacturing of composite parts. Design of the mold, filling time prediction, optimization of the composite manufacturing parameters i.e. inlet and outlet locations have been executed by trial and error approaches, so far. It is essential to estimate the resin flow in LCM process, correctly. The resin flow simulation in LCM process is done with finite element based softwares like PAM-RTM [33] LIMS [34] and Poly-Worx [35]. The basis of the finite element solution to simulate the filling process stems originally from Darcy's law [36]. It states that the flow volume averaged velocity of fluid ( $\mathbf{v}$ ), is proportional to the pressure gradient ( $\Delta p$ ), fluid viscosity ( $\mu$ ), and preform permeability tensor ( $\mathbf{K}$ ) as:

$$\mathbf{v} = -\frac{\mathbf{K}}{\mu} \Delta p \quad (2.1)$$

Solving this equation needs an important and crucial input parameter of fabric i.e. permeability. It depends on the local compression of the preform during the molding. To predict the filling time and flow front pattern, a complete characterization of material property is necessary for simulations. The preform permeability in porous media is anisotropic such that a second order tensor describes this property as follows:

$$\mathbf{K} = \begin{bmatrix} K_{xx} & K_{xy} & K_{xz} \\ K_{yx} & K_{yy} & K_{yz} \\ K_{zx} & K_{zy} & K_{zz} \end{bmatrix} \quad (2.2)$$

Where  $K_{xx}$  is the permeability for flow in the  $x$  direction as driven by a pressure gradient in the  $x$  direction,  $K_{yx}$  and  $K_{zx}$  are the permeabilities for flows in  $y$  and  $z$  directions as driven by a pressure gradient in the  $x$  direction.

This tensor can be diagonalized to obtain the principle permeabilities. It is assumed that the first two principle permeabilities lie in the fabric plane while the third one is oriented perpendicular to the fabric plane [17]. However, it can be argued that the last one can be omitted for practical purposes for preforms in general [37].

There are various methods for permeability measurements. They can be divided into three classifications: flow geometry (radial-2D, rectilinear-1D), injection boundary condition (constant pressure, constant flow rate) and saturation status of the method (saturated, unsaturated).

As studied in [15], two approaches are commonly used to determine the in-plane permeability: radial [38–41] and rectilinear techniques [42–44]. The radial method looks attractive for permeability measurements because it is bidirectional measurement and half lengths of major and minor axes of the elliptic fluid flow pattern gives the in-plane principle permeability. Some difficulties are reported [45–48] in relation to the radial method. It requires a complex data acquisition setup.

Deformation of reinforcement and vacuum bag during the process, also sensitivity of the flow pattern to radius and shape of the inlet port increase this complexity. Because of all these problems, the permeability measurement does not seem straightforward.

The second approach which is called rectilinear method derives the principle permeabilities  $K_1$ ,  $K_2$  and orientation of the permeability tensor from at least three unidirectional measurements. Moreover, this experiment is less complicated and easier to track the flow front. However, the race tracking that may occur during tests limits this approach [49–51].

In recent years, since composites use has increased dramatically, several experimental and analytical studies have been conducted to characterize the in-plane permeability in shell-like structures [52]. However, there is a complete lack of standardization for permeability measurements. In this respect, Parnas R. S. [53] proposed a 3D woven fabric as a standard reference material for the permeability characterization. However, it is not used as a standard method.

There are several researches associated with permeability determination in both RTM and VARTM molding in 3D and 2D [15]. Although there are different approaches to characterize permeability, obtaining a repeatable value is one of the challenges that researchers face and report in their studies. The calculated preform permeabilities show variation of 20-50% for the same process and tests in the same laboratory [17,18]. First international benchmark exercise presents a wide scatter up to 90% for two different fabrics with different processes used by participants [18]. For the second benchmark despite having a common procedure, there is still a significant scatter up to 20% in their results. The reasons for scatter are due to the process type, race tracking, human factors, preparation of the specimens and repeatability of experimental condition [17,18].

Lugo et al. [54] presented an analytical and experimental approach to determine the multiple permeability components from a single rectilinear experiment. By their approach in-plane permeabilities as well as the transverse (through-thickness) one and the one for a distribution media can be estimated.

Claudio Di Fratta et al. [55] introduced a novel approach to estimate the permeability of the fabric as a function of fiber volume fraction in a single unidirectional RTM experiment with an exclusive injection.

Claudio Di Fratta et al. [16,56] presented an efficient and cost-effective approach compared with the conventional one because it needs fewer experiments and preform samples. Their approach is based on the angle measurement in unidirectional experiment, which reduces the time, cost and number of tests required. By this approach, two different preform directions are implemented to measure the angle between the flow front and the measurement direction, and to determine the in-plane preform permeability tensor. Therefore, this approach reduces the number of tests for determining in-plane principle values from 3 to 2.

This chapter will demonstrate a single experiment permeability measurement method in the infusion process for determining the in-plane permeability. This method is based on the flow tracking as a function of time where fabrics are placed one after the other in three different directions i.e.  $0^\circ$ ,  $45^\circ$ , and  $90^\circ$ . This work provides an analytical approach to calculate the permeabilities in the second and third sections as well as the first section. Whereas the first zone permeability is obtained according to the conventional unidirectional method. After finding the first-zone permeability, it is applied to calculate the second zone value and finally both are used to estimate the permeability of the last zone. Therefore, the presented analytical and experimental strategy allows the determination of principle permeabilities in just one experiment.

For this process, it is essential to track the flow front. In this study, it is achieved by an image processing system developed. In order to generate a reproducible and reliable measurement, a specific vacuum bag design is utilized. Finally, experimental tests are conducted to validate the proposed methodology.

## **2.2 Analytical determination of in-plane permeability**

The following analytical approach is used for the estimation of in-plane permeability of preforms from a single rectilinear experiment. Presented method is an approach to estimate the permeability of multiple fabrics with distinct properties and/or having different directions. These preform sections are saturated sequentially. The flow front

form with respect to time plot is used to estimate permeabilities of each component. Figure 2.1 shows the schematic of the layup of configuration. It is to extract the relation for obtaining the permeabilities of each zone that infused from the left side as a gate line to right side as an outline. Here,  $L_1$ ,  $L_2$  and  $L_3$  are the distance of each zone end to the gate, and  $L$  is the flow front location from the gate at time  $t$ .

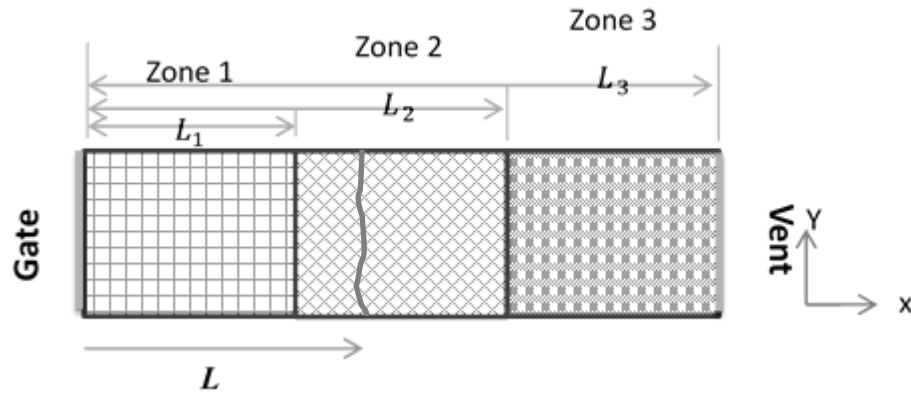


Figure 2.1. Schematic of the experiment lay-up

Darcy's law is used as the governing equation to determine the flow through permeable fabric, the simplest of which is for a 1D (thin and long plate, the length and width of preform are relatively much larger than its thickness) preform and for a constant fluid viscosity:

$$Q = -\frac{K_{xx}(x)h(x)}{\mu} \frac{dp}{dx} \quad (2.3)$$

where  $Q$  is the flowrate per unit width of the preform (in units of volume per unit time),  $K_{xx}$  is the permeability of the formation that may vary with location,  $h$  is the local thickness of the formation,  $\mu$  is the viscosity of the fluid,  $dp/dx$  represents the pressure change per unit length of the formation.

Integration of the resin pressure from the inlet pressure at  $x_0$  to pressure at the flow front (i.e. vacuum pressure) and from the inlet line ( $x = 0$ ) to flow front position ( $L$ ):

$$\Delta p = Q\mu \int_0^L \frac{dx}{K_{xx}(x)h(x)} \quad (2.4)$$

By rearranging, it can be written as a relation of the flow rate  $Q$  and the flow front location  $L$  as follows:

$$Q = \frac{\Delta p}{\mu} \frac{1}{\int_0^L \frac{dx}{K_{xx}h(x)}} \quad (2.5)$$

The flow front progress can be expressed as:

$$\frac{dL}{dt} = \dot{L} = \frac{Q}{\varphi(L)h(L)} \quad (2.6)$$

where  $\varphi$  is porosity of the preform that is equal to  $(1 - v_f)$ , where  $v_f$  is the fiber volume fraction. Substituting Eq. (2.5) into Eq. (2.6) gives the differential equation for flow front progress as:

$$\dot{L} = \frac{\Delta p}{\mu h(L)\varphi(L)} \frac{1}{\int_0^L \frac{dx}{K_{xx}(x)h(x)}} \quad (2.7)$$

This equation can be integrated for transient inlet pressure with time to obtain the transient flow front position:

$$\int_0^L \left[ h(\omega)\varphi(\omega) \int_0^\omega \frac{dx}{K_{xx}(x)h(x)} \right] d\omega = \int_0^t \left( \frac{\Delta p(\theta)}{\mu} \right) d\theta \quad (2.8)$$

It includes the change in thickness, porosity and permeability with position. The suggested experimental approach records the flow front position during constant-pressure infusion through three parts with different permeability. Eq. (2.8) is used to evaluate the permeability of all components. These characterizations are done step by step by determining the permeability in the all parts for three different preform

directions. In each component, permeability, porosity and thickness are assumed independent of position.

Integration of each side of Eq. (2.8) gives the familiar relation for the flow front as:

$$L^2(t) = \frac{2K_{xx1}\Delta p}{\mu\varphi_1}t \quad (2.9)$$

Here,  $K_{xx1}$  and  $\varphi_1$  are the effective permeability and porosity of the preform in the first zone.

The permeability of the first zone ( $K_{xx1}$ ) is obtained from the slope of the best-fit line by plotting  $L^2$  as a function of  $t$ .

Similarly, for the second zone, where  $x > L_1$  with  $h_2$  and  $\varphi_2$ , the effective permeability of the fabric is  $K_{xx2}$ . Integrating Eq. (2.7) from the second zone start line ( $L_1$ ) and the time that the resin flow front reaches to the end of the first zone end  $L_1$  i.e.  $t_1$ :

$$\int_{L_1}^L \left[ h_2\varphi_2 \left( \frac{L_1}{K_{xx1}h_1} + \frac{\omega - L_1}{K_{xx2}h_2} \right) \right] d\omega = \int_{t_1}^t \left( \frac{\Delta p(\theta)}{\mu} \right) d\theta \quad (2.10)$$

where  $K_{xx1}$  is the first segment permeability,  $t_1$  is the time that flow front reaches to the end of the first component. Integration results in:

$$\begin{aligned} h_2\varphi_2 \left( \frac{L_1L}{K_{xx1}h_1} + \frac{L^2 - 2L_1L}{2K_{xx2}h_2} - \frac{L_1^2}{K_{xx1}h_1} - \frac{L_1^2 - 2L_1^2}{2K_{xx2}h_2} \right) \\ = \frac{\Delta p}{\mu} (t - t_1) \end{aligned} \quad (2.11)$$

re-arranging this expression to estimate the second component permeability as:

$$\frac{1}{2h_2} (L - L_1)^2 = K_{xx2} \left( \left( \frac{\Delta p}{\mu h_2 \varphi_2} \right) (t - t_1) - \frac{L_1}{K_{xx1} h_1} (L - L_1) \right) \quad (2.12)$$

The second permeability in component two,  $K_{xx2}$ , is determined as the slope of this expression.

Finally, for the last component,  $x > L_2$  with  $h_3$  and  $\varphi_3$ , the permeability  $K_{xx3}$  is obtained from the integration of Eq. (2.7) from  $L_2$  and  $t_2$  as:

$$\int_{L_2}^L \left[ h_3 \varphi_3 \left( \frac{L_1}{K_{xx1} h_1} + \frac{L_2 - L_1}{K_{xx2} h_2} + \frac{\omega - L_2}{K_{xx3} h_3} \right) \right] d\omega = \int_{t_2}^t \left( \frac{\Delta p(\theta)}{\mu} \right) d\theta \quad (2.13)$$

This integration gives:

$$h_3 \varphi_3 \left( \frac{L_1 L}{K_{xx1} h_1} + \frac{(L_2 - L_1) L}{K_{xx2} h_2} + \frac{L^2 - 2L_2 L}{2K_{xx3} h_3} - \frac{L_1 L_2}{K_{xx1} h_1} - \frac{(L_2 - L_1) L_2}{K_{xx2} h_2} - \frac{L_2^2 - 2L_2^2}{2K_{xx3} h_3} \right) = \frac{\Delta p}{\mu} (t - t_2) \quad (2.14)$$

By re-arranging this relation as shown below:

$$\begin{aligned} & \frac{1}{2 h_3} (L^2 - 2L_2 L + L_2^2) \\ &= K_{xx3} \left( \frac{\Delta p}{\mu h_3 \varphi_3} (t - t_2) - \frac{L_1(L - L_2)}{K_{xx1} h_1} - \frac{(L_2 - L_1)(L - L_2)}{K_{xx2} h_2} \right) \end{aligned} \quad (2.15)$$

Where the permeability of the last segment,  $K_{xx3}$ , is determined as the slope of this function.

Thus, by this approach, the permeability of each component are determined by the presented relations Eq. (2.9), (2.12) and (2.15) for the preforms in  $0^\circ$ ,  $45^\circ$  and  $90^\circ$  directions. After determining the permeability for each combination, the in-plane permeability tensor could be extracted.

Therefore, one can determine the principal permeability and direction of fabrics by this approach.

### 2.3 Principle permeability calculation methodology

Once the values of each zone in three different preform directions are obtained, the principle permeabilities can be obtained. Based on the literature [43], that the square root of the permeability along any fabric direction follows an ellipse as shown in Figure 2.2. For the elliptic flow pattern, half of major and minor axes gives the square root of in-plane principle permeabilities  $K_1$  and  $K_2$  as follows:

$$K_1 = K_{xx}^{0^\circ} \frac{\alpha_1 - \alpha_2}{\alpha_1 - \frac{\alpha_2}{\cos(2\beta)}} \quad (2.16)$$

and

$$K_2 = K_{xx}^{90^\circ} \frac{\alpha_1 + \alpha_2}{\alpha_1 + \frac{\alpha_2}{\cos(2\beta)}} \quad (2.17)$$

where  $\alpha_1$ ,  $\alpha_2$  and  $\beta$  are given by

$$\alpha_1 = \frac{K_{xx}^{0^\circ} + K_{xx}^{90^\circ}}{2} \quad (2.18)$$

$$\alpha_2 = \frac{K_{xx}^{0^\circ} - K_{xx}^{90^\circ}}{2} \quad (2.19)$$

$$\beta = \frac{1}{2} \tan^{-1} \left( \frac{\alpha_1}{\alpha_2} - \frac{\alpha_1^2 - \alpha_2^2}{\alpha_2 \cdot K_{xx}^{45^\circ}} \right) \quad (2.20)$$

Where  $K_{xx}^{0^\circ}$ ,  $K_{xx}^{45^\circ}$ ,  $K_{xx}^{90^\circ}$  and  $\beta$  are permeability of the preform along  $0^\circ$ ,  $45^\circ$ ,  $90^\circ$  orientations and the angle of elliptic pattern and warp direction of fabric.

Figure 2.2 shows the principle permeability values from the experimental permeability data.

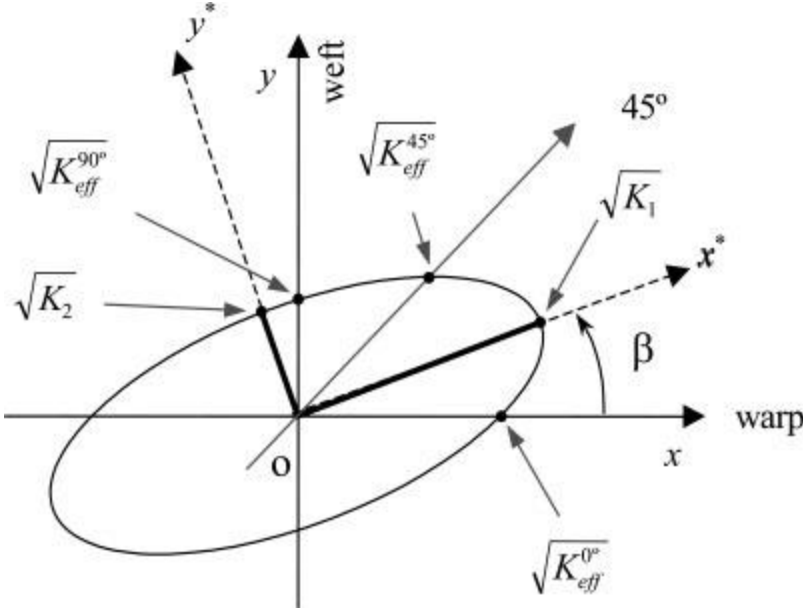


Figure 2.2. Flow front elliptical pattern,  $K_1, K_2$  and  $\beta$  are principle permeabilities and angle of flow elliptical [43]

**2.4 Permeability measurement experiment**

**2.4.1 Test set-up**

Experimental set up composes of upper flexible mold as a vacuum bag and transparent glass mold as shown schematically in Figure 2.3. Bottom mold allows tracking of the flow through the reinforcement. The port on the left edge of the sample is used as the resin inlet and the one on the very right is used as the vacuum port.

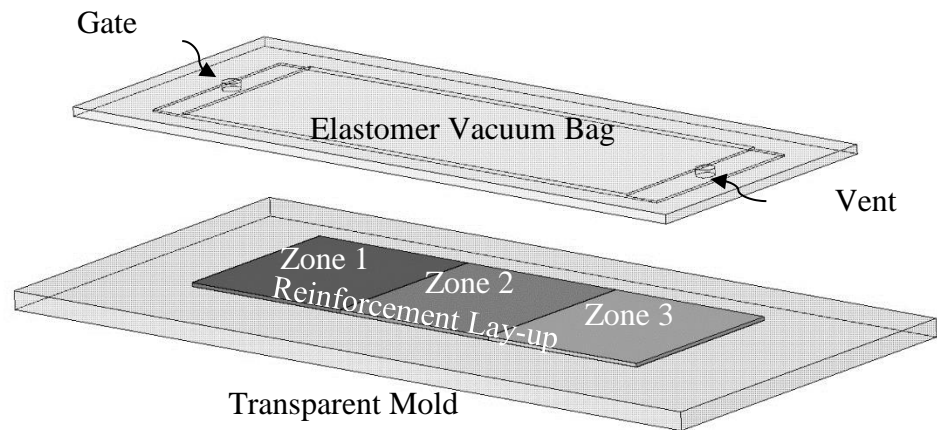


Figure 2.3. Typical experiment mold

For the detection of the flow front, a MATLAB program is written which is working coupled with an image processing unit. The program takes images as bitmap at selected time intervals, corrects the camera related perspective distortion and detects the flow front edge. From the detected front, this program calculates the average distance from the resin inlet.

#### 2.4.2 Elastomer silicone vacuum bag

Silicone rubber is an elastomer that is extensively used in the industry with various formulations. Platinum-based silicone rubbers cure rapidly and have many advantages, such as almost no shrinkage (not more than 0.1%), high chemical resistance to most of the resins used in composites field, high tear strength, good degree of precision in reproduction, high dimensional stability over time and non-deformability, high resistance to high temperatures and aging [32].

In VARTM process, race-tracks are frequently formed at the edge due to the inability of the fabric layers or the vacuum bag to stretch into gaps around the edge, this point is schematically represented in Figure 2.4. Race-tracking is an important issue independent of how fabric layers are cut. This is a problem, and during the vacuum infusion process, it often occurs due to low resistance along the edges of the mold, such that resin has higher velocity in these gaps.

Using silicon type of vacuum bag may prevent possible race-tracking channels as shown in Figure 2.4. Liquid rubber fills gaps and creates a suitable mold form along the edges. As presented in the analytical section, the experiment is conducted in a VARTM process and preforms are covered with silicone type of vacuum bag.

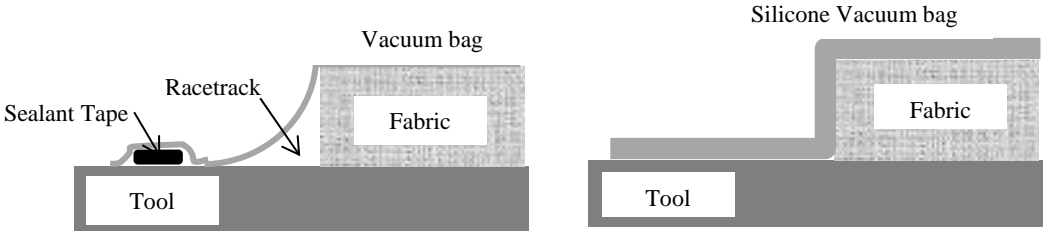


Figure 2.4. Race-tracking and its elimination by an elastomer vacuum bag

**2.4.3 Permeability calculation**

The described permeability measurement methodology is experimentally validated by a series of tests to characterize the permeability of E-Glass fiber multiaxial fabric with nominal areal weight of 600 g/m<sup>2</sup> at 0°, 45° and 90° orientations in a single test. Five number of layers are stacked for each segment. As displayed in Figure 2.5, testing directions at 0° and 90° are defined respectively in the warp and weft of the roll. The 45° testing orientation is obtained between the 0° and 90° directions.

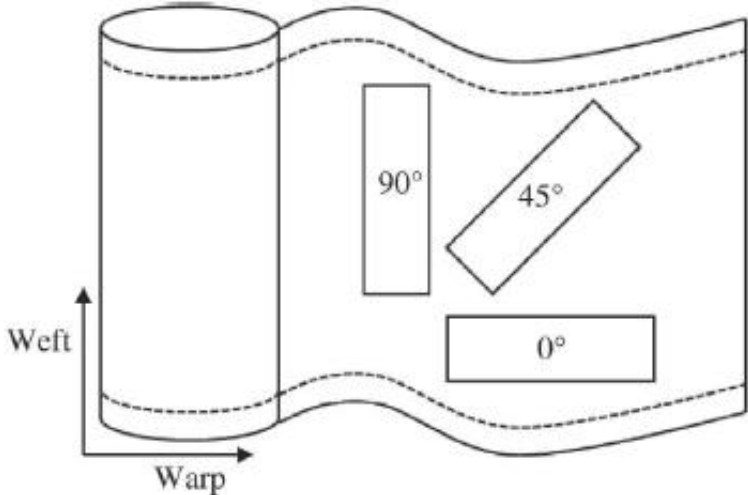


Figure 2.5. Directions of each segments layers in the reinforcement roll [17]

For a good resin flow uniformity, mold size of 100 mm × 300 mm (aspect ratio of 3) is used. Dimension of each segment (laminate with 0°, 45°, and 90° fabric orientation) is 100 × 100 mm as shown in Figure 2.6. It illustrates the layup of preforms at 0° – 90° – 45° sequences.

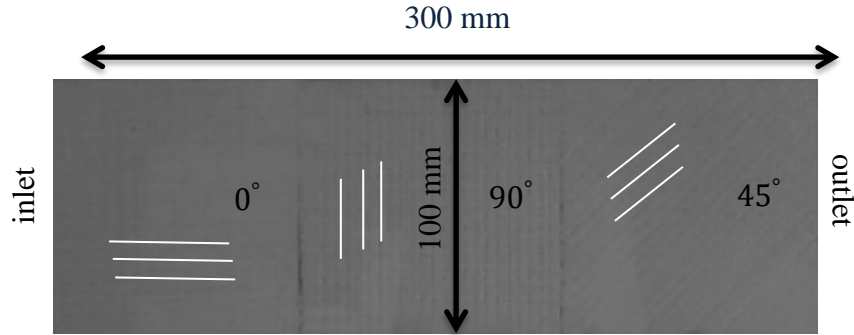


Figure 2.6. Placement of fabrics on the transparent mold

After placing the fabrics, silicone vacuum bag is placed over them and then vacuum is applied to the mold. A motor oil with viscosity of 0.16 Pa.s at 25°C is used as the test liquid.

To calculate the permeability of the fabric, the porosity  $\varphi$  of the fabric or the fiber volume fraction is required. The fiber volume fraction is dependent on the total mass of fabric  $m_f$ , length  $l$  and width  $w$  of preform, preform thickness  $h$  and the density of the fabric  $\rho_f$  as following:

$$V_f = \frac{m_f}{lwh\rho_f} \quad (2.21)$$

The porosity  $\varphi$  of the fabric can thus be calculated as:

$$\varphi = 1 - V_f \quad (2.22)$$

In infusion experiments, the sequence of reinforcements with different directions in each test may influence the permeability measured in each zone. To evaluate and

consider these effects, experiments are conducted for all possible permutations of these three different fabric orientations as summarized in Table 2.1.

Table 2.1. Permeabilities of zone sequences and their codes

| Test          | Code | Zone sequence |
|---------------|------|---------------|
| Permutation 1 | P1   | (0-45-90)     |
| Permutation 2 | P2   | (0-90-45)     |
| Permutation 3 | P3   | (45-0-90)     |
| Permutation 4 | P4   | (45-90-0)     |
| Permutation 5 | P5   | (90-0-45)     |
| Permutation 6 | P6   | (90-45-0)     |

## 2.5 Results and discussion

The flow front positions for each test recorded are shown in Figure 2.7. In this graph, the flow front position is given as a function of time. The effect of lay-up sequence on the flow front profile and filling time can easily be observed. Obviously, it is due to impregnation property of the fabric in different orientations and varying the permeability of segment. Investigating the results shows that placing the preform with a lower permeability close to the infusion line increases the filling time. This result can easily be seen by comparing the filling time values. Similarly, as Figure 2.8, it can be observed that placing the preform with  $90^\circ$  close to the inlet increases the filling time. The trend is shown by a solid line. Preform of  $45^\circ$  has a moderate permeability and dash lines illustrate this effect in the form of an increase in the filling time. The more low permeability preform closer to the inlet is the more increasing filling time. This can be seen in this figure and from the comparison of permutations 1 and 3. This result is also valid for comparing P2 and P4 also P 5 and P 6. It can be justified by the fact that; the low permeability preform close to the infusion line has more resistance and during the filling process less flow is delivered through the preform and it increases the filling time.

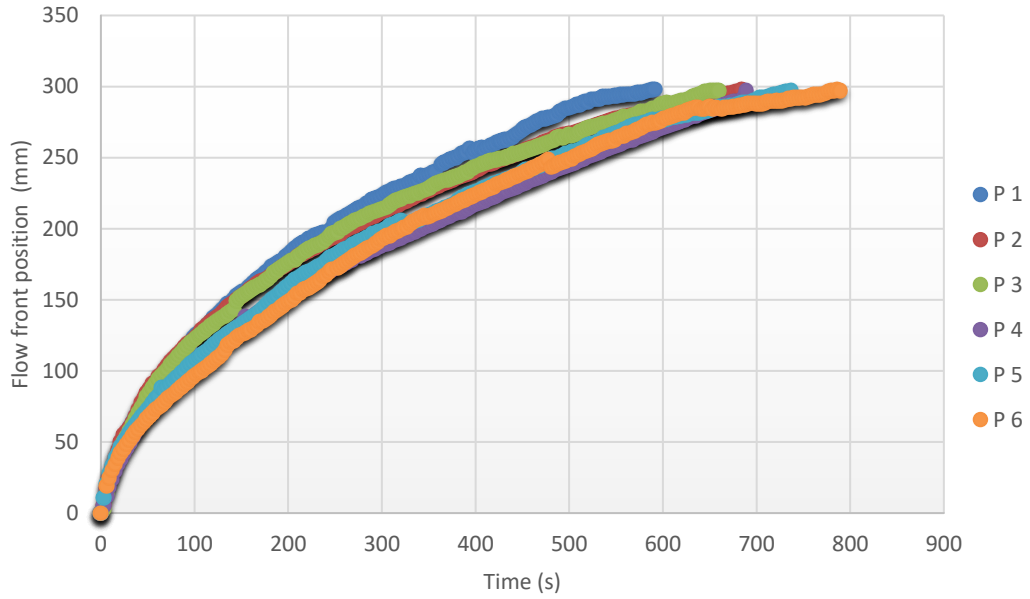


Figure 2.7. Flow front position as a function of time

| Permutation No. | Zone 1 | Zone 2 | Zone 3 |
|-----------------|--------|--------|--------|
| P 1             | 0      | 45     | 90     |
| P 3             | 45     | 0      | 90     |
| P 2             | 0      | 90     | 45     |
| P 4             | 45     | 90     | 0      |
| P 5             | 90     | 0      | 45     |
| P 6             | 90     | 45     | 0      |

Figure 2.8. Effect of placement on filling time

Experimentally speaking, a similar process with the analytical calculations is repeated here. Using the flow front position in each zone and lay-up sequence, permeability of each zone is calculated in the first, second and third zones sequentially. For the first zone, the slope of the best fit-line for square flow front position in this section versus time is given in Figure 2.9 for P 3. For the second and

third zones, the slope of the best fit-line of the Eq. (2.12) and Eq. (2.15) as  $f_2(L) = K_{xx2} g_2(L, t)$  and  $f_3(L) = K_{xx3} g_2(L, t)$ , sequentially, are given in Figure 2.10 and Figure 2.11.

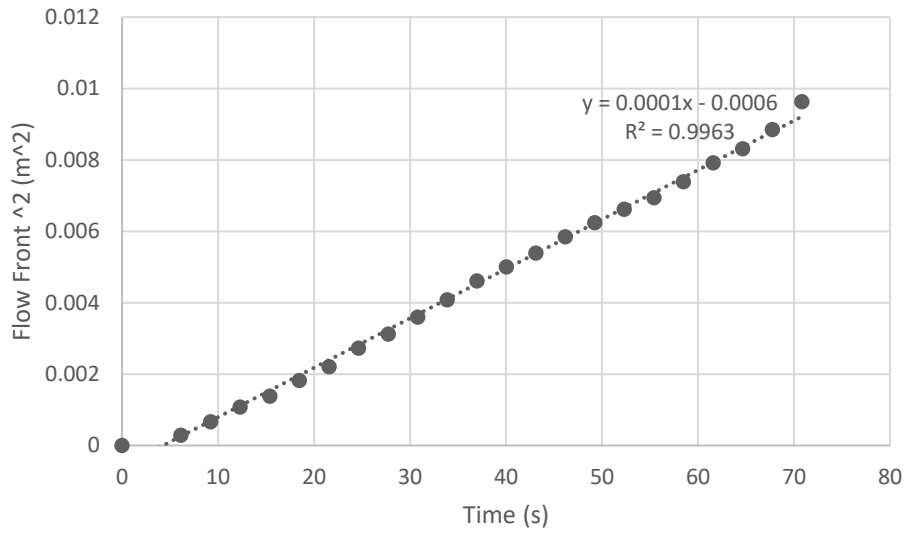


Figure 2.9. Flow front position vs. time for the first zone in P3

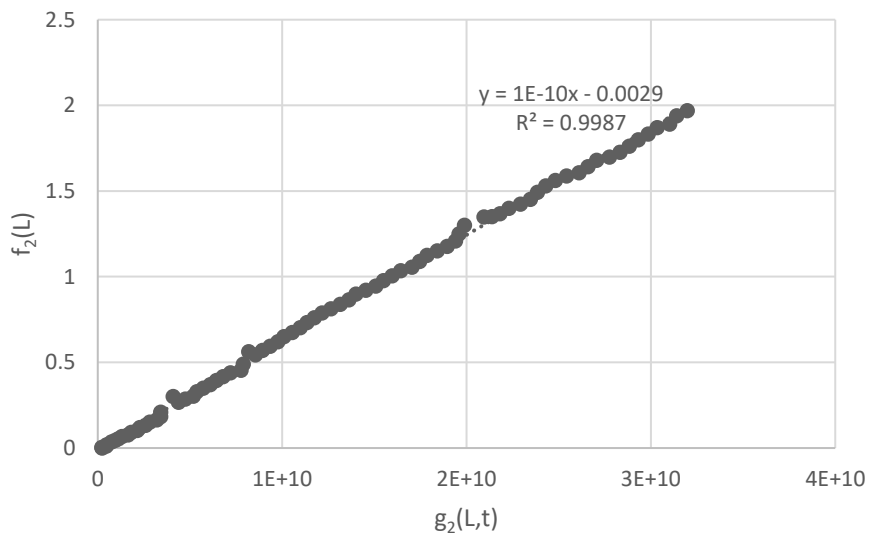


Figure 2.10. Permeability of the second zone with  $0^\circ$  for P3 test

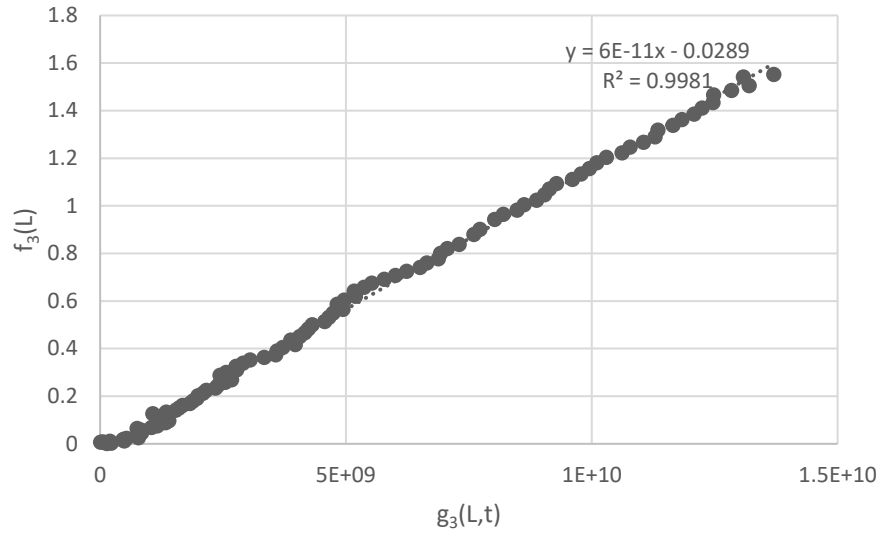


Figure 2.11. Permeability of the third zone with  $90^\circ$  for P3

Table 2.2. Permeability of the reinforcements at different orientation

| Test series             | Permeability ( $10^{-10} m^2$ ) |            |            |
|-------------------------|---------------------------------|------------|------------|
|                         | Fabric orientation              |            |            |
|                         | $0^\circ$                       | $45^\circ$ | $90^\circ$ |
| Permutation 1 (0-45-90) | 1.1                             | 0.84       | 0.68       |
| Permutation 2 (0-90-45) | 1.02                            | 0.77       | 0.62       |
| Permutation 3 (45-0-90) | 1.08                            | 0.73       | 0.63       |
| Permutation 4 (45-90-0) | 1.12                            | 0.82       | 0.6        |
| Permutation 5 (90-0-45) | 1.05                            | 0.75       | 0.64       |
| Permutation 6 (90-45-0) | 1.01                            | 0.8        | 0.61       |
| Total average           | 1.06                            | 0.78       | 0.63       |
| Reference               | 1.06                            | 0.77       | 0.62       |

All results are given in Table 2.2 and Figure 2.12. The reference data for each preform orientation is return to the average of the two permutations that include the same orientation in the first zone. The reason for tacking this values as a reference is that in the first zone permeability calculation is based on the well-known equation for

a single component. Investigating the results presents that this approach reduces the scatter significantly in comparison with the benchmarks results.

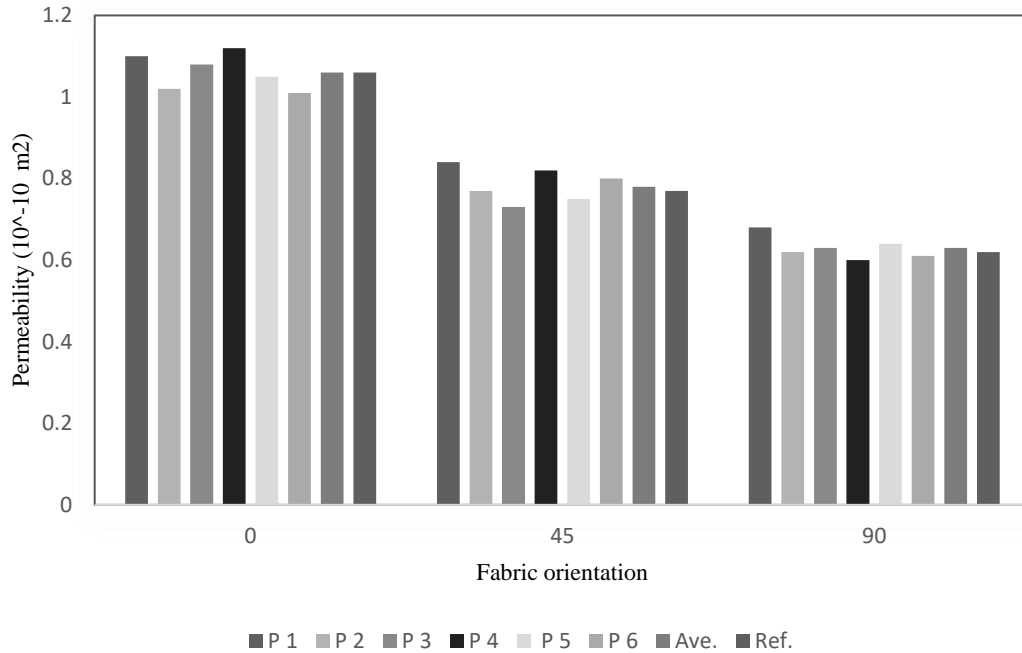


Figure 2.12. Permeability for 0°, 45° and 90° orientations

Once the permeability of preform in three different directions are calculated, it is possible to create the permeability ellipse, the principal axes of which fully defining the in-plane permeability tensor of the fibrous reinforcement. From Eq. (2.16), Eq. (2.17) and Eq. (2.20) principle permeabilities and orientation of the elliptic angle are calculated as below:

$$K_1 = 1.68E-10, K_2 = 6.18E-11 \text{ and } \beta = -10^\circ$$

Therefore, by using these data, finding the flow ellipse centered at (0,0) that passes through the three points  $(\sqrt{K_{xx}^{0^\circ}}, 0)$ ,  $(\sqrt{K_{xx}^{45^\circ}} \times \cos(45), \sqrt{K_{xx}^{45^\circ}} \times \sin(45))$ , and  $(0, \sqrt{K_{xx}^{90^\circ}})$  is possible. The elliptic pattern of the effective permeability and the principle permeabilities for the preform of this study is shown in the following Figure 2.13.

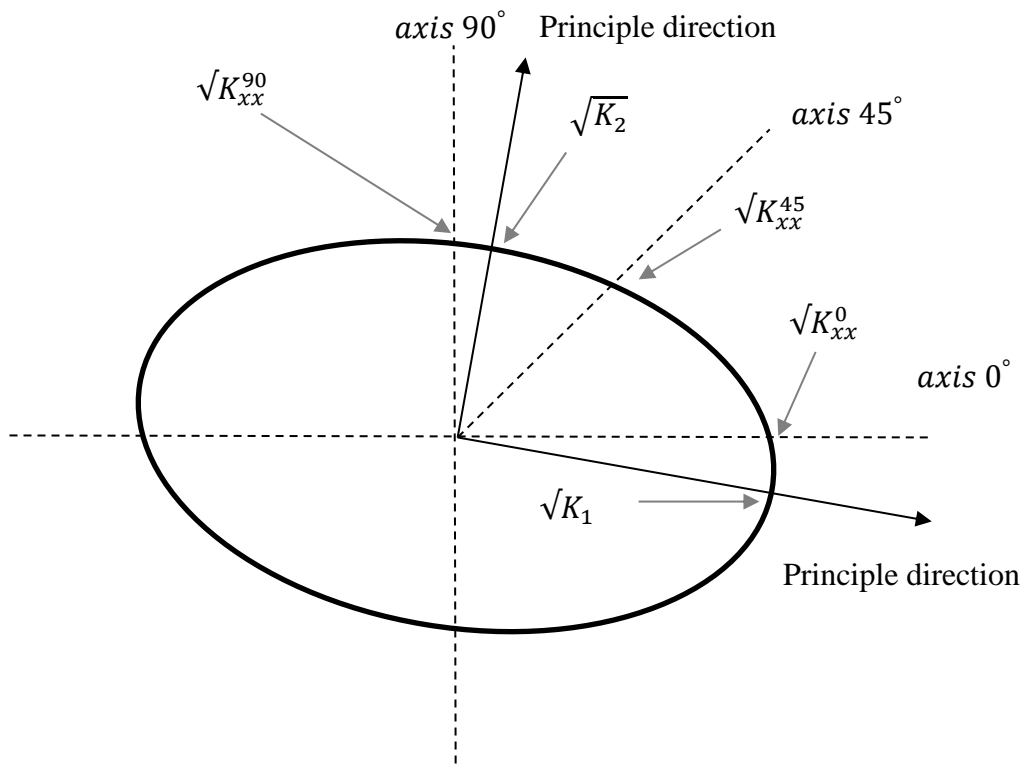


Figure 2.13. Elliptic pattern of permeability for preform used

## 2.6 Summary

The present study introduces a novel approach to estimate the principle in-plane permeabilities of fabrics in a single rectilinear experiment. The methodology consists of placing the preforms in a single VARTM infusion process one after the other with different orientations. This work introduces an analytical approach to characterize the permeability of each zone. For the first zone, the method is same as the current method. For the second and third sections, Darcy's law is extended to calculate their permeability values, sequentially. To track the flow front as a function of time, image processing is used by writing a program in MATLAB. To prevent the formation of race-tracking and to have a repeatable and reliable process, a silicone vacuum bag is used.

The experimental validation of the presented approach is carried out for all possible permutations. The experimental results show the accuracy and reproducibility of the

methodology in a more efficient way with just a single test. Results show that the permeability values are very close to the reference values.

Presented approach is not only to estimate the in-plane principle permeability values but it is also applicable to find the permeability of several fabrics of different materials in a single test.

## CHAPTER 3

### FLOW CORRECTION CONTROL WITH ELECTROMAGNETICALLY INDUCED PREFORM RESTING PROCESS

Resin Flow Correction Control with Electromagnetically Induced Preform Resting (EIPR) Process, a new variation of VARTM process called Electromagnetically Induced Preform Resting (EIPR) for dynamically resin flow controlling is introduced to manipulate the flow front and local permeability to prevent formation of dry spots. This chapter proposes an active and real-time flow controlling approach implemented during the composite laminate infusion. EIPR process applies an electromagnetic field source to pinch (raise) and vibrate the upper flexible mold to rest the fiber preform and increase the local permeability. Vibration action delivers the fluid through the preform. The EIPR process includes a new and creative upper flexible vacuum bag with the embedded elements to lift and make locally vibration via an automated gantry system. The control methodology is carried out by tracking the flow front with a real-time correction. System capability is demonstrated with three configurations of preform having different preform permeability in each experiment. A low permeability preform is employed in these configurations to disturb the flow pattern and cause an artificial problem or pseudo problem during the filling process. Results show that this system fills the mold completely without any dry spot and therefore create no waste material.

#### **3.1 Introduction**

Fiber reinforced composite manufacturing have more variation to create strong lightweight parts from various types of fibers and thermosetting resins. Vacuum-assisted resin transfer molding (VARTM) is an attractive manufacturing process due to its cost effective operating conditions to produce large scale composite structures [32,57–59]. In this process, fiber preforms are cut, placed in a single side hard mold,

and covered with a vacuum bag to impregnate dry fabrics under a pressure gradient [60,61].

Irrespective of the manufacturing type, the complete saturation of dry fabrics is a critical factor for producing quality structural parts [62]. Dry spots and voids are entrapped during the infusion due to irregular resin flow patterns caused by wrinkling of vacuum bag, misalignment of the preform, inherent preform permeability variation and race tracking. These types of problems are introduced as a source of defect and material waste created during the filling stage [62–64]. By simulating the infusion process and optimizing the inlet and outlet locations, some of these problems are solvable to some extent. However, a real time control of resin flow is necessary to have a reliable and repeatable process to prevent formation of dry spots and eliminate human related errors [65,66].

There are some research efforts to manipulate the filling process by different approaches in liquid composite molding process. Hsiao [26] presented an intelligent open/close gate/vent approach for RTM and VARTM processes with a correct timing based on flow sensing sensors in the mold to prevent unexpected distribution failures during the mold filling stage by combining a genetic algorithm with filling simulation.

Nielsen et al. [64,67,68] developed a model based on a resin flow control approach in liquid composite molding using an intelligent neural network to control gate pressure and gate flow rate in real time. Nalla et al. [29] focused on a multi-segment injection lines, each operating independently to deliver the resin to different locations by a closed-loop controller. Johnson et al. [4,64] presented an active control method where resin is locally heated to reduce viscosity and, thereby, enhance preform permeation to eliminate void entrapment and dry spots. Dhiren Modi [28] suggested another active control system which is capable of detecting flow front, identifying flow disturbances and implementing real time corrective action by computer controlled ports.

Ryosuke Matsuzaki et al. [69] proposed an active flow control approach by progressive forecasting of the flow front pattern from numerical simulation in VARTM process to correct the flow front using dielectric heating at a specific

targeted location to decrease the viscosity of the resin and as a result increase the flow speed.

In studying flow control, Justin Alms et al. [31] investigated a new method of resin delivery called the flow flooding chamber to reduce the filling time and material waste. Their method stretches the vacuum bag by a chamber above that using vacuum to rest the preform. This chamber accumulates the resin into the rested preform and after releasing the vacuum, atmospheric pressure drives the resin into the preform. Justin B. Alms [30] has worked on another approach called the vacuum induced preform relaxation uses an external local vacuum pressure to reduce the preform compaction and manipulate the permeability. The automated feature of this system is used to control flow in real time manner.

In the present study, we proposed a new online resin flow front controlling approach to eliminate the limitations of VARTM process during the filling. The present method called Electromagnetic Induced Preform Resting (EIPR) can alter the permeability of fabrics locally to prevent the formation of the dry spots and voids by accelerating the flow front at target positions. The system automatically detects the problematic regions by monitoring the flow during molding using an image processing method. Objective of this study is to improve the reliability and repeatability of the resin infusion process by a new online control methodology.

### **3.2 EIPR process for resin flow controlling**

The key disadvantage of the VARTM process is its inability to precisely manipulate the resin flow front during the filling in real time. Electromagnetically induced preform resting (EIPR) process is a new variation of VARTM and SCRIMP, which incorporates a creative upper flexible mold with embedded elements for locally lifting and vibrating vacuum bag to rest the preform by an electromagnetic field source. EIPR process consists of an elastomer vacuum bag with embedded aluminum elements during the manufacturing of the upper mold, an automated gantry system carrying the electromagnetic and resin flow front detection system. Aluminum elements are scattered in vacuum bag so that resin flow control is possible almost anywhere in the composite mold. The principle of this approach is locally disturbing and vibrating the elastomer vacuum bag to rest the preform and decrease the

resistance against the resin flow locally at problematic locations. Resin is delivered faster in these locations where an unpredictable permeability variation occurs to compensate the resin flow perturbation in real time. This correction action reduces the compaction pressure which increases the fabric preform porosity. The process is schematically demonstrated in Figure 3.1.

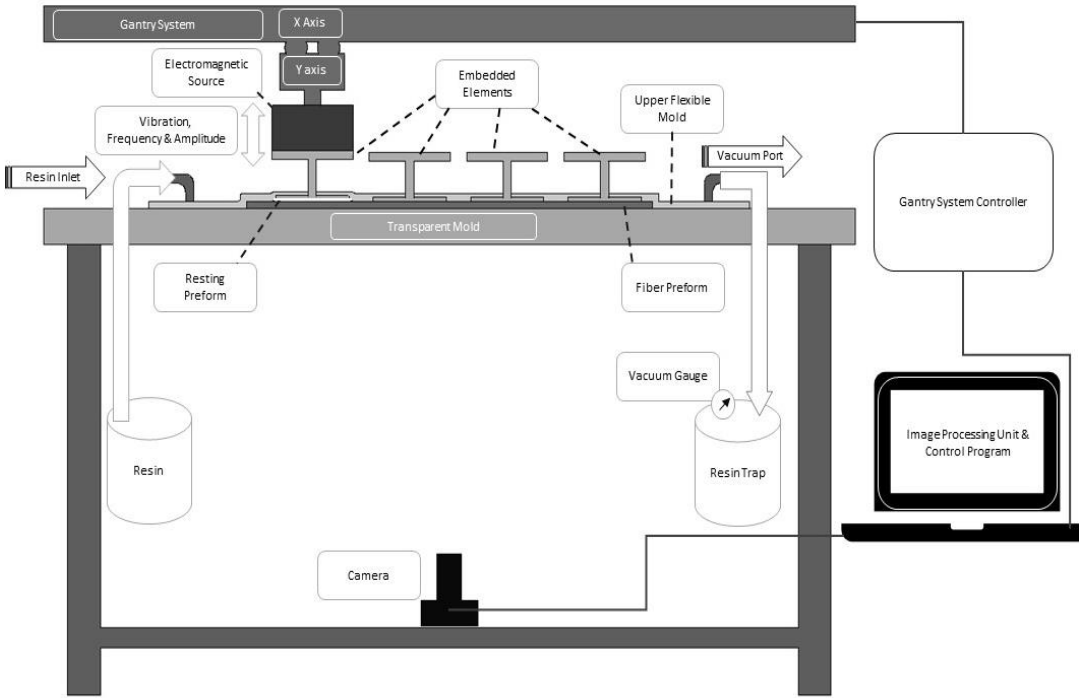


Figure 3.1. Schematics of EIPR process

Evaluating of the process unveiled significant parameters to be amplitude and frequency of vibration. The amplitude is the distance between the external electromagnet and the corresponding embedded element, and the frequency denotes the rate of electromagnetic force engagement on the corresponding the vacuum bag location. Figure 3.2. illustrates these parameters where their influences are investigated experimentally on three different levels to find the optimum process parameters. The relation between these parameters and local permeability are obtained experimentally. In this chapter, to qualify the EIPR performance, a system with an amplitude of 0.5 mm and frequency of 5.5 Hz is executed.

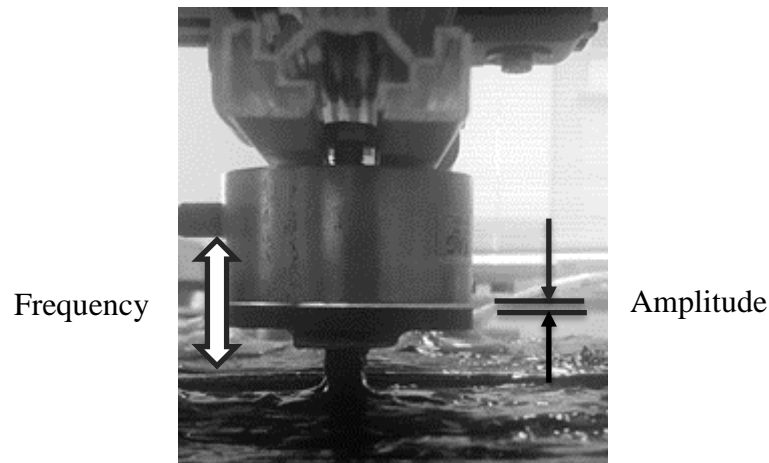


Figure 3.2. Amplitude and frequency of EIPR process

### 3.2.1 Embedded element and array

Shape of embedded elements plays a significant effect on flow manipulation and flow front correction. Some experiments are conducted to select a proper element for the presented process as discussed. A square element shape of  $45 \times 45$  mm is selected for embedding them into the upper flexible mold, as shown in Figure 3.3. This type of element is preferred to achieve the aim of the EIPR process that compensates and delivers the fluid, uniformly. In order to activate the entire low permeability area, elements are placed in the form of  $60 \times 60$  mm patterns for the case studies.

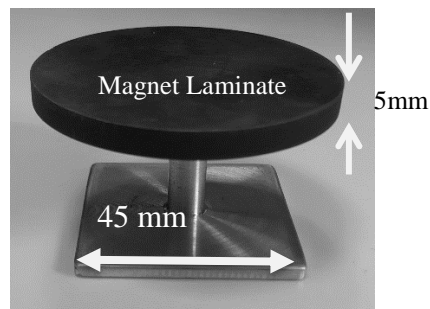


Figure 3.3. Element shape

These elements are assembled with laminates of magnetic material. A type of material that is easily magnetized and de-magnetized is required to vibrate the flexible upper mold regularly.

When a ferromagnetic material is magnetized in one direction, it will not relax back to zero magnetization when the imposed magnetizing field is removed. It must be driven back to zero by a field in the opposite direction. If an alternating magnetic field is applied to the material, its magnetization will trace out a loop called a hysteresis loop. The lack of retraceability of the magnetization curve is the property called hysteresis and it is related to the existence of magnetic domains in the material. Once the magnetic domains are reoriented, it takes some energy to turn them back again. This property of ferromagnetic materials is useful as a magnetic "memory" [70].

Soft ferromagnetic materials such as iron or silicon steel have very narrow magnetic hysteresis loops, as shown in Figure 3.4, resulting in very small amounts of residual magnetism rather than hard ferromagnetic making them ideal for use in relays, solenoids and transformers as they can be easily magnetized and demagnetized. These materials are used to make temporary magnets. Susceptibility and permeability of these materials are relatively high and magnetic energy stored in them is comparatively less.

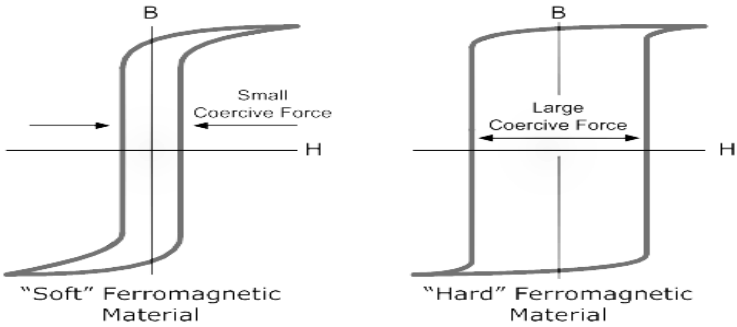


Figure 3.4. Hysteresis loops of soft and hard ferromagnetic material [106]

A soft ferromagnetic ‘thin non-oriented grades steel no 20’ is selected as the magnet laminate in this study. Fifty layers of this material are stacked to make a 5-mm magnet laminate, as shown in Figure 3.3.

### 3.3 Control methodology design

A closed-loop control scheme is designed to prevent the formation of dry spots, reduce the filling time and achieve complete preform saturation without any defects. Inlet and outlet positions are defined as a reference measurement, initially. The geometry of the mold for selected case studies is shown in Figure 3.5. The low permeability zone for each case has different dimensions however for all cases they are located in section 2. The controller for the given geometry divides the model into three longitudinal sections and the average flow front distance of each section from the inlet line measured as  $L_i(t)$  is depicted in Figure 3.5. Index  $i$  changes from one to three, denoting the section number. The measured length is the distance of the flow front from the inlet line on the analyzed image. The flow front of second section is compared to the average of the first and third ones to onset the correction action. For a difference of 10 mm or more, the controller chooses the best action and sends a command to the automated gantry system to position the electromagnet over the appropriate element to raise and start vibration for increasing the porosity of the preform locally. The online control technique for this work is represented in a flow chart in Figure 3.6. It illustrates the controller steps from the very start to the end of the infusion process that is conducted by a program written in both MATLAB and ARDUNIO.

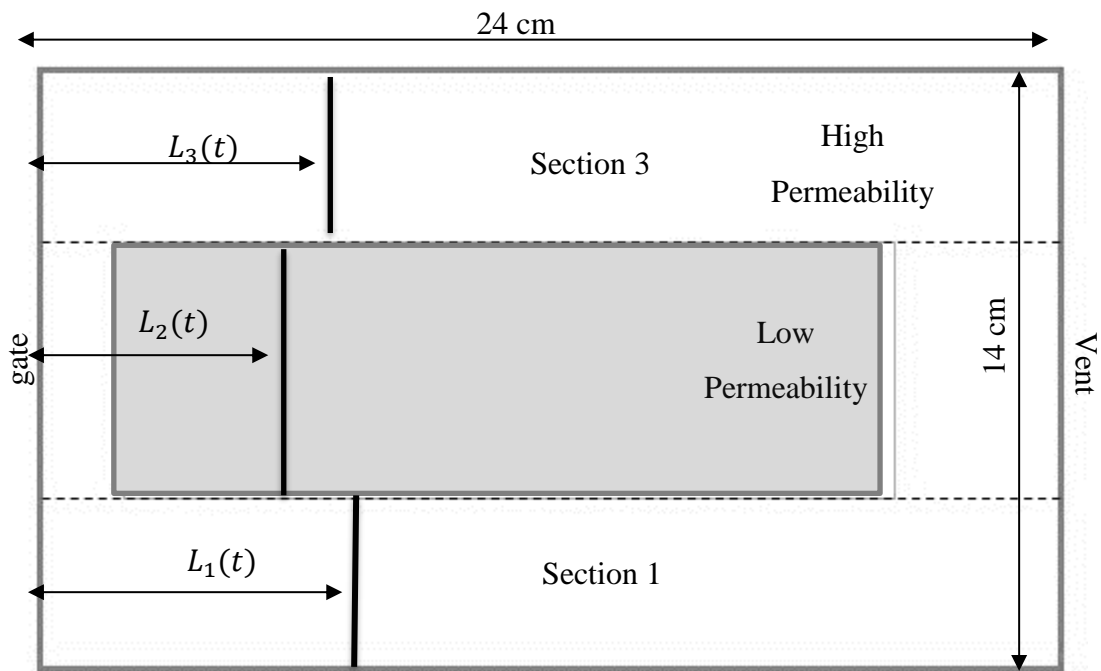


Figure 3.5. Geometry of the mold for the case studies and distance of flow front for each section from inlet line.

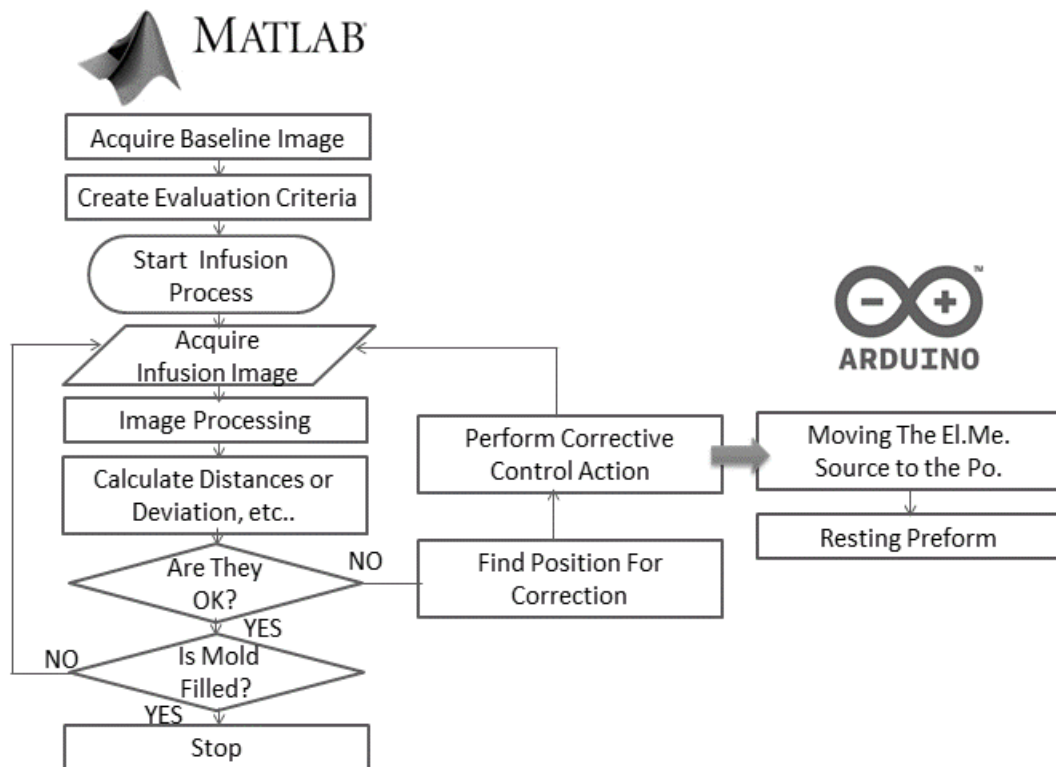


Figure 3.6. Control flowchart used in case studies

The model is basically implemented by taking a baseline image, creating the inlet and outlet, correcting the perspective distortion and calibrating the image to evaluate the subsequent online images. The process starts by opening the resin gate, and the camera takes digital images in desired intervals (3 seconds in EIPR system evaluation). The analysis and detection of the flow front is performed for each section. Depending on the evaluation criteria, the correct area is identified in MATLAB program. For these case studies, this criterion is 10-mm distance difference between the flow front average of the side sections with the middle section. Then the electromagnet is positioned over the identified element and invokes the element to rest the preform in accordance with the program written in Arduino. This control loop is repeated for manipulating the flow front until the mold is filled.

Note that the proposed control methodology requires a priori knowledge of the optimum values for the EIPR process parameters.

### **3.4 Experimental set up**

Three different scenarios are planned for addressing the disturbance in flow front. For creating such a disturbance, each scenario has a model where the middle of the sample is inserted a low permeability preform as shown in Figure 3.7.

Three case studies are considered in this work. Plates used in these tests have a rectangular geometry of  $140 \times 240$  mm. They have a thickness of about 2.5 mm with different layup of fabric preforms, where the inlet and outlet are placed along the short opposite sides. Each case study with two types of fabric preforms are shown in Figure 3.7. In all case studies, the same flexible mold is utilized.

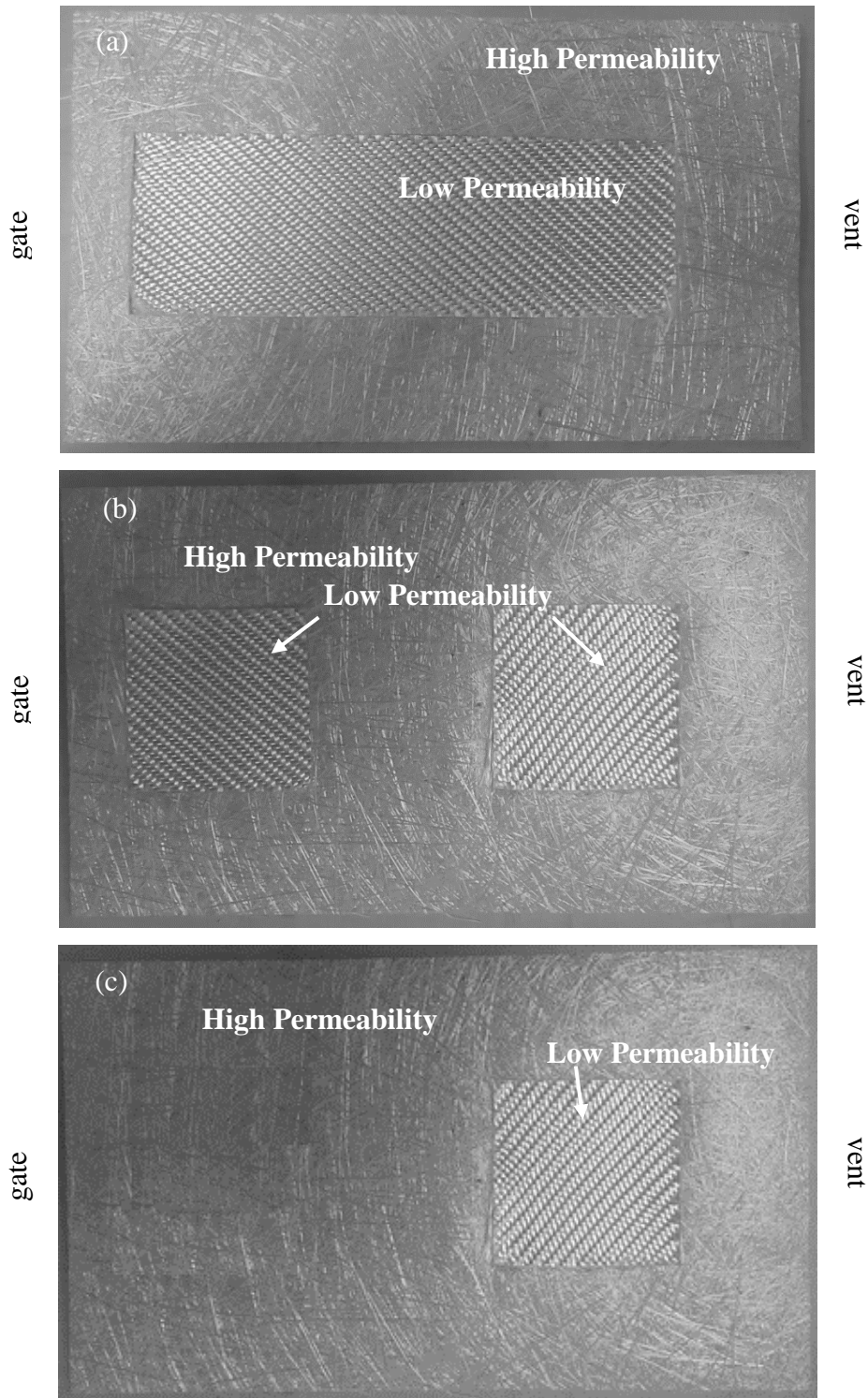


Figure 3.7. Case studies for infusion where a high permeability preform stiffened with low permeability one

### 3.4.1 Preparation of upper flexible mold

First, to produce the upper flexible mold with its internal elements, a transparent tool made of glass is cleaned and a plate with the dimensions of test sample is placed on the tool. The edges of part profile are sealed with a tape first and then inlet and outlet ports are located with a double-sided tape. Tubes as inlet and outlet lines are taped at both ends of the plate to form the vacuum and inlet channels. Aluminum elements that stiffened with a reinforcing cloth were positioned in their places carefully. First layer of silicone rubber was brushed over all surfaces. Then first layer is let to partially cure “tacky” at room temperature before applying the second layer. A portion of vacuum and infusion channels are covered with reinforcing cloth and followed by silicone rubber brushing to build up a thickness. Finally, the silicone rubber is allowed to fully cure for 4-5 hours at room temperature. The special vacuum bag cured in this process is carefully removed from the tool. The finished upper flexible mold is reusable and guaranties a repeatable process for all experiments as shown in Figure 3.8.

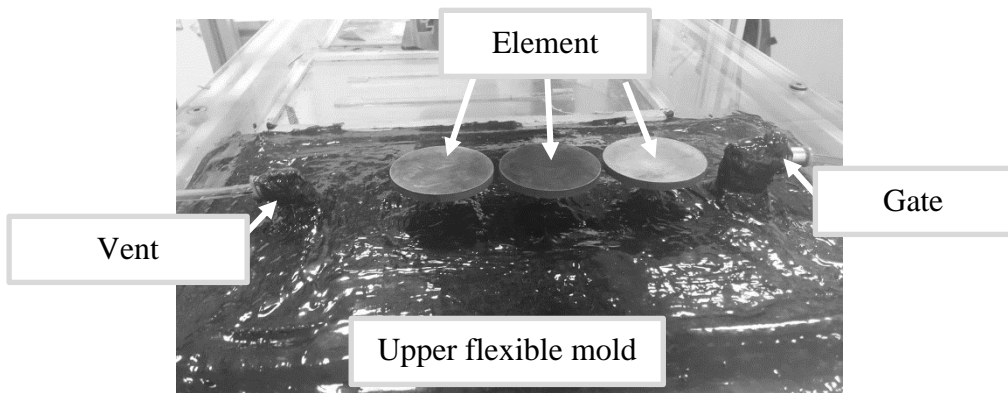


Figure 3.8. Special reusable vacuum bag with embedded elements

### 3.4.2 Flow front monitoring

The image acquisition and analysis system operates with the on-line controlling of flow progression which is made possible by the bottom transparent mold. The special toolbox in MATLAB has a comprehensive set of reference-standard algorithms, functions and applications for image processing, analysis, visualization, and algorithm development.

To distinguish the resin flow front, an image processing analysis is required. This process is done by writing a code in MATLAB. This code captures images from a Logitech C310 Hp 720p webcam at regular time intervals to conduct a real-time image processing. The captured images are processed to select the area of the filling part. Captured images always have a perspective distortion where an image correction is necessary before trying to recognize the flow front in these images. Sequentially, this program first converts the true color RGB image to a grayscale one. Then a filter is applied to convert the grayscale image to a blurred image. This image is then converted to a binary image and finally resin flow front is detected by using the edge function in MATLAB. The camera is positioned with respect to the mold and calibrated before the onset of the infusion process.

### **3.4.3 Automated gantry system**

To implement and develop the EIPR process for manipulation and correction of the resin flow front and filling the mold, a 2-axis control system is constructed. Aluminum  $45 \times 45 \text{ mm}$  profiles are used to construct the platform of the EIPR system. Two linear guides representing  $x$  and  $y$  axes are installed to provide the motion of the electromagnet in  $x$ - $y$  plane. Step motors are utilized to control and position the electromagnet anywhere in this plane based on the controller commands. The camera is installed under the mold to track the flow front during the filling process. All of system components are schematically shown in Figure 3.9.

The motion control of electromagnet to increase the local permeability is done by a program generated in ARDUINO UNO that sends the control signal to the driver board TB6560.

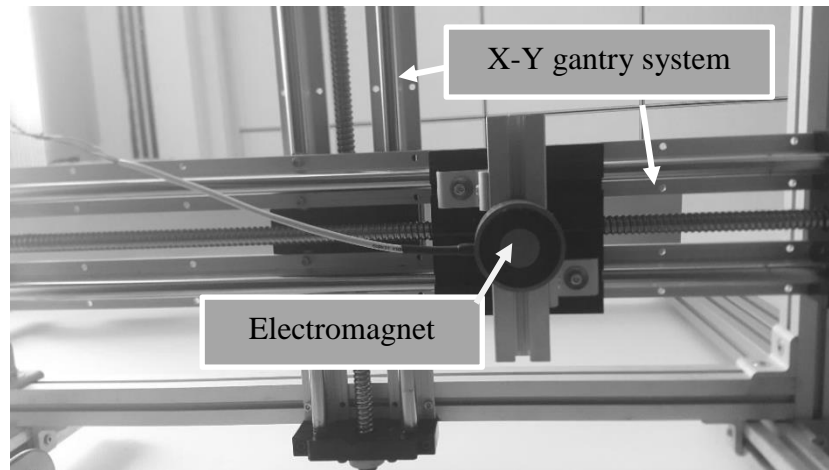


Figure 3.9. 2D automated gantry system with electromagnet

### 3.5 Experimental validation

To evaluate the presented resin flow manipulation method and implement a control scheme, a workstation is prepared and set up with the necessary hardware. The workstation is composed of a transparent mold with an upper special flexible mold, an image processing unit, an automated gantry system and an electromagnet field source.

#### 3.5.1 Preform configurations

High and low permeability preforms are selected to create an artificial disturbance in the flow pattern. The criterion for selection is their permeability values. The selected fibers for this study are: E-Glass fiber fabric twill 300 gr/m<sup>2</sup> as a low permeability reinforcement and chopped E-Glass fiber EMAT1-450 kg/m<sup>2</sup> as a high permeability reinforcement. Since the low permeability section is under the flow controlling action, the permeability of this preform is determined for both flow control and no-control options. The permeability characteristics of preforms are given in Table 3.1.

Table 3.1. Material permeability for flow control and no-control options

| Material | Permeability $m^2$     |                        |
|----------|------------------------|------------------------|
|          | No-control             | Controlled             |
| Mat      | $8.47 \times 10^{-11}$ | -                      |
| Twill    | $1.72 \times 10^{-11}$ | $6.30 \times 10^{-11}$ |

### 3.5.2 Test fluid

Since viscosity of the thermoset resins varies during the process and they have a Newtonian behavior especially before the gelation [71]. Therefore, a motor oil 20W50 is used to have repeatable and reliable measurement, as recommended in [17]. Its viscosity is 0.165 Pa.s with a density of 900 kg/m<sup>3</sup>.

### 3.5.3 Experimental procedure

The preforms which are stiffened in the middle of the plate are placed on the transparent mold and covered with the flexible mold and compressed under 500 mmHg vacuum pressure.

Next, optimum values for the process parameters are given to the controller program as input to start vibrations of the elements whenever necessary and increase the permeability locally. Before commencing the infusion, the image processing unit that includes a camera under the transparent mold is calibrated. It is programmed to record the images with regular intervals and it is able to capture flow front during the filling process.

Finally, the infusion process and the EIPR system are initiated simultaneously. The flow front detecting unit follows the front at 3s time intervals and calculates the distance of flow front in each segment from the infusion line. It evaluates the flow pattern in divided sections and makes a proper correction action for its position. The electromagnetic field source is driven to the position by 2D gantry system. The electromagnet source invokes the element and starts vibrating the vacuum bag to ease the delivery of fluid through the low permeability preform.

### **3.6 Results and discussion**

In order to prove the efficiency of the EIPR process, a comparison study is conducted for the filling process by considering different case studies. Two types of processes, one controlled with the current EIPR process for resin flow correction and the other uncontrolled without any resting are performed and resin flow front patterns are recorded in each experiment through the filling process. The flow progress in these experiments is tracked to study the efficiency of the system. In all experiments, left side of the plate is used for the infusion line while the right side is the vacuum line. The effectiveness of the flow manipulation with the current system can be seen in Figure 3.10. It shows successive frames of filling by clearly indicating how this process compensates flow pattern disturbances. The frames in this figure belong to the first case study. First frame displays the flow pattern before the flow reaches the low permeability zone. After calculating the distance of flow front from the inlet line for each section and approving a lag in the second section, the low permeability zone, controlling action is activated as in the second frame of this figure.

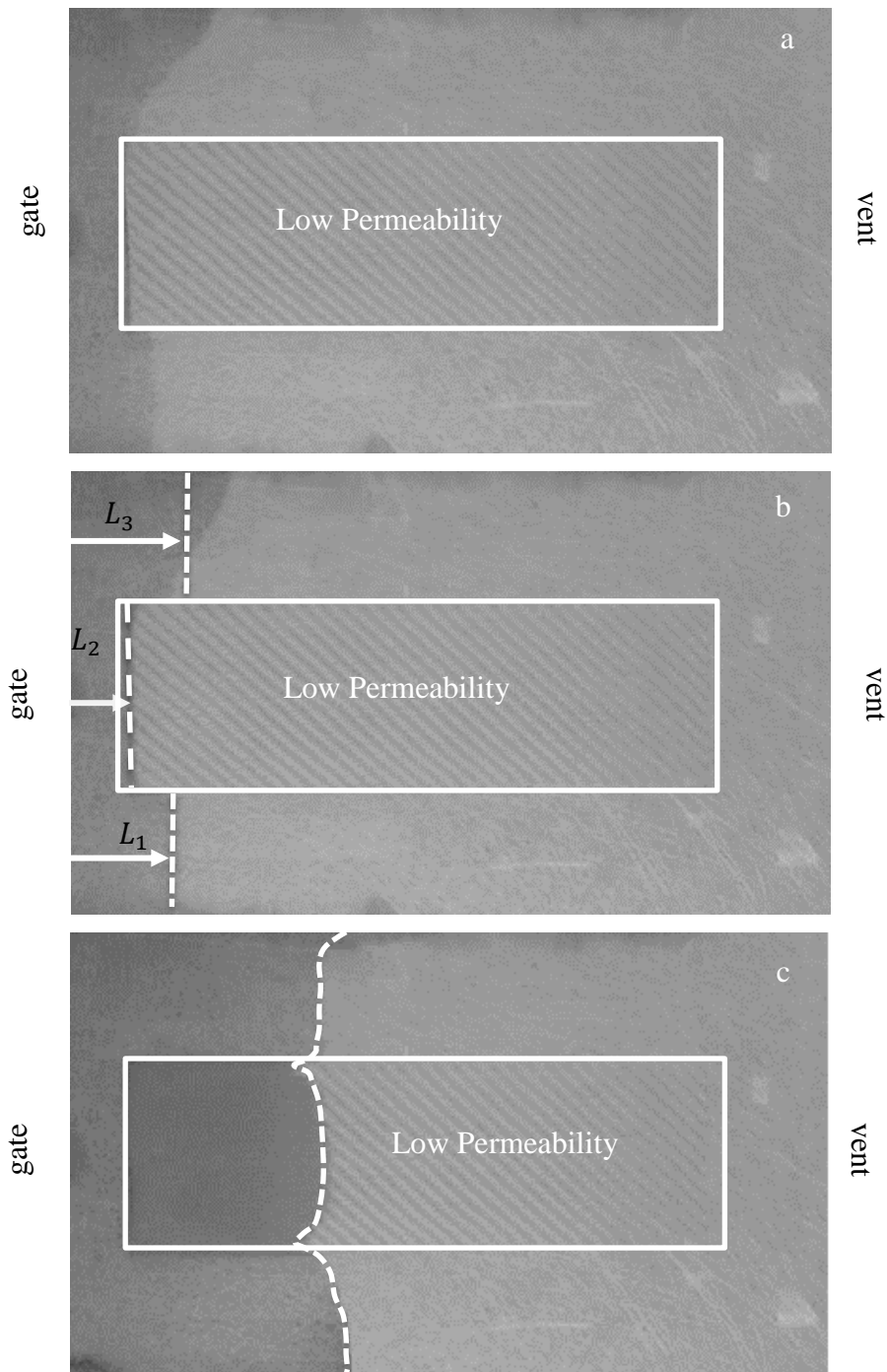


Figure 3.10. Filling process before (a) and after (b, c) frames of filling process

Dry spot or air trap appears at the end of the low permeability zones. The air trap is formed because of the divergent flux during the infusion. According to the ideal gases law, pressure of the air trap increases and its volume becomes smaller and smaller until the pressure in the air trap close to the infusion pressure, which means

that the pressure gradient is very small and the resin cannot move and eventually form dry spot.

To inspect the process efficiency, formation of any dry spots while the fluid is filling the mold is closely watched. After the evaluation of the state of the flow front of each divided section if any such formation is determined to happen, one of the appropriate elements is invoked to create a relaxation in the preform and start vibrating the upper flexible mold around this particular location. The system during the filling process continually evaluates the flow pattern and invokes the second element to improve the flow front. Consequently, the third one is induced to help filling the mold by not allowing the formation of any dry spots. Figure 3.11 illustrates this ability by comparing it with no-flow-control process. Two frames of the controlled and non-controlled processes are compared in the figure. In the non-controlled case, dry spot forms at the end of the low permeability zone. In these frames and resin is infused from the left side to the right side.

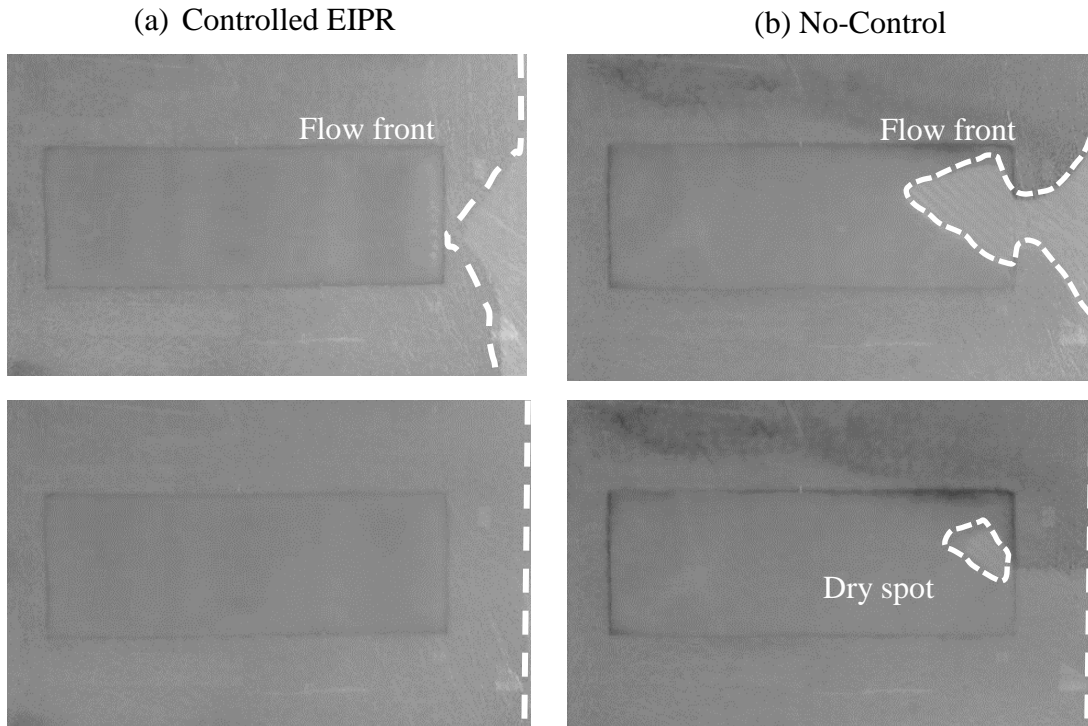


Figure 3.11. Case 1: (a) Effect of EIPR process preventing dry spot formation, (b) Formation of a dry spot for no-controlled process

For the second case, the correction action is done by invoking the first and third elements based on results of the image processing analysis Figure 3.12 shows the frames of controlled and non-controlled flow patterns after the first low permeability zone. Frames in the second row of this figure present the fully saturated reinforcement under the controlled process rather than the non-controlled one. These frames show the infusion from the left side to the right side. Two dry spots forms in non-controlled case as shown in the figure while the EIPR one fills the mold perfectly without having any void formation.

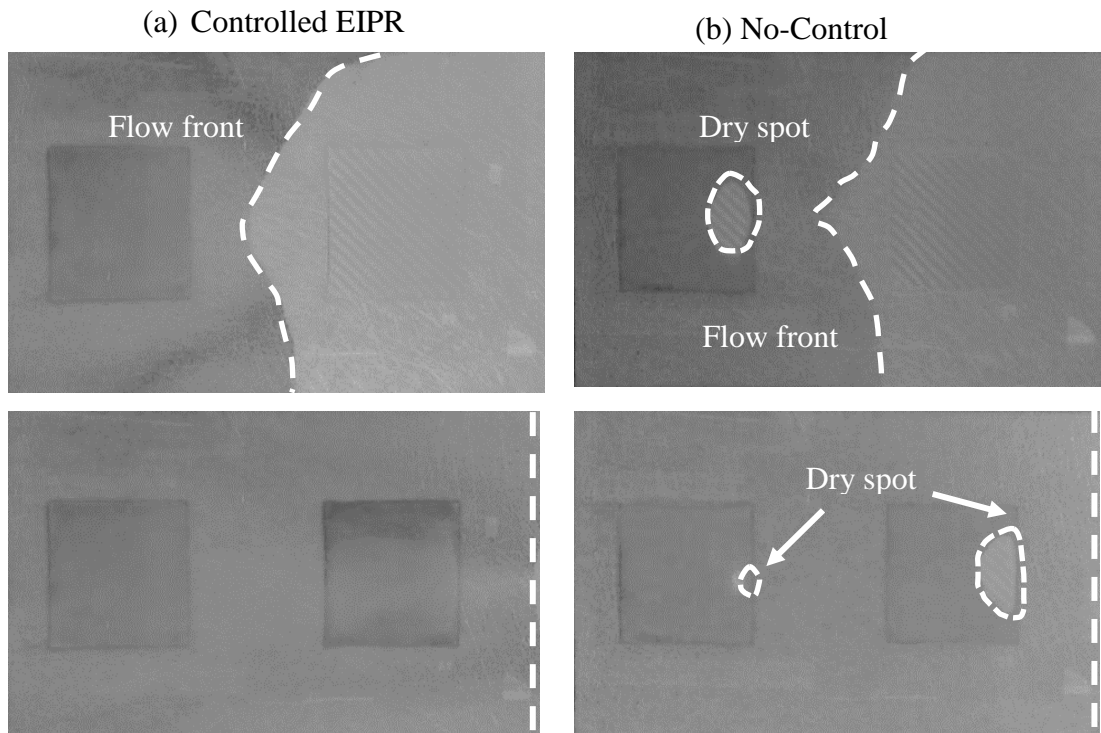


Figure 3.12. Case 2: (a) Effect of the EIPR process preventing dry spot formation, (b) Formation of a dry spot for no-controlled process

Last case also shows the efficiency of this approach clearly by preventing the dry spot formation. In this case, the third element is activated by the controller to fill the mold as shown in Figure 3.13. In this case, resin is also infused from the left side to the right side.

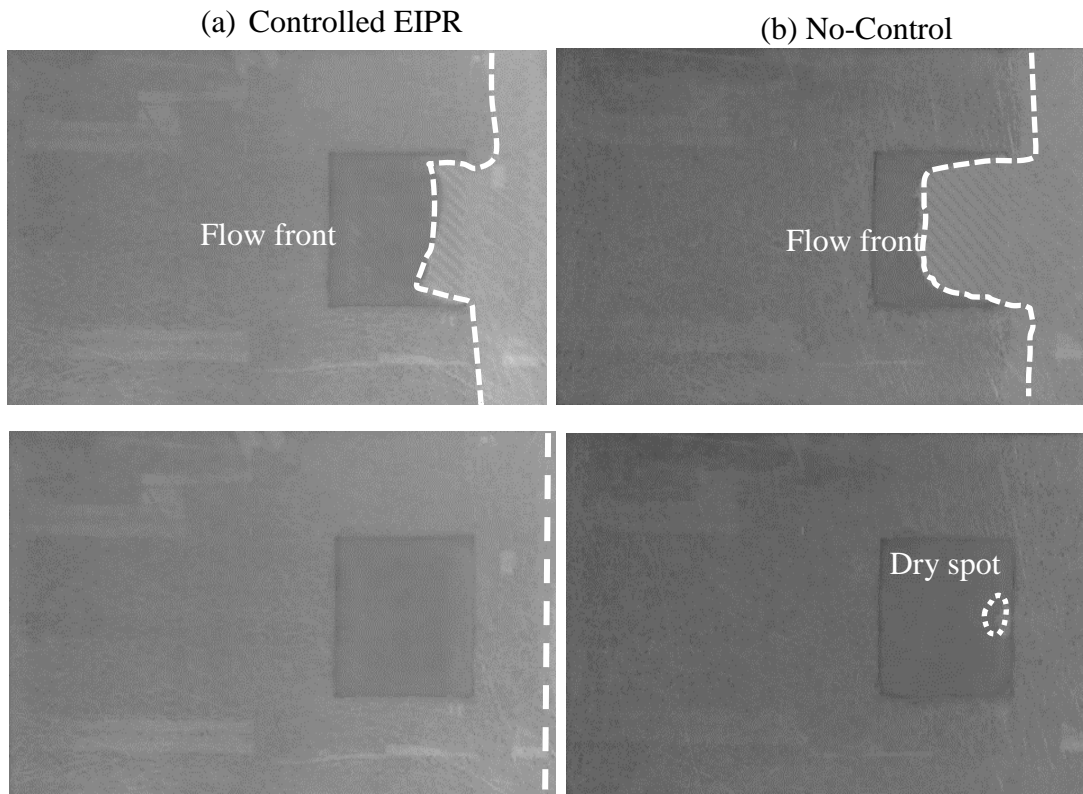


Figure 3.13. Case 3: (a) Effect of EIPR process on flow front preventing dry spot formation, (b) Formation of dry spot for no-controlled process

Case studies presented in this part obviously reveal the efficiency and performance of the suggested approach. This process is also shown to decrease the filling time and prevent any wasting of resin in an infusion process.

### 3.7 Summary

A new variation of the resin infusion process to manipulate the flow front in real time, called the EIPR process is introduced and its performance in infusion of the composite preforms is evaluated without having any defect during the filling. The introduced approach is based on the principle that it changes the permeability of preforms locally, and this way resting the preform and increasing the porosity. To implement this flow controlling system, a special vacuum bag with embedded elements is proposed to vibrate the vacuum bag and ease the resin flow through the preform. The elements are invoked with electromagnetic field source. In order to create an effective vibration, 'thin non-oriented grades steel NO20' with small amounts of residual magnetism is used. To automate the system and for the flow

control, a computer program written in MATLAB and Arduino is utilized. A workstation to mount the automated 2D gantry and transparent mold is built. To evaluate the system, three case studies with two types of preforms in each case are studied. These preforms have a large difference in their permeability values. The experimental results of the controlled processes in comparison with uncontrolled ones clearly unveil the EIPR process efficiency. Results show that this approach not only can manipulate and control the flow front but also assure the repeatability and reliability of the infusion process.



## CHAPTER 4

### CHARACTERIZATION AND MODELING OF IN-PLANE PERMEABILITY IN ELECTROMAGNETICALLY INDUCED PREFORM RESTING PROCESS

Electromagnetically induced preform resting (EIPR) process is a new version of vacuum-assisted resin transfer molding (VARTM) which allows the manipulation and correction of the resin flow during the filling process. The EIPR process enhances the permeability of fiber preforms locally in case of undesirable flow front situations by the vibrating upper flexible mold locally through embedded ferromagnetic elements. This technique ensures the perfect filling despite the existence of inherent permeability variation in various preforms. To utilize the EIPR process, its comprehensive characterization is necessary. Amplitude, frequency of vibration and primary permeability of the preform as a material index recognized as independent factors that must be considered. For each factor, three different values are considered as a parameter in to establish a mathematical model for the permeability of preforms. The maximum and minimum values of the frequency and amplitude are determined based on the observations in acceptable composite manufacturing and in-plane permeability characterization. In current study, frequency and amplitude with three different values (levels) are taken as continuous factors and the primary permeability of preform (material) is taken as a categorical factor with three levels. Response Surface Methodology (RSM) approach is used to model the permeability of EIPR process. Results show that the optimum response values occur at a frequency of 5.6 Hz and an amplitude of 0.56 mm for selected preforms.

## 4.1 Introduction

Fiber reinforced composite structures have been utilized greatly in high technology applications such as aerospace, auto, marine and wind energy industries. High specific stiffness and strength properties of these materials make them candidates for new applications. Composite materials have been facing strong competition from traditional materials. So, cost effective manufacturing approaches of these materials are an important issue [72–75]. Nowadays for example, high tech industry have been using out-of-autoclave process to manufacture composite parts [76–78] Liquid Composite Molding (LCM) is a branch of composite material manufacturing process which allows the production of strong lightweight structures. Some well-known LCM processes are Resin Transfer Molding (RTM) and Vacuum Assisted Resin Transfer Molding (VARTM) in which preforms are first placed in the mold and then resin is transformed to saturate the dry preform. In VARTM process, a vacuum bag covers the preform from one side as a tool surfaces and this lowers the process cost which therefore makes this process more usable especially for structural and large parts. Undesirable resin flow development and resulting air entrapments causes waste of resources which limits the effective VARTM process [79–81].

One of the major reasons of dry spots is undesirable flow front formations due to inherent variation in the preform permeability. According to the ideal gas law ( $Pressure * Volume = constant$ ), pressure increases in this dry spot area and the volume becomes smaller and smaller until the pressure in the air trap becomes close to the infusion pressure. As a result, the pressure gradient gets very small and the resin can no longer moves and forms dry spots [82,83].

Resin flow control has received abundant attention for making VARTM process as a viable one in high technology applications. One of the identified challenges in this process is the race tracking that disturbs the flow front. Preform alignment problems, preform warping and wrinkling of vacuum bags are other inherent problems associated with this process [80]. Some studies have been conducted in order enhance the simulations with real data from resin flow monitoring by image processing which is used along with various types of sensors to modify the flow

pattern by controlling pressure, flow rate and auxiliary gate/ vent ports [17,28,29,67,84–87].

Another type of active control method in VARTM process for controlling the resin flow is to increase the resin flow velocity through the preform. Decreasing the resin viscosity is in this category type obtained by heating the resin [4,65,69,88,89]. Increasing the permeability of the preform by relaxing the preform by a vacuum chamber placed over the vacuum bag is another category for speeding up the resin [30,31,65]. However, the resin gelation time and application condition are the limitation of these processes.

Justin et al. [6] presented a numerical approach to characterize the permeability of the preforms in vacuum infusion process with fiber relaxation (VIPR) in which the preforms undergoes the vacuum chamber externally. This approach presents the permeability as a function of the chamber vacuum pressure.

Electromagnetically Induced Preform Resting (EIPR) is a new approach that manipulates the flow front by lifting and vibrating the upper flexible mold. By this method, one can increase the permeability, locally. To implement this process, a thorough understanding and full characterization of EIPR process is required to effectively predict the resin flow and permeability of the preform.

In the EIPR process, various factors may affect significantly and control these factors and their optimization seems to be necessary. The experimental design and Response Surface Method (RSM) are statistical and mathematical approaches that help one to understand and optimize the process. RSM is often applied to refine models after determining significant factors using factorial designs; especially for curvature in the response surface. This method is widely used by researchers for modeling their response that uses a few tests to obtain the relationship among major factors and the response of the system [65,88,90].

In this study, the permeability of preform under EIPR process with different parameters of this approach are calculated in order to optimize and characterize the increased permeability as a function of amplitude and frequencies of vibration for

three different preforms. Characterizing the permeability under this controlling approach enables one to apply this method to manipulate the flow front correctly.

#### **4.2 EIPR process**

The key disadvantage of the VARTM process is its inability to precisely manipulate the resin flow front during the filling in real time. The electromagnetically induced preform resting (EIPR) process is a new variation of VARTM and SCRIMP, which incorporate a creative upper flexible mold with embedded elements for lifting and vibrating vacuum bag to relaxing the preform by an electromagnetic field source. EIPR process consists of this type of vacuum bag (silicone vacuum bag with embedded metal elements) and an automated gantry system which carries the electromagnetic and resin flow front detecting system. The elements are distributed within the vacuum bag so that the resin flow control is possible anywhere in the composite mold. The principle of this approach is stretching and vibrating the elastomer vacuum bag to relax the preform and decrease the resistance against the resin flow locally at the predetermined positions. Resin flow then eases through the induced relaxation locations of preform. This correction action reduces the compaction pressure therefore increase the fabric preform porosity. A schematic representation of this process is demonstrated in Figure 4.1.

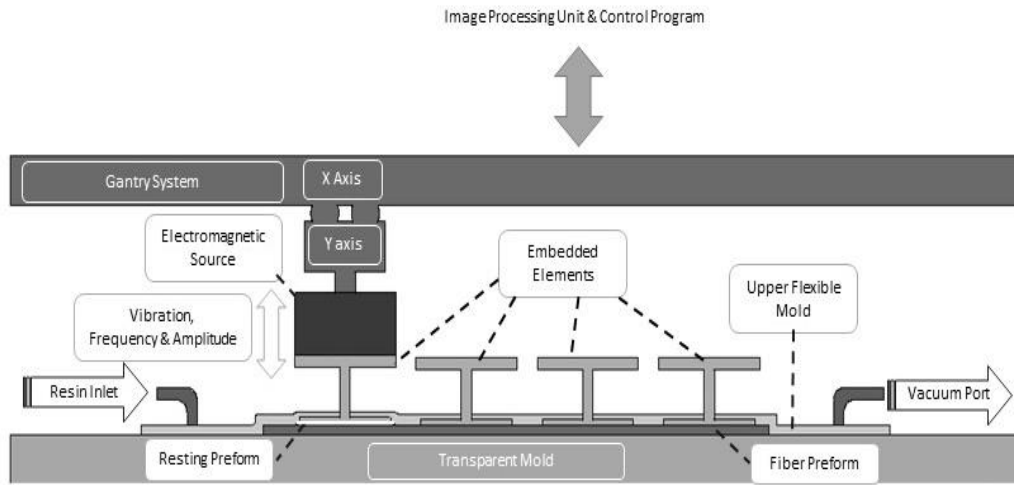


Figure 4.1. Schematic of EIPR process

### 4.3 Permeability measurement method

For the unsaturated rectilinear flow at constant pressure, the permeability is calculated from linear infusion of fluid as inlet line into the fiber preform. The flow front is assumed uniform and oriented parallel to the inlet line. Darcy's law [36] gives the permeability as:

$$K_{xx} = -\frac{x_{ff}\mu\varphi}{2\Delta Pt} \quad (4.1)$$

where  $x_{ff}$  is the position of flow front at time  $t$ ,  $\Delta p$  is the pressure difference between infusion and vent line,  $\mu$  is the fluid viscosity, and  $\varphi$  is the preform porosity. Here

$$\varphi = 1 - v_f \quad (4.2)$$

And  $v_f$  is the fiber volume fraction.

#### 4.4 Design of experiment

Box and Wilson [91] pioneered a statistical method that is called Response Surface Method (RSM). It is an approach for experiment design, finding significant parameters of a process and modeling the response, mathematically. This method is used to relate the response to the significant parameters with a first or second order polynomial. The quadratic equation is used to model the curvature response, it takes the following form:

$$Y = \beta_0 + \sum_{i=1}^k \beta_i X_i + \sum_{i=1}^k \beta_{ii} X_i^2 + \sum_{i < j} \beta_{ij} X_i X_j + \varepsilon \quad (4.3)$$

where,  $\beta_0, \beta_i, \beta_{ii}$  and  $\beta_{ij}$  are the constant, linear, quadratic and interaction coefficients, respectively. Also  $X_i$  and  $\varepsilon$  are parameters and the error term, respectively.

#### 4.5 Experiments

##### 4.5.1 Set-up

An experimental setup is developed in which there is a transparent mold as the rigid part of mold and an upper flexible mold with embedded metal elements used in EIPR process to lift and vibrate the vacuum bag to increase the permeability as shown in Figure 4.1. In this study to characterize the EIPR process, an elastomer vacuum bag with two embedded ferromagnetic (FM) elements is used where the upper flexible vacuum bag is illustrated in Figure 4.2. The aim of using these two FM elements is to investigate the effect of the element location with respect to the infusion line.

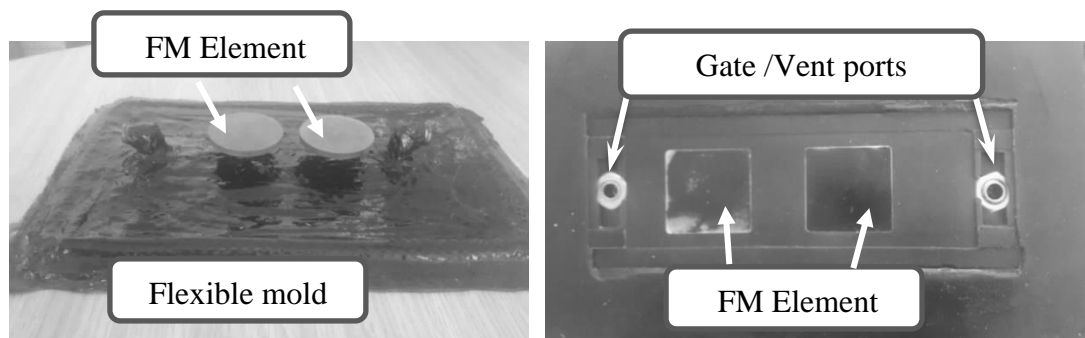


Figure 4.2. Upper flexible mold with two embedded FM elements for permeability measurement

## 4.5.2 Material

### Preforms

Three different preforms are selected to explore the permeability feature. The criterion for selection is their different permeability values. Selected fibers for this study are: E-Glass multiaxial fabric with  $600 \text{ gr/m}^2$ , E-glass twill of  $300 \text{ gr/m}^2$ , Mat E-glass EMAT1 with  $450 \text{ g/m}^2$ .

Preform size for these experiments is  $60 \times 180 \text{ mm}$ . To avoid the race-tracking phenomena during the filling process and have better preform samples, while laying each fabric, they are held by infusion adhesive and then cut carefully. Number of layers for twill, multiaxial and mat samples are 12, 5 and 5, respectively. Prepared samples are shown in Figure 4.3.

### Test fluid

Since viscosity of thermoset resins varies during the process and they have a Newtonian behavior before the gelation, instead a test fluid (Motor oil 20W50) is used to have repeatable and reliable measurement, as recommended in [17]. The test fluid viscosity is  $0.165 \text{ Pa s}$  with a density of  $900 \text{ kg/m}^3$ .

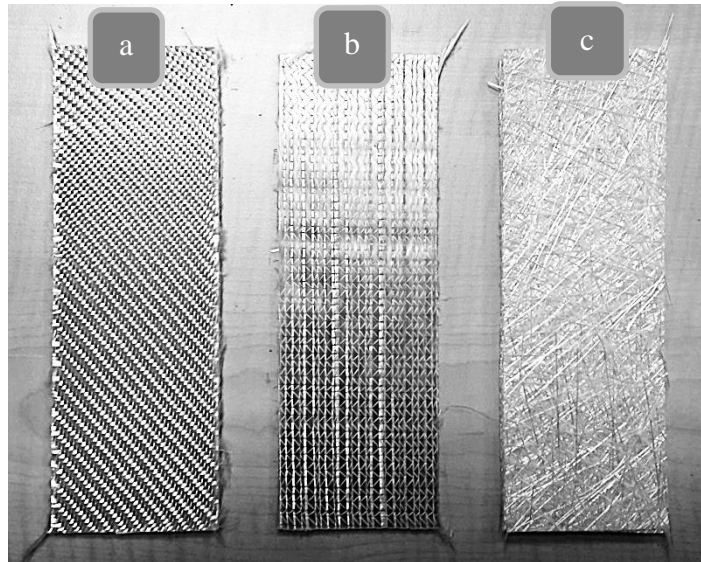


Figure 4.3. E-Glass samples: a) Twill b) Multiaxial c) Mat

#### 4.5.3 Permeability characterization for EIPR process

To fully understand EIPR Process, it is essential to characterize it. Before applying it for resin flow controlling understanding this process must be discovered. In this respect, the FM element shape, its distance from the fluid inlet, frequency of the vibration and amplitude for each preform type are investigated.

First, the shape of FM element is considered. A circular element with a radius of 45 mm and a square with a side length of 45 mm are selected as shown in Figure 4.4. Obviously, area of these shapes is not equal. Here, the aim of study is to evaluate the shape of the reform flow pattern and identify a proper shape for permeability evaluation of the EIPR process. Preform relaxation is provided by both shapes, and the corresponding flow front progresses are inspected. Circular element causes a flow front in the form of a curve or a semicircle to be precise where the speed of fluid under the center of the element is the highest. It is more suitable for a case where the race-tracking is likely to occur, since it can reduce the race tracking effect. Figure 4.5 (a) shows the contribution of circular element to the flow front. However, the square element generates a straight flow front as shown Figure 4.5 (b). Later is selected for EIPR permeability characterization study, since a uniform flow front is needed to calculate the permeability based on the Darcy's law.

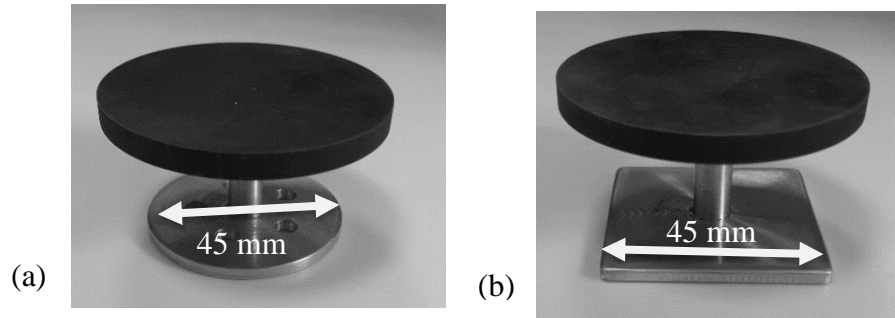


Figure 4.4. Element shapes: a) circle b) square

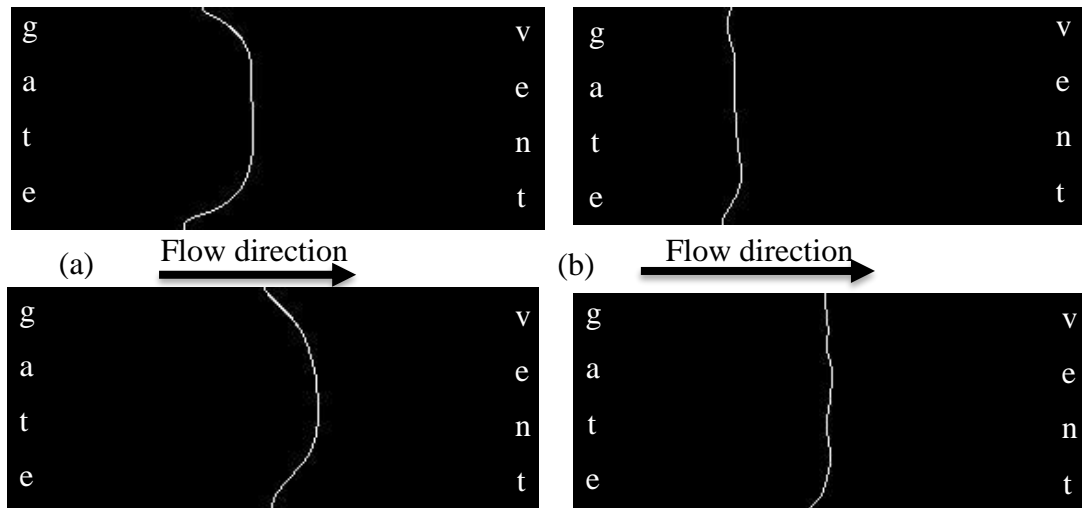


Figure 4.5. Flow front patterns for 2 different elements of a) circular shape b) square shape

The second parameter investigated is the FM element distance from the infusion gate line. It has an important role in fluid motion or to be specific the fluid velocity. A number of element positions are studied in which conducted cases are shown in Figure 4.6. To study the element distance from the infusion line two ports as a gate and vent lines and two elements are used to create different distances from the same mold. Results showed that the distance of the element from the infusion gate line has a significant effect for increasing the fluid velocity. Figure 4.7 shows the filling time at the same flow front with/without the EIPR process position. It can be observed

that shorter distances lower the filling time while the larger one does not have a significant change in the filling time.

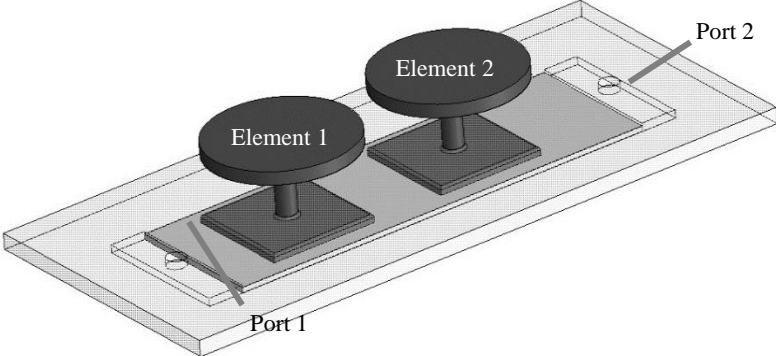


Figure 4.6. Case studies of element distance from gate line

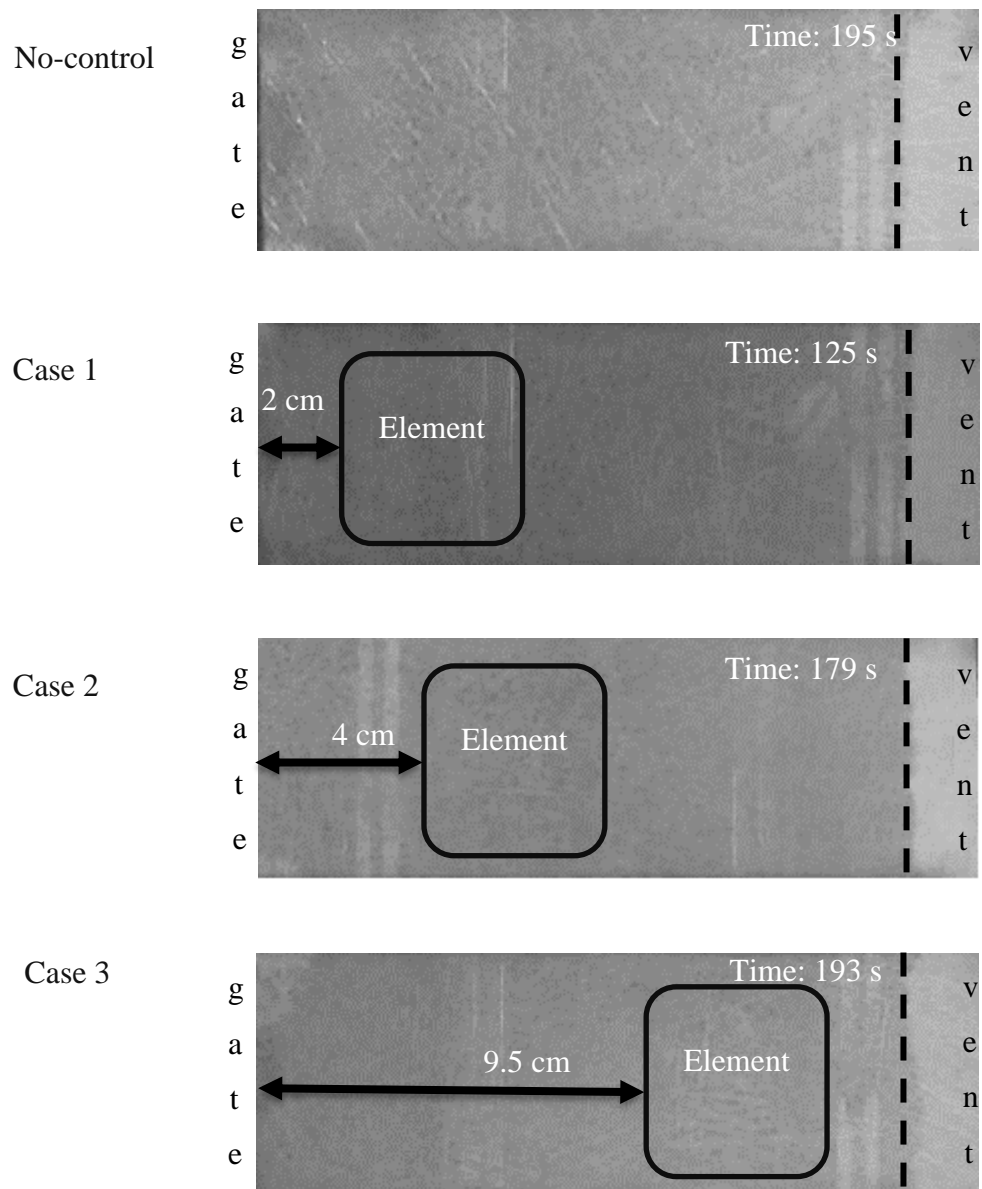


Figure 4.7. Effect of element position on the filling time compared with uncontrolled process

After selecting shape of the element and the effective distance, full characterization of the EIPR process to relax preform and increasing the velocity of fluid through preform must be examined. Tapping frequency and amplitude of element vibration are selected as characterization factors. In this study, amplitude refers to the distance that EM force can lift the element as illustrated in Figure 4.8.

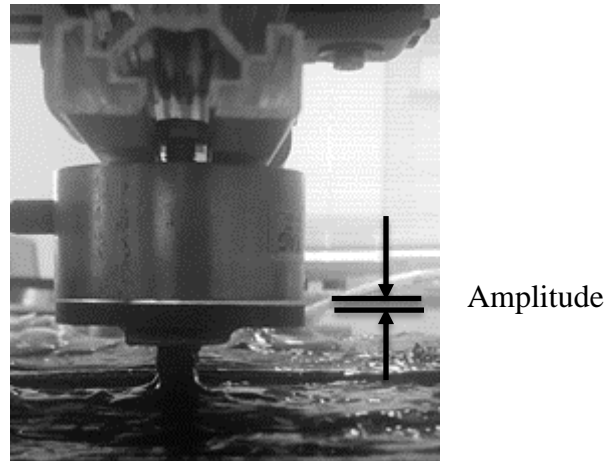


Figure 4.8. Amplitude of EIPR process

Range of amplitude and frequency are obtained by running several tests. The effective range for amplitude is found to be between 0.2 and 0.8 mm. and for frequency it is varied between 1 and 10 Hz. Amplitudes over 0.8 mm create an excessive gap between the vacuum bag and upper surface of the preform. This causes an undesirable filling because the gap provides a very high permeability channel over the preform and it is significantly different from the in-plane permeability of the preform. Also, this gap cumulates the resin under the vacuum bag and decreases the fluid velocity. For the frequencies over 10 Hz, the electromagnet practically clings to the element, where the vibration ceases.

#### 4.5.4 Permeability measurements

The characterization of the process is conducted on the selected preforms by using frequency and amplitude as parameters and three levels are considered for each.

Central Composite Design (CCD) was utilized for the design experiment of surface response method. Full factorial design with center point was used for design of two

continues factors and one categorical factor. A total of 39 experiments are designed for three factors with 4 replications at the center point of each categorical factor.

#### **4.5.5 Test procedure**

First, prepared preforms are placed on the transparent mold and then covered with the flexible mold and a vacuum pressure of 500 mmHg is applied into the mold. For the in-plane permeability measurement and to avoid through-the-thickness infusion distribution fabric or mesh fabric is not used. Figure 4.1 shows the cross section of layout.

Next, frequencies for each test as is given as an input to the control program to create the vibration of element and increase the porosity of the preform thereby increase the permeability. Before commencing the infusion, the camera under the transparent mold and the coupled image processing software are calibrated. The calibration is based on the flow front during the filling process. The image processing program takes images of the filling process at desired intervals and calculates the permeability immediately after the filling process. For calculations, the program detects the flow front and calculates the average flow front distance from the infusion line.

Sequentially, the EIPR system is located over the element and the amplitude is set on the instrument. Finally, the infusion process itself, permeability calculator program and EIPR system are initiated. The EM field source induces the element and causes vibration, this way porosity is enhanced, namely permeability is improved and the fluid is delivered through the preform. Flow front position versus time data and permeability values of the preform under different conditions are determined.

Additionally, the permeability of each preform without the EIPR process like VARTM process are calculated as a comparison tool.

### **4.6 Results and discussion**

#### **4.6.1 Permeability and filling time**

For each fiber preform type, tests with controlled process having three levels of parameters for frequency and amplitude are carried out in addition VARTM tests for comparison purposes. The selected levels for the frequency are 1.0, 5.5 and 10.0 Hz and for the amplitude are 0.2, 0.5, and 0.8 mm. Note that parameters exceeding the

threshold values are not desirable for acceptable filling. Table 4.1 demonstrates the coded and actual level values for design parameters and experiments. The value after latter F shows the frequency and the one after the latter A shows the amplitude of the system. According to these codes the F0A0 one shows the non-controlled experiment results.

Table 4.1 Actual and coded levels of parameters in this study

| Factors       | Levels  |            |          |
|---------------|---------|------------|----------|
|               | Low (1) | Medium (2) | High (3) |
| Frequency (F) | 1       | 5.5        | 10       |
| Amplitude (A) | 0.2     | 0.5        | 0.8      |

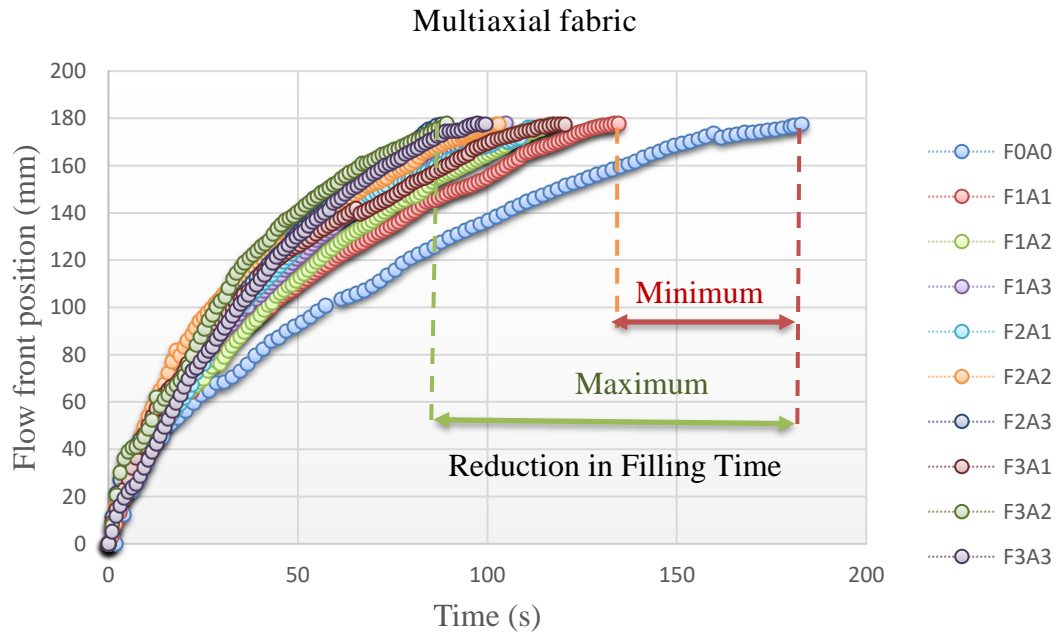
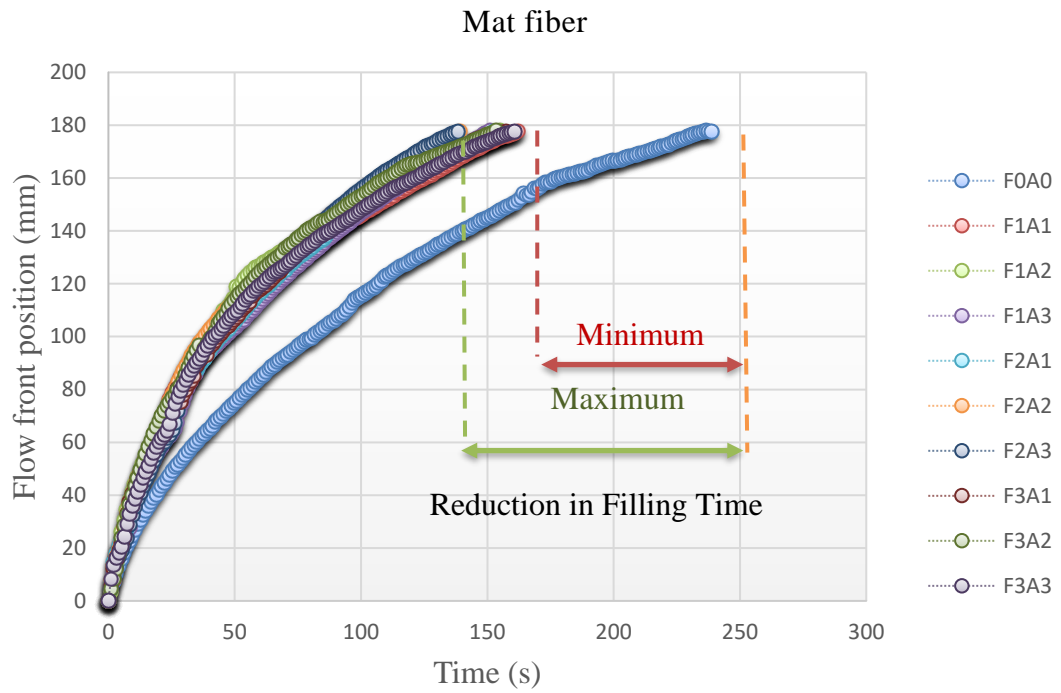
Three preform types has low, mean and high permeability values. First primary permeability of preforms without any controlling (VARTM) are obtained and given in Table 4.2. as a reference. Each test is repeated three times and the average of these is presented. All experiments with or without EIPR process are run in the same mold geometry, test conditions and test fluid.

Table 4.2. Permeability and filling time for the preforms without EIPR process (VARTM)

| Material   | Permeability ( $m^2$ ) | Filling time (s) |
|------------|------------------------|------------------|
| Mat        | 8.476E-11              | 250              |
| Multiaxial | 1.05 E-10              | 168              |
| Twill      | 1.72 E-11              | 1099             |

In each experiment, the flow front position versus time is detected and recorded by the program written in MATLAB. This program calculates the flow front distance from the infusion line by using image processing. Table demonstrates the coded and

actual level values for all the experiments. The results for flow front position versus time for all preforms are shown in Figure 4.9.



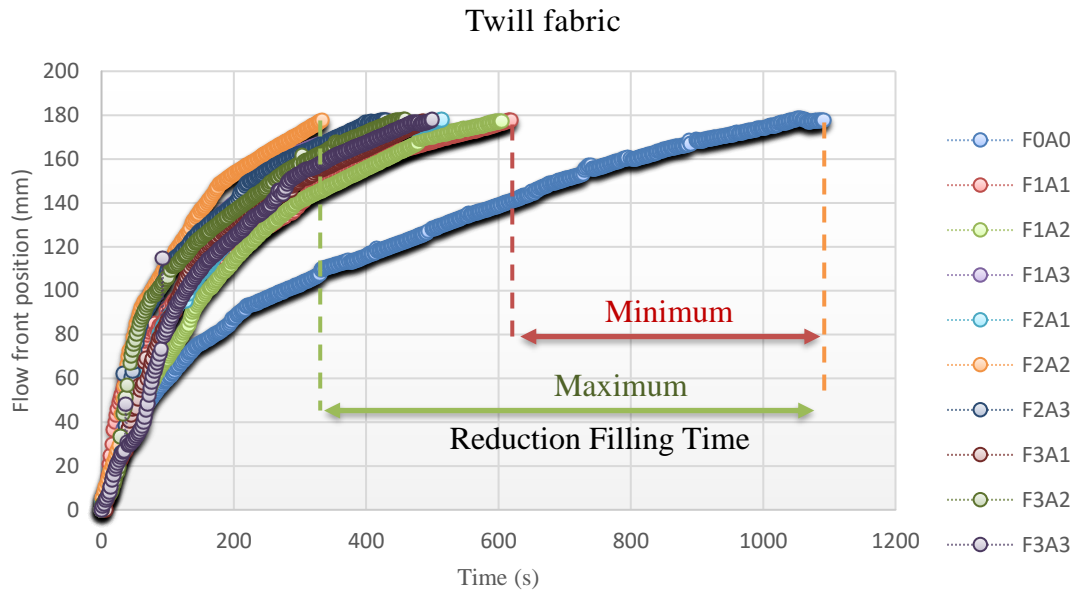


Figure 4.9. Flow front progression through (a) Mat (b) Multiaxial (c) Twill

Figure 4.9 (a) represents the results for mat preform. In this figure, one can see the effect of the EIPR process in reducing the filling time. It reduces the filling time from 34% to 44% regarding different process parameters. The lowest filling time belongs to test number Freq. 5.5 Amp. 0.5.

Similarly, the flow progression is presented for the multiaxial one in Figure 4.9 (b). By comparing, we can see that there is a reduction from 20% to 44% in filling time for this case.

Sequentially, recorded flow front with respect to time for twill is given in Figure 4.9 (c). Twill fabrics has the lowest permeability among the preforms. In this case, there is a 42% to 60% reduction in filling time. The lowest filling time belongs to Freq. 5.5 Amp. 0.5 test.

From the filling time of the experiments, it can be concluded that the EIPR process is more effective for the low permeability preforms rather than high permeability ones.

#### **4.6.2 Response surface analysis and regression model for EIPR process permeability**

Table 4.3 displays the permeability responses for the generated experiments by CCD method where frequency and amplitudes are continuous factors and material is a categorical factor.

Table 4.3. Experimental design and corresponding response

| Experiment code | Experiment no. | Frequency Hz (Freq.) | Amplitude mm (Amp.) | Material (Mat.) | Permeability $\times 10^{-11}m^2$ |
|-----------------|----------------|----------------------|---------------------|-----------------|-----------------------------------|
| F1A1            | 1              | 1                    | 0.2                 | Mat             | 11.56                             |
| F3A1            | 2              | 10                   | 0.2                 | Mat             | 12.60                             |
| F1A3            | 3              | 1                    | 0.8                 | Mat             | 12.89                             |
| F3A3            | 4              | 10                   | 0.8                 | Mat             | 12.10                             |
| F1A2            | 5              | 1                    | 0.5                 | Mat             | 12.40                             |
| F3A2            | 6              | 10                   | 0.5                 | Mat             | 13.29                             |
| F2A1            | 7              | 5.5                  | 0.2                 | Mat             | 12.80                             |
| F2A3            | 8              | 5.5                  | 0.8                 | Mat             | 14.50                             |
| F2A2            | 9              | 5.5                  | 0.5                 | Mat             | 13.77                             |
| F2A2            | 10 (C)         | 5.5                  | 0.5                 | Mat             | 14.50                             |
| F2A2            | 11 (C)         | 5.5                  | 0.5                 | Mat             | 13.00                             |
| F2A2            | 12 (C)         | 5.5                  | 0.5                 | Mat             | 14.50                             |
| F2A2            | 13 (C)         | 5.5                  | 0.5                 | Mat             | 13.95                             |
| F1A1            | 14             | 1                    | 0.2                 | Multiaxial      | 16.070                            |
| F3A1            | 15             | 10                   | 0.2                 | Multiaxial      | 18.900                            |
| F1A3            | 16             | 1                    | 0.8                 | Multiaxial      | 20.450                            |
| F3A3            | 17             | 10                   | 0.8                 | Multiaxial      | 23.780                            |
| F1A2            | 18             | 1                    | 0.5                 | Multiaxial      | 18.750                            |
| F3A2            | 19             | 10                   | 0.5                 | Multiaxial      | 24.100                            |
| F2A1            | 20             | 5.5                  | 0.2                 | Multiaxial      | 20.380                            |
| F2A3            | 21             | 5.5                  | 0.8                 | Multiaxial      | 24.810                            |
| F2A2            | 22             | 5.5                  | 0.5                 | Multiaxial      | 24.800                            |
| F2A2            | 23 (C)         | 5.5                  | 0.5                 | Multiaxial      | 24.000                            |
| F2A2            | 24 (C)         | 5.5                  | 0.5                 | Multiaxial      | 25.100                            |
| F2A2            | 25 (C)         | 5.5                  | 0.5                 | Multiaxial      | 24.700                            |
| F2A2            | 26 (C)         | 5.5                  | 0.5                 | Multiaxial      | 24.400                            |
| F1A1            | 27             | 1                    | 0.2                 | Twill           | 3.610                             |
| F3A1            | 28             | 10                   | 0.2                 | Twill           | 4.301                             |
| F1A3            | 29             | 1                    | 0.8                 | Twill           | 5.790                             |
| F3A3            | 30             | 10                   | 0.8                 | Twill           | 5.460                             |
| F1A2            | 31             | 1                    | 0.5                 | Twill           | 4.802                             |
| F3A2            | 32             | 10                   | 0.5                 | Twill           | 5.448                             |
| F2A1            | 33             | 5.5                  | 0.2                 | Twill           | 4.810                             |
| F2A3            | 34             | 5.5                  | 0.8                 | Twill           | 6.360                             |
| F2A2            | 35             | 5.5                  | 0.5                 | Twill           | 6.300                             |
| F2A2            | 36 (C)         | 5.5                  | 0.5                 | Twill           | 6.700                             |
| F2A2            | 37 (C)         | 5.5                  | 0.5                 | Twill           | 5.962                             |
| F2A2            | 38 (C)         | 5.5                  | 0.5                 | Twill           | 6.100                             |
| F2A2            | 39 (C)         | 5.5                  | 0.5                 | Twill           | 6.000                             |

For obtaining a model for permeability under the EIPR process, a statistical analysis is required. As mentioned before, the tapping frequency and amplitude are taken as independent factors. In this stage, for evaluating the effect of these factors on the corresponding responses is done using MINITAB 18 software. In this analysis, results are investigated based for a confidence factor of 95% by taking P-value  $\alpha = 0.05$ . Therefore, when the probability of factors is more than 95% or  $\alpha \leq 0.05$ , it is considered as a significant factor. For P-values more than 0.05, the factors are rejected as insignificant.

Results of RSM analysis are given in terms of permeability are shown in Table 3. The probability values for frequency and amplitude are more than 99%. Therefore, these factors are effective and significant. Also, P-value for material effect is more than 99% which shows its significance. It is observable that the interactions of factor squares are effective and significant. P-values of all are more than 99% expect for frequency/amplitude and frequency/material interactions, these values are 96%. Figure 4.10 shows Patreo charts that illustrates the effectiveness of the independent factors on the preform permeability under EIPR process.

Table 4.4. Analysis of variance for transformed response

| Source            | DF | Adj SS  | Adj MS   | F-Value | P-Value |
|-------------------|----|---------|----------|---------|---------|
| Model             | 11 | 1.61980 | 0.147255 | 593.47  | 0.000   |
| Linear            | 4  | 1.57425 | 0.393562 | 1586.14 | 0.000   |
| Freq.             | 1  | 0.00575 | 0.005748 | 23.17   | 0.000   |
| Amp.              | 1  | 0.02128 | 0.021280 | 85.76   | 0.000   |
| Mat.              | 2  | 1.54722 | 0.773610 | 3117.82 | 0.000   |
| Square            | 2  | 0.03624 | 0.018121 | 73.03   | 0.000   |
| Freq.*Freq.       | 1  | 0.01847 | 0.018470 | 74.44   | 0.000   |
| Amp.*Amp.         | 1  | 0.00511 | 0.005110 | 20.60   | 0.000   |
| 2-Way Interaction | 5  | 0.00932 | 0.001863 | 7.51    | 0.000   |
| Freq.*Amp.        | 1  | 0.00121 | 0.001207 | 4.86    | 0.036   |
| Freq.*Mat.        | 2  | 0.00334 | 0.001669 | 6.72    | 0.004   |
| Amp.*Mat.         | 2  | 0.00477 | 0.002386 | 9.62    | 0.001   |
| Error             | 27 | 0.00670 | 0.000248 |         |         |
| Lack-of-Fit       | 15 | 0.00459 | 0.000306 | 1.74    | 0.170   |
| Pure Error        | 12 | 0.00211 | 0.000176 |         |         |
| Total             | 38 | 1.62650 |          |         |         |

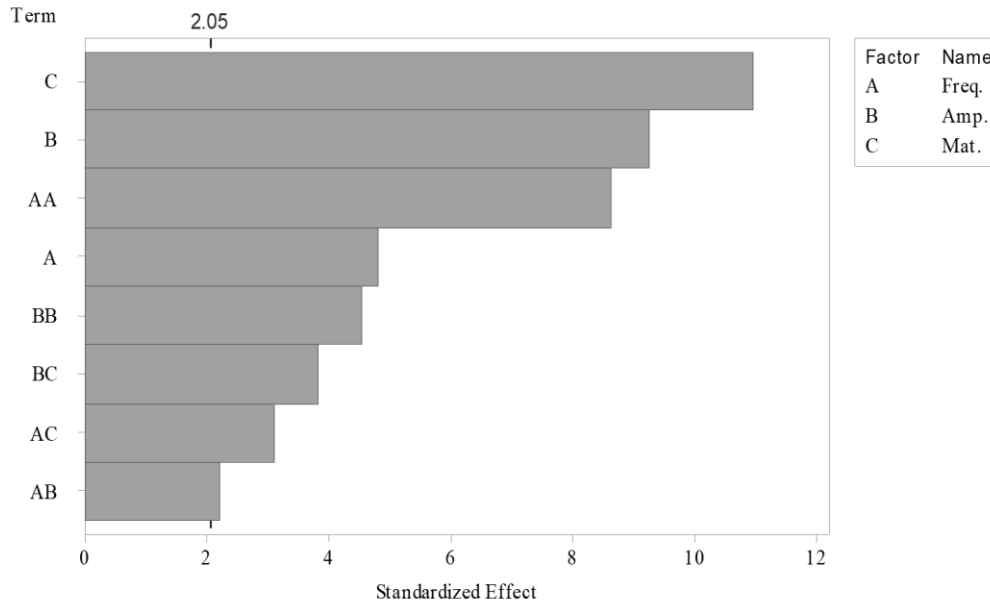


Figure 4.10. Effectiveness of terms in form of Pareto chart for permeability ( $\alpha = 0,05$ )

Lack-of-fit is an index that shows a regression model is not significantly describe the extracted model between the factors and response. If lack-of-fit is significant it can be due to exclude of quadratic terms or exist of unusually large residual results from the fitting the model. Moreover, in this analysis Lak-of-fit is not significant with P-value 0.122, so the extracted model fit the experiment data satisfactorily.

The transformed regression model with the determined coefficients for forecasting response of permeability for all materials tack the following form:

For mat fiber :

$$\begin{aligned}
 Permeability^{0.208834} &= 1.5614 + 0.03057 F + 0.3551 A \\
 &- 0.002332 F * F - 0.2759 A * A \\
 &- 0.00743 F * A
 \end{aligned}
 \tag{4.4}$$

For multiaxial fabric:

$$\begin{aligned}
 Permeability^{0.208834} &= 1.6656 + 0.03754 F + 0.4622 A \\
 &- 0.002332 F * F - 0.2759 A * A \\
 &- 0.00743 F * A
 \end{aligned}
 \tag{4.5}$$

For twill fabric:

$$\begin{aligned}
 \text{Permeability}^{0.208834} &= 1.2044 + 0.03189 F + 0.4769 A \\
 &- 0.002332 F * F - 0.2759 A * A \\
 &- 0.00743 F * A
 \end{aligned}
 \tag{4.6}$$

Where  $F$  and  $A$  in these equations are frequency and amplitude of the system.

$R^2$  is another criterion to evaluate the regression model in predicting results. The more this value is close to 100%, is the more accurate prediction result. Table 4.5 presents the  $R^2$  values for the transformed response.

Table 4.5. Model summary for transformed response

| S         | R-sq   | R-sq(adj) | R-sq(pred) |
|-----------|--------|-----------|------------|
| 0.0157520 | 99.59% | 99.42%    | 98.99%     |

Figure 4.11 (a) and (b) illustrate the normal probability of residuals for the preform permeability response. This type of plots reveals whether a particular distribution fits to the collected data and allows the comparison of sample distributions. Points close to the distribution line and close together mean good fitness of the selected distribution. We can see that the points are very close to the fit line, i.e. the normality assumption is valid in this analysis. The histogram plot, Figure 4.11 (c), also shows the normal distribution without skew and existence of outliers. Residuals Versus Fitted-Values plot shows a random pattern of residuals on both sides of zero. And this confirms the constant variance assumption in experiment data. From the residuals versus order of data, it is noticeable that the residuals are uncorrelated with each other.

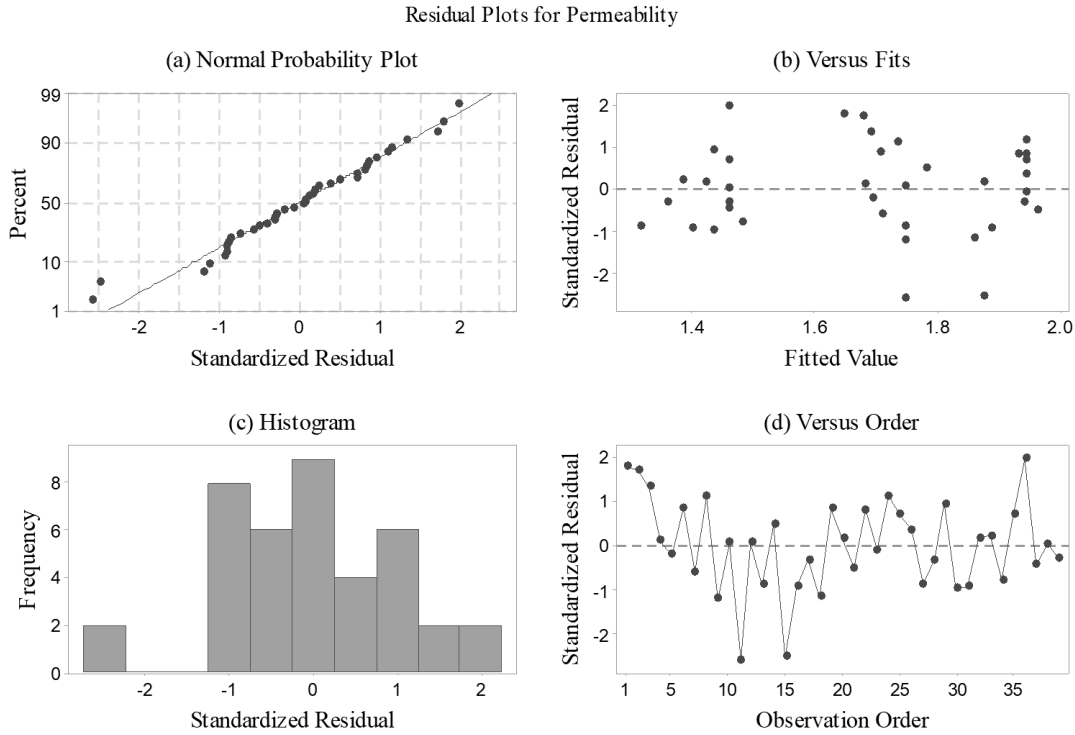


Figure 4.11. Residual plots for permeability. (a) Normal probability (b) versus fits (c) histogram (d) versus order

### 4.6.3 3D surface and 2D contour plots for preform permeability of EIPR process

3D surface and 2D contour plots are utilized to show the effect of the independent variables, i.e. frequency and amplitude of the EIPR process, on the permeability, while holding the material at fixed level at the same time.

Figure 4.12-14 display 3D surface and 2D contour plots for frequency and amplitude while the material factor is kept constant for mat, multiaxial and twill fabrics respectively. It is observable as Figure 4.15, the preform permeability increases and then decreases with increasing frequency. However, it increases with increasing amplitude.

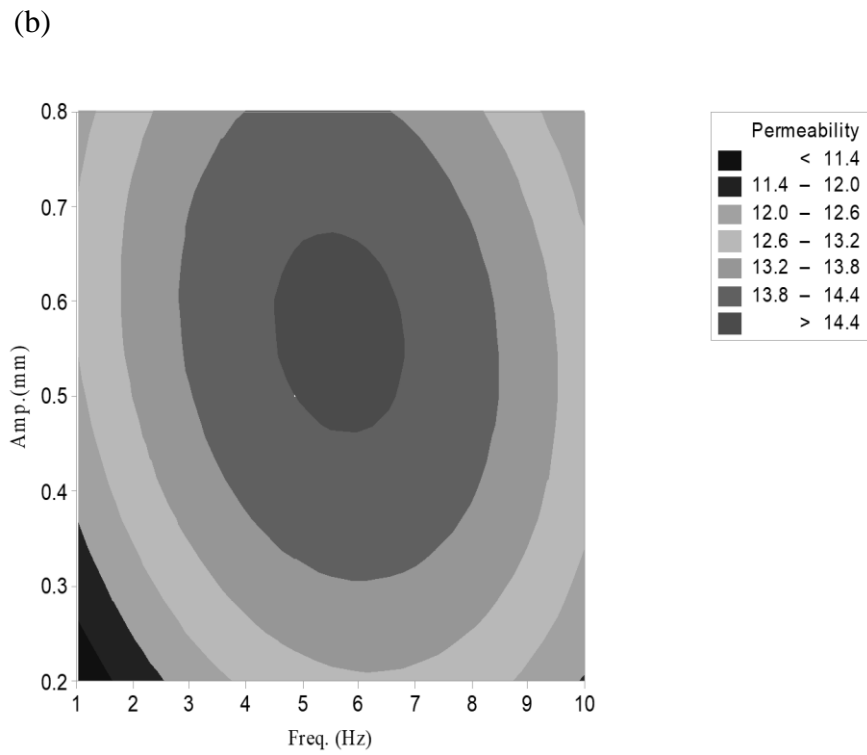
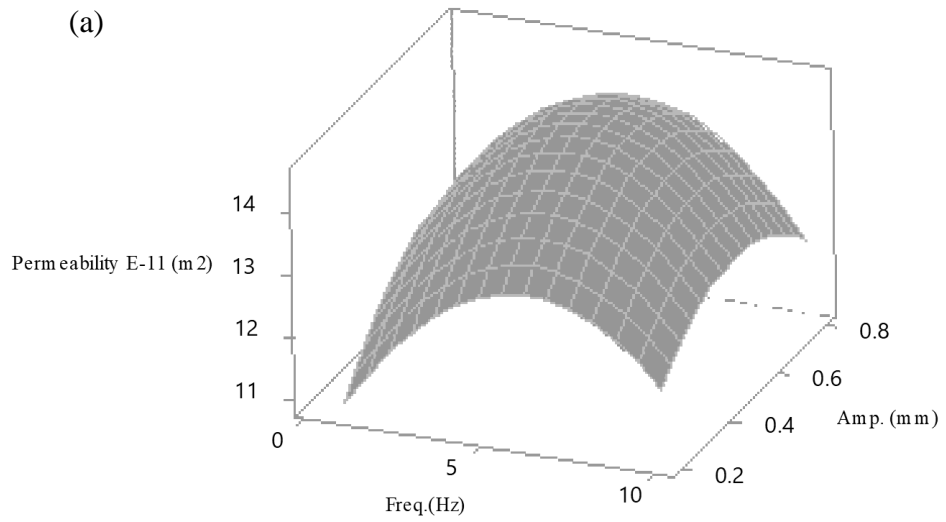


Figure 4.12. (a) 3D surface and (b) 2D contour plot for mat preform on permeability

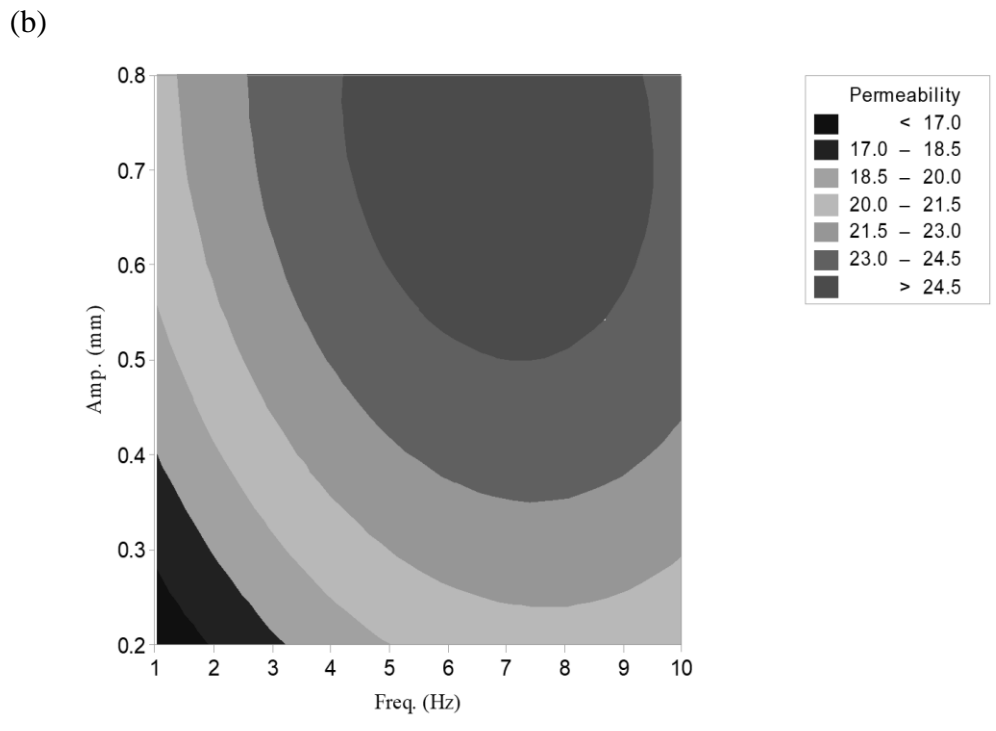
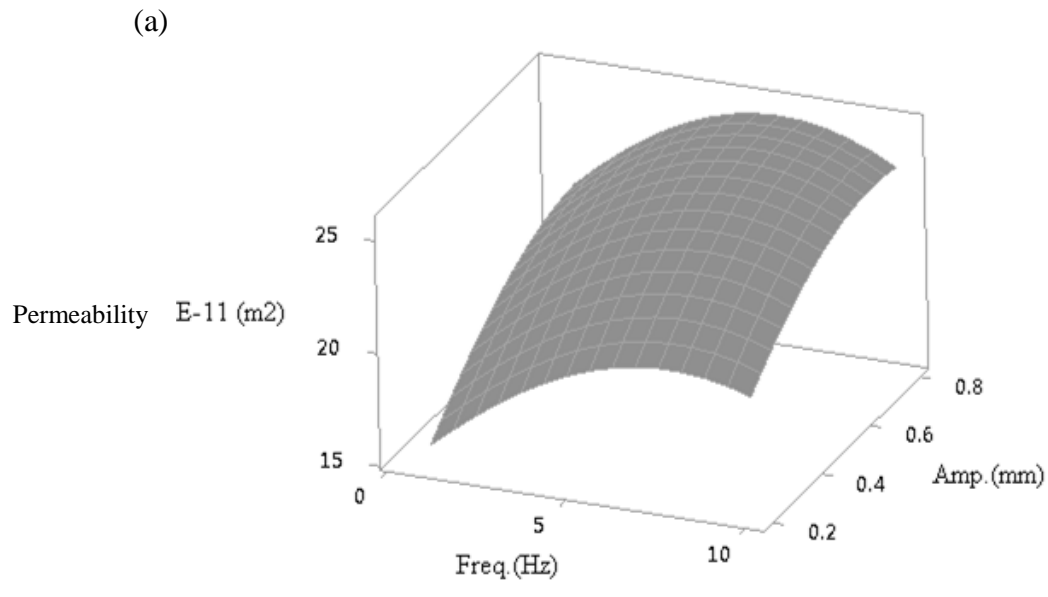


Figure 4.13. (a) 3D surface and (b) 2D contour plot for Multiaxial on permeability

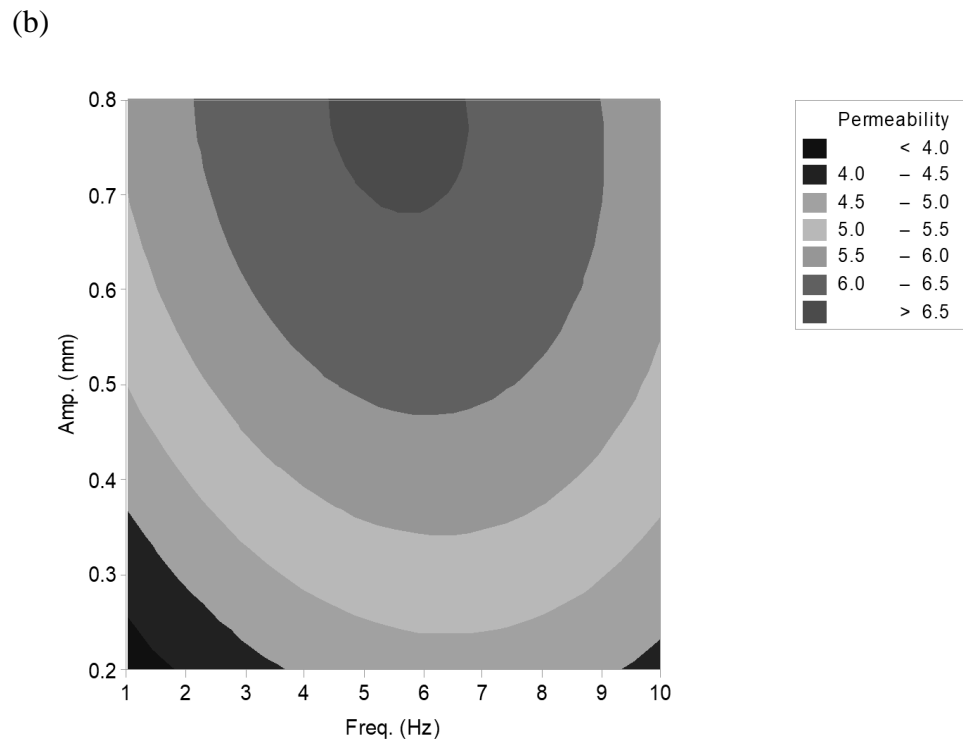
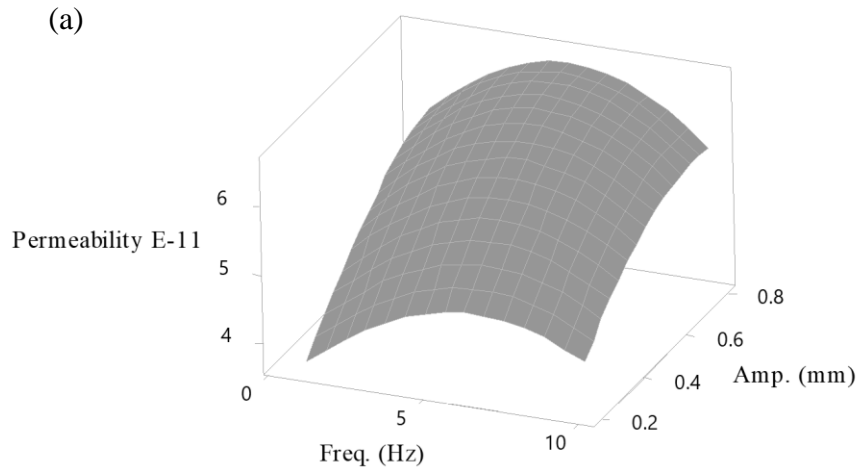


Figure 4.14. (a) 3D surface and (b) 2D contour plot for twill on permeability

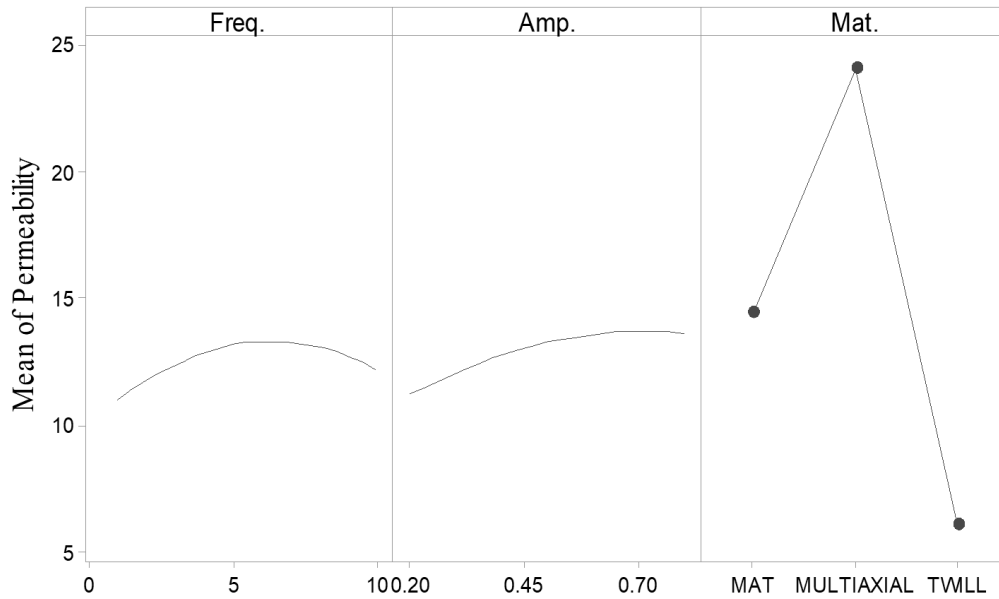


Figure 4.15. Mean effects plot of frequency, amplitude and material on preform permeability fitted mean

#### 4.6.4 Optimization

Finally, an optimization study is performed for preform permeability by using the response optimizer where the aim is to maximize the permeability. The optimum values depend on the preforms for frequency and amplitude are found to be 5.6-5.7 Hz and 0.5-0.7 mm, respectively. Obviously, these values are the optimum values for the selected range of these parameters. For the frequency these values may change by applying different materials for the elements and different electromagnetic forces. Corresponding permeability for mat, multiaxial and twill fabrics are  $14.580 \times 10^{-11}$ ,  $24.93 \times 10^{-11}$  and  $6.183 \times 10^{-11} m^2$ , respectively.

#### 4.7 Summary

In this study, the preform permeability under the EIPR process is characterized. Leading factors of the process are identified including frequency and amplitude of vibration. In order to evaluate this process and obtain a confident model, three preform types with permeabilities of high, medium and low values are selected. CCD method is used for the design of experiment. A total of 39 experiments are conducted to study the effect of the factors on the preform permeability under the EIPR process. The filling time of preform infusion under the EIPR process shows a significant

reduction from 20% to 60% depending on the material and factor levels. High reduction values relate to the low permeability preform. The response surface methodology (RSM) is utilized to analyze and model the permeability response. A mathematical model is obtained as a function of frequency and amplitude for each material. It shows that the response defined in terms of permeability first increases with increasing frequency and then reduces. Meanwhile it has an ever increasing trend with increasing amplitude. The maximum preform permeability of the EIPR process is obtained for each preform.



## CHAPTER 5

### MODELING AND EVALUATION OF ELECTROMAGNETICALLY INDUCED PREFORM RESTING (EIPR) PROCESS

Unexpected flow patterns of resin in the infusion process may occur due to the vacuum bag wrinkling and inherent permeability variation of preforms. The EIPR process is a relatively new derivative of Vacuum Assisted Resin Transfer Molding (VARTM) processes. The resin flow can be controlled and manipulated during the process in real time. In this method, the permeability of the preform locally by resting the preform, increasing the porosity and therefore delivering the resin through the fiber reinforcement accordingly. The aim here is to model and assess the parameters of the EIPR process numerically. The flow simulation for the process like many new processes is required to ensure its utilization to produce near perfect composite parts without any defects. In order to conduct a more reliable simulation, the permeability of preform is determined experimentally with and without EIPR. The ones with EIPR are used as an equivalent permeability in the sections which are obtained with the flow control. The obtained data is used to simulate the EIPR process for the selected case studies. Two case studies involving two different permeability zones are designed for evaluation purposes. In each case, a low permeability preform is placed in the middle of high permeability one to create an artificial disturbance during the filling process. Comparing the results of the simulation with the experimental data demonstrates that an acceptable accuracy is obtained in simulations.

#### 5.1 Introduction

Resin infusion processes are one of the alternatives for out-of-autoclave processes. It has been more noticeable in composites manufacturing especially for large structures. This category of the liquid composite molding reduces tool cost with

respect to the well-known Resin Transfer Molding (RTM) process. Additionally, VARTM process is known to release relatively less volatile organic compounds into the atmosphere. In VARTM process, defects such as dry spots, voids and welding lines often arise during the mold filling and thereby they decrease the mechanical properties of the produced parts [92,93]. These defects may often occur due to unexpected resin flow in the current vacuum bags [61]. To evaluate VARTM process with rival approaches i.e. autoclave and RTM process, elimination of limitations caused by such defects is required.

Resin flow controlling is needed to prevent the formation of voids and dry spots. In general, resin flow controlling systems have two types as off-line and on-line control. The off-line control is done before any infusion by optimizing gate and vent lines or ports using numerical approaches [22,94–98]. Since the off-line approaches are done before the real infusion process, these methods do not intervene during the filling process for unexpected cases. However, the on-line methods are conducted during the infusion. In recent years, some approaches to control and to manipulate the resin flow have been suggested. These approaches involve gate/vent closing/opening and pressure control, increasing resin viscosity by heating, increasing porosity of preform by vacuum induced preform relaxation, resin delivering by flow flooding chamber (FFC) [23,28,30,31,65,69,82,95,99]. As presented in this study, the compaction of preforms can be obtained by electromagnetically induced preform rest (EIPR) approach to enhance permeability and speed the resin flow locally.

### **5.1.1 EIPR process**

The VARTM process is incapable of manipulating resin flow front during the filling in real time. Electromagnetically induced preform resting (EIPR) process is a new variation of VARTM and Seemann's Composites Resin Infusion Molding Process (SCRIMP), which incorporates a creative upper flexible mold with embedded elements for lifting and vibrating the vacuum bag to rest the preform by an electromagnetic field source. EIPR process consists of this type of vacuum bag, an automated gantry system which carries the electromagnet and a camera to trace the resin flow front development. The elements are distributed within the vacuum bag so that a resin flow control is possible anywhere in the composite mold. The principle of this approach is raising and vibrating the elastomer vacuum bag to relax the preform

and decrease the resistance against the resin flow locally at selected positions. Resin flow speeds up at induced preform resting positions to compensate the resin flow disturbance in real time. This correction action reduces the compaction pressure therefore it increases the porosity of fabric preform. Figure 5.1 schematically displays this process.

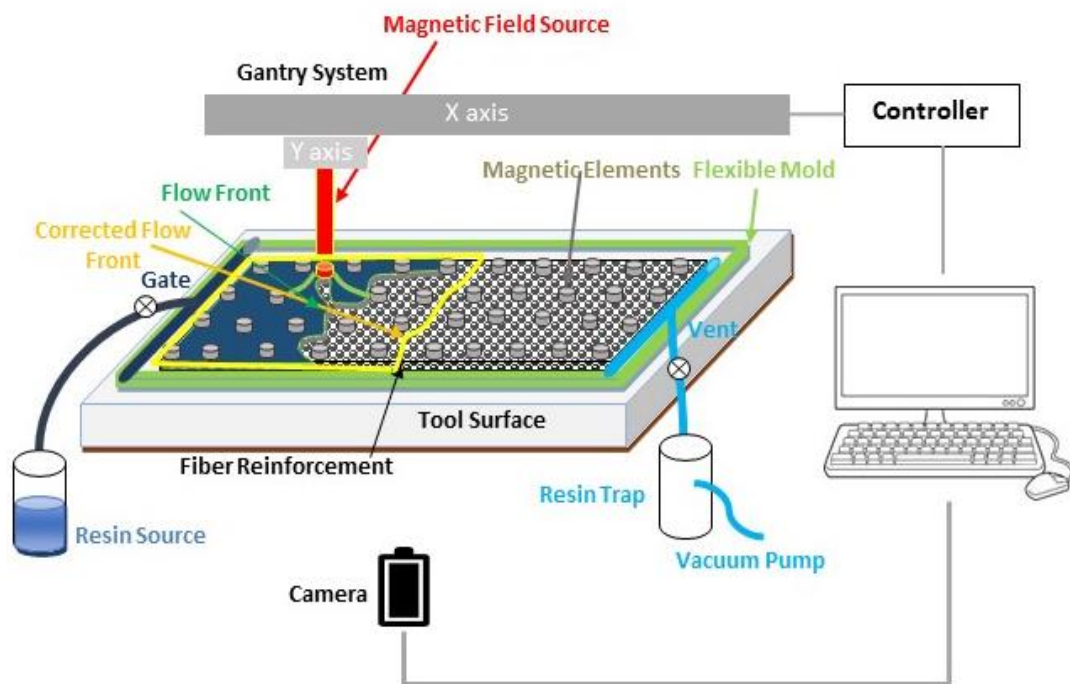


Figure 5.1. EIPR process and its components

Significant parameters of this system are: amplitude refers to the height that the electromagnetic (EM) force can lift the element, tapping frequency of EM force for resting the vacuum bag and primary permeability of fabric preforms. Influences of these parameters are investigated experimentally with three different levels to find the optimum process factors. The relation between these parameters and local permeability values are obtained. In this chapter, the optimum parameter values used are 0.5 mm for amplitude and 5.5 Hz for frequency. Like the other processes of liquid composite molding (LCM) development of this process also needs to model and evaluate numerically.

### 5.1.2 Resin flow simulation

In a VARTM process, any unsaturated area of fiber preforms may cause for the produced composite parts to be scrapped. For making LCM processes more reliable, the resin flow saturation in fiber preform is needed to be understood numerically. Numerical analysis enables one to optimize the filling process and evaluate the resin filling processes. In recent years, various VARTM process simulations have been conducted extensively.

Simulations for the liquid composite molding require defining boundary conditions, in addition to preform characteristics such as compressibility and permeability.

There are several programs for the simulation of composite laminate molding mostly with an acceptable approximation. For simulation of filling molds, commercial softwares such as LIMS from the University of Delaware [34], RTM-Worx from the Polyworx [35], FLUENT from Ansys, Abaqus CFD from Simulia Abaqus and PAM-RTM from ESI group [33] have been extensively used. The resin flow simulation of LCM process in 2D, 2.5D with a layer of shell and 3D perspective has been studied by several authors [100–104]. The essential ingredient for generating successful simulation for mold filling is the material characterization which includes: permeability and compressibility. It is explained in more detail in the following section.

### 5.1.3 Material characterization

#### **Permeability:**

The permeability of fiber reinforced preforms is an important parameter that must be given as an input to the simulation software. It is in a way representation of the resistance of preform against the resin flow. Darcy's law [36] states that velocity of fluid per flow volume ( $\mathbf{v}$ ), is proportional to the pressure gradient ( $\Delta p$ ), fluid viscosity ( $\mu$ ), and preform permeability tensor ( $\mathbf{K}$ ) as:

$$\mathbf{v} = -\frac{\mathbf{K}}{\mu}\Delta p \quad (5.1)$$

where its solution requires permeability of fabric preform. This parameter depends on the local compression of the preform during resin infusion molding. To predict

the filling time and flow front pattern, a complete characterization of material property is necessary. Permeability is known to be anisotropic in porous media [16] such that a second order tensor describes this property as follows:

$$\mathbf{K} = \begin{bmatrix} K_{xx} & K_{xy} & K_{xz} \\ K_{yx} & K_{yy} & K_{yz} \\ K_{zx} & K_{zy} & K_{zz} \end{bmatrix} \quad (5.2)$$

This tensor can be diagonalized to obtain what is known as the principle permeability. It is assumed that the first two principle permeability values lie in the fabric plane while the third one is orthogonal to the fabric plan. To find the principle permeabilities three permeability measurements are needed at  $0^\circ, 45^\circ, 90^\circ$  direction of the preforms. Once these values are obtained calculation of principle permeabilities ( $K_1, K_2$ ) is possible as follows [17]:

$$K_1 = K_{xx}^{0^\circ} \frac{\alpha_1 - \alpha_2}{\alpha_1 - \frac{\alpha_2}{\cos(2\beta)}} \quad (5.3)$$

and

$$K_2 = K_{xx}^{90^\circ} \frac{\alpha_1 + \alpha_2}{\alpha_1 + \frac{\alpha_2}{\cos(2\beta)}} \quad (5.4)$$

where  $\alpha_1$  and  $\alpha_2$  are:

$$\alpha_1 = \frac{K_{xx}^{0^\circ} + K_{xx}^{90^\circ}}{2} \quad (5.5)$$

$$\alpha_2 = \frac{K_{xx}^{0^\circ} - K_{xx}^{90^\circ}}{2} \quad (5.6)$$

$$\beta = \frac{1}{2} \tan^{-1} \left( \frac{\alpha_1}{\alpha_2} - \frac{\alpha_1^2 - \alpha_2^2}{\alpha_2 \cdot K_{xx}^{45^\circ}} \right) \quad (5.7)$$

where  $K_{xx}^0, K_{xx}^{45}, K_{xx}^{90}$  and  $\beta$  are permeability of the preform along  $0^\circ, 45^\circ, 90^\circ$  orientations and the angle between the elliptic pattern of flow and warp direction of fabric.

### **Compressibility:**

The fabric compressibility is another important factor in all VARTM processes, and it affects both the material and process related properties of a part. As the fabric is compressed by fluid pressure or the mold surface, fibers get compacted and the corresponding fiber volume fraction increases. This decreases the thickness of the part, in other words the porosity and as a result it decreases the permeability. The compressibility is more important to understand in one-sided molding processes like VARTM than in closed-mold processes like RTM. In a closed mold process, the permeability and fabric thickness are fixed at a certain value which is determined by the mold gap. Throughout the process, the permeability is constant and independent of the injection pressure. In one-sided molding processes, the compaction of the fabric can lead to several important phenomena. In processes where the flow is in the plane of the fabric such as VARTM and SCRIMP, an area with non-uniform thickness can be created since the net compaction pressure varies throughout the mold.

According to Darcy's law, an increase in pressure will increase the velocity of the fluid through the fabric. However, on the other side, increasing the pressure of the fluid will increase the compaction pressure and lower the permeability. It could be possible in certain cases for an increase in pressure to have a decrease in injection time, although this is not common. For most fabrics, the decrease in thickness tends to compensate for the decreased permeability in through-thickness flow. The effect of compaction on permeability is very dependent on the fabric architecture, which means some fabrics are more affected than others. The fabric compaction also affects the porosity of the fabric, which will affect the saturation time for unsaturated flow. This fact adds yet another complication to the problem. Although permeability decreases with compaction, the decrease in porosity can increase the velocity of the fluid through a preform. Since this parameter has an important effect on the permeability of the preform and processability of the composite parts, to get accurate values for fabric compaction, compressibility values of preforms are required. It is

defined as a function of preform thickness ( $h$ ) of the pressure applied on the preform surface:  $h = f(P_{com})$ . In LCM processes, the compressibility of the preform directly define the fiber volume fraction by  $V_f(P_{com}) = (\frac{m}{h(P_{com})\rho})$ , where  $m$  is areal density of the fiber preform,  $\rho$  is fiber density and  $h$  is the preform thickness.

During the infusion process, the resin pressure that is calculated from the Darcy's equation has a gradient along the saturation path from the atmospheric pressure at infusion line side to the vacuum pressure at vent line side. This pressure difference ( $P_{atm} - P_{vac}$ ) is constant and taken as external pressure. Thickness ( $h$ ) of the mold is not constant due to balancing property of vacuum bags on the pressure gradient against the summation of resin pressure and reinforcement compaction pressure that is computed from compressibility curve [82,100,105].

$$P_{ext} = P_{resin} + P_{com} \quad (5.8)$$

The aim of this part of the study is to present and evaluate a predictive model of mold filling for the EIPR process using PAM-RTM software package. Therefore, a procedure for the numerical simulation of the EIPR process is presented here. The material properties including permeability and compressibility of fiber reinforced preforms are obtained with and without EIPR processes for resin flow control. The permeability of reinforcements under the EIPR process is taken as an equivalent property of preform in process modeling.

## 5.2 Experimental characterization of materials

### 5.2.1 Material

High and low permeability preforms are selected to create artificial disturbances in the flow pattern of a given sample. The criterion for selection is its permeability value. The selected fibers for this study are: E-Glass fiber fabric twill with 300 gr/m<sup>2</sup> areal density as low permeability reinforcement and E-Glass fiber EMAT1-450 g/m<sup>2</sup> (Mat) as high permeability reinforcement. A view of material samples for permeability measurement tests are shown in Figure 5.2.



Figure 5.2. Fabric samples, twill (left), mat (right)

Since viscosity of thermoset resins varies during the process and they have a Newtonian behavior before the gelation, therefore a test fluid (Motor oil 20W50) is used to have repeatable and reliable measurements, as recommended in [17]. Test fluid viscosity is 0.165 Pa.s with a density of 900 kg/m<sup>3</sup>.

### 5.2.2 Permeability measurement for fiber preforms

For characterizing the in-plane permeability of fiber preforms, an experimental setup is designed and implemented. Use of an elastomer vacuum bag during tests is shown to provide a uniform flow front and eliminate race tracking phenomena. An image processing code written in MATLAB is used to detect the flow front with respect to time. It measures the flow front position from the inlet line. Two types of processes are applied for measuring the permeability of preforms. The first one was VARTM process without any flow control scheme and the other one is with the EIPR approach.

In-plane permeability of mat fiber has an isotropic behavior, hence one experiment is sufficient to obtain the in-plane permeability of this material. For the twill preform, measurements for three different directions are needed to calculate the principle permeabilities. In the VARTM process resin infused starting from the gate line flowing toward the vent line. Schematic of the experiment to characterize the in-plane permeability of the fabrics during the EIPR process is detailed in Figure 5.3.

Note that for this process, the ferromagnetic element is not invoked. In the EIPR process, optimum values for test parameters (frequency of 5.5Hz, amplitude of 0.5 mm) are implemented for the experiments. The region with low permeability preform of the case studies is treated with the flow controlling action, permeabilities of them are determined in three directions ( $0^\circ, 45^\circ, 90^\circ$ ).

For both approaches, the permeability of preforms is calculated according to Darcy's law which says that the slope of the line fitted to the square flow front with respect to time  $t$  gives the permeability  $K_{xx}$  as follow:

$$K_{xx} = \frac{L_{ff} \varphi \mu}{2pt} \quad (5.9)$$

where  $L_{ff}$  is the flow front at instant  $t$ ,  $\varphi$  is the preform porosity,  $\mu$  is the fluid viscosity and  $p$  is the vacuum pressure. In this relation, porosity of the preform is calculated from:

$$\varphi = 1 - V_f \quad (5.10)$$

where  $V_f$  is the fiber volume fraction that is obtained as:

$$V_f = \frac{m}{l \cdot w \cdot h \cdot \rho} \quad (5.11)$$

where  $m$  is the total mass of the preform,  $l$ ,  $w$  and  $h$  are the dimensions of the composite part, and  $\rho$  is the density of the preform.

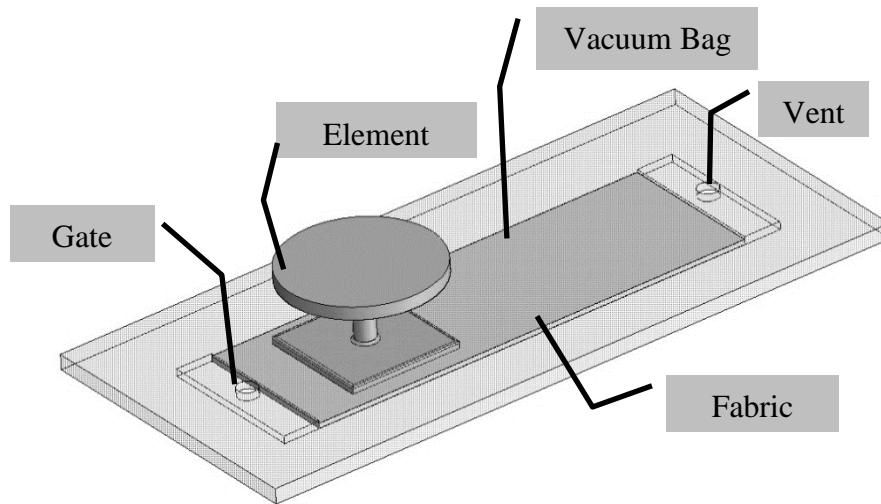


Figure 5.3. Schematic of experiment for characterization of in-plane permeabilities

### 5.2.3 Fabric compressibility

For this purpose, the out-of-plane compression response of preforms is tested on a displacement-controlled Instron machine. Three specimens for each with the size of  $60 \times 60 \text{ mm}$  and 5 and 12 plies for mat and twill preforms, respectively as shown in Figure 5.4. In Figure 5.5 and Figure 5.6, the pressure response of preforms are demonstrated as a function of fiber volume fraction. In Table 5.1, the compressibility values of preforms based on power law are given.

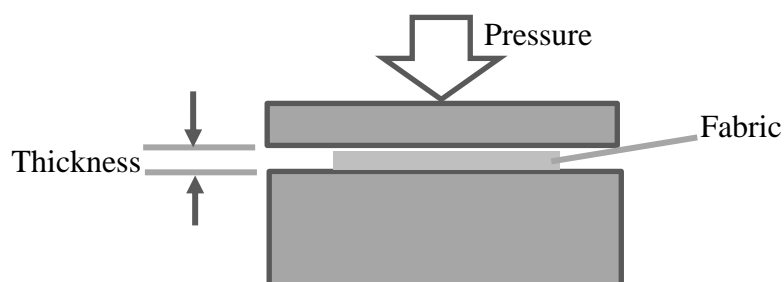


Figure 5.4. Test set-up for measuring compressibility of preforms

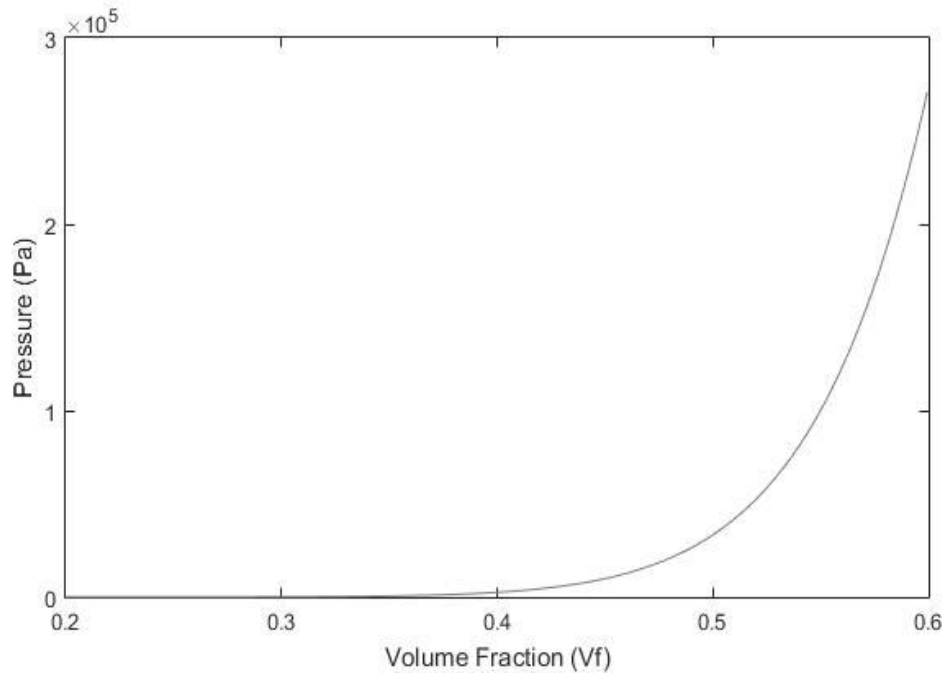


Figure 5.5. Pressure response of twill preform

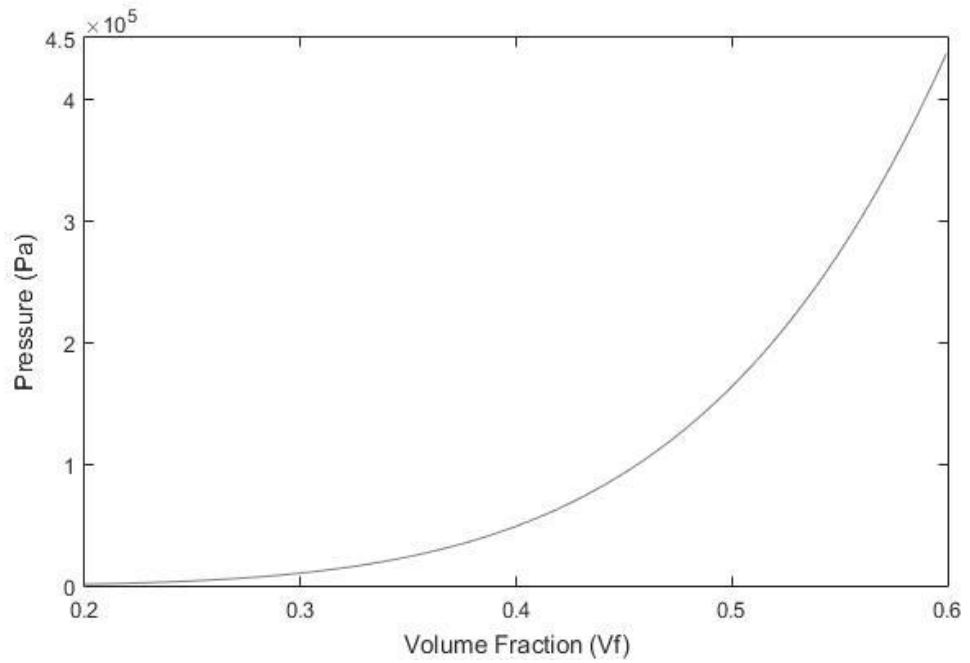


Figure 5.6. Pressure response of mat

Table 5.1 Compressibility of preforms used

|       |   |
|-------|---|
| Mat   | $P_{com} = 7 \times 10^6 \cdot V_f^{5.42}$  |
| Twill | $P_{com} = 1 \times 10^8 \cdot V_f^{11.55}$ |

### 5.3 EIPR process simulation

Simulation of EIPR process can incorporate the resin flow control in real time. The equivalent permeability of the low permeability preform is taken as material property for this section that is under the resin control action.

For simulating the filling process, the fluid flowing through the preform is assumed to be isothermal and incompressible Newtonian. Continuity of the incompressible flow gives:

$$\nabla \cdot V = 0 \quad (5.12)$$

where flow velocity vector [m/s] through the preform is

$$V = -\frac{K_{xx}}{\mu} \nabla p \quad (5.13)$$

Substituting  $V$  in Eq. (5.12) yields the Laplacian for the pressure:

$$\nabla^2 p = 0 \quad (5.14)$$

where  $\nabla p$  is the pressure gradient [Pa/m] and  $\mu$  is the fluid viscosity [Pa.s].

Two case studies are conducted to model the EIPR process numerically. The models of infusion simulation are  $0.14 \times 0.24 \text{ m}$  plate with a thickness of about  $0.002 \text{ m}$ , where the middle of the plates is stiffened with a low permeability preform, a twill fabric. Figure 5.7 shows these models with the dimensions and the boundary conditions of simulation. Infusion pressure is atmospheric pressure at the left side and vacuum pressure is  $500 \text{ mmHg}$  which is at the flow front or the right side of the models. The model is meshed using triangular 2D elements. Filling the mold for the

selected case studies are simulated for both VARTM (with no resin flow control) and EIPR process (with flow control) to see the efficiency of the process.

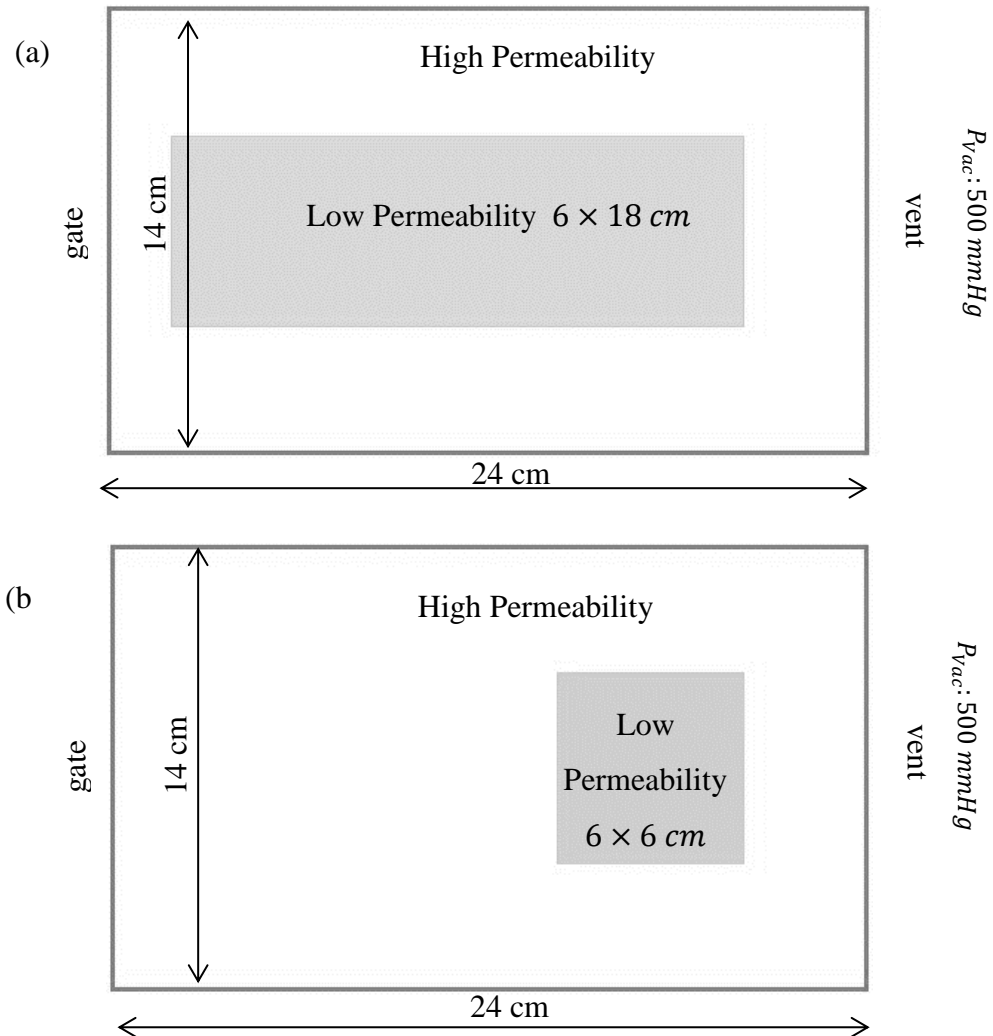


Figure 5.7. Geometry of plates in case studies (a) case 1 (b) case 2

#### 5.4 Validation

In order to evaluate the simulation of resin flow with EIPR, a workstation is designed and set up with all hardware. It is composed of a transparent mold with an upper special flexible mold, an image processing unit, an automated gantry system and an electro-magnetic (EM) field source. In this section, the experiments performed on this workstation are presented.

### 5.4.1 Permeability of preform with/without EIPR process

The permeability characterization of selected preforms is conducted for both processes. For determining the principle permeability of twill fabric, a permeability measurement test at  $0^\circ$ ,  $45^\circ$  and  $90^\circ$  directions are conducted for both with/without EIPR processes. For mat performs, permeability is only measured at  $0^\circ$  without any control process. The effective permeability at different directions, principle permeabilities, orientation angle. ( $\beta$ ) of the elliptical flow shape for both processes are presented in Table 5.2.

Table 5.2 Effective and principle permeability, and orientation of elliptical flow

| Process | Material | Permeability<br>( $10^{-11} m^2$ ) |                     |                     |       |       | Ellipse<br>orientation |
|---------|----------|------------------------------------|---------------------|---------------------|-------|-------|------------------------|
|         |          | $K_{xx}^{0^\circ}$                 | $K_{xx}^{45^\circ}$ | $K_{xx}^{90^\circ}$ | $K_1$ | $K_2$ | $\beta$                |
| EIPR    | Twill    | 6.29                               | 6.78                | 7.74                | 7.77  | 6.28  | $96.2^\circ$           |
| VARTM   | Mat      | 8.47                               | -                   | -                   | 8.47  | 8.47  | $0^\circ$              |
|         | Twill    | 1.72                               | 1.86                | 2.42                | 2.47  | 1.68  | 102.1                  |

### 5.4.2 Experimental procedure

For the EIPR process, the prepared preform with the additional reinforcement in the middle of the plate are placed on the transparent mold and then covered with the flexible mold and kept under 500 mmHg vacuum pressure. Next, the optimum values of the process i.e. frequency of 5.5 Hz and amplitude of 0.5 mm are set as input into the workstation. Finally, infusion process and the EIPR system are initiated simultaneously. Flow front detecting unit follows the front at 3s time intervals and calculates the distance of flow front of each segment from the infusion line and then evaluates flow pattern and decides a proper correction action. The EM field source is carried out to the position by the 2D gantry system. It invokes the element and tap the vacuum bag to deliver fluid through the low preform region to compensate the low permeability zone effects on flow pattern.

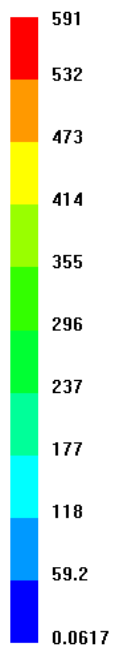
For the no-control process, the experiments are implemented as VARTM process. For these experiments, after placing the preforms and covering them with vacuum bag, preforms are taken under the vacuum pressure and then process is started.

## **5.5 Results and discussion**

Figure 5.8 shows the forecasted filling pattern of case 1 for EIPR process in comparison with two frames of experimental results at 300 and 550 seconds of infusion. In the figure, the low permeability zone is illustrated with a black rectangle. As these frames show, simulation of EIPR process predicts flow patterns and filling time correctly. As it is expected, the EIPR process is shown to avoid the formation of dry spots both in simulations and in experiments. For comparison purposes, one can easily see the dry spot formation for the no-control process, as shown in Figure 5.9. The flow starts from the left side of the plate in the EIPR process and it progresses towards the low permeability section in the center. As shown in this figure, when flow reaches the low permeability zone which is at the center, it faces a resistance in this region and it flows faster around this section through two high permeability channels. Finally, the fluid flow in these two channels join in the right-hand side of the low permeability zone and a dry spot is formed there.

The simulation also predicts the unsaturated zone in VARTM process correctly. In the presented figure, a frame of flow pattern before air entrapment and formed dry spot at the end of filling process, Figure 5.9 (c) and (d), experimentally and numerically is exemplified. Figure 5.9 (a) and (b) depicts flow front at 445s of process of simulation and experiment.

Filling\_Times



Time : 0 s.

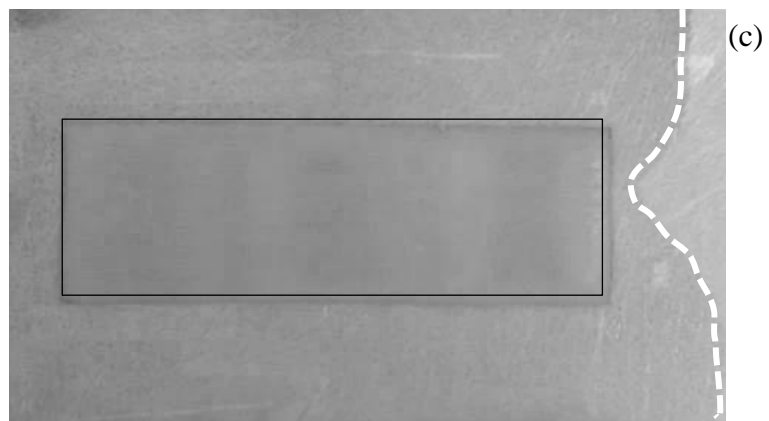
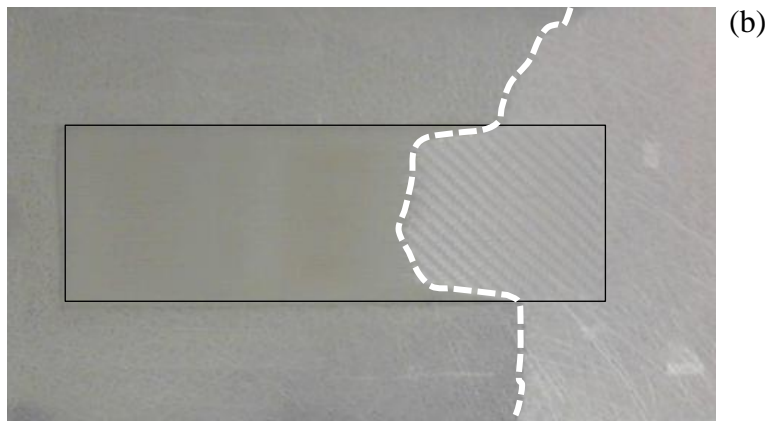
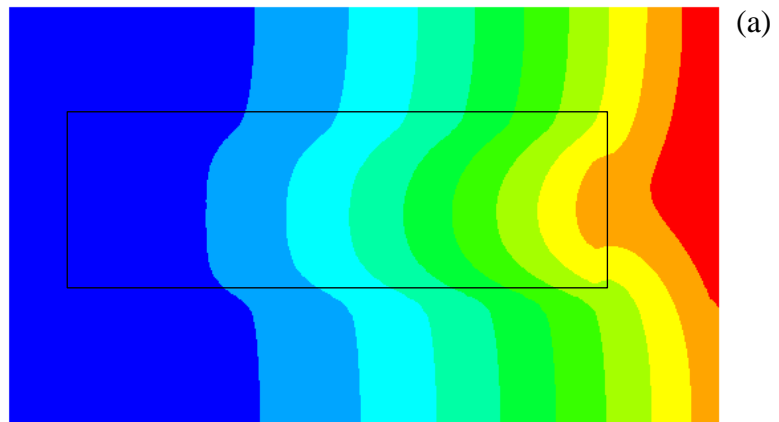
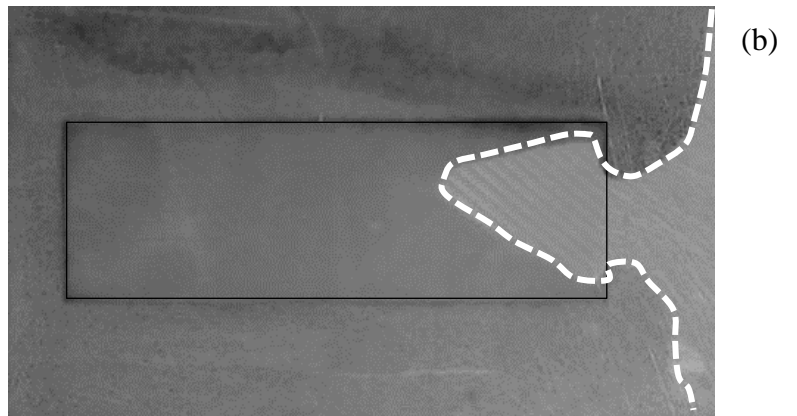
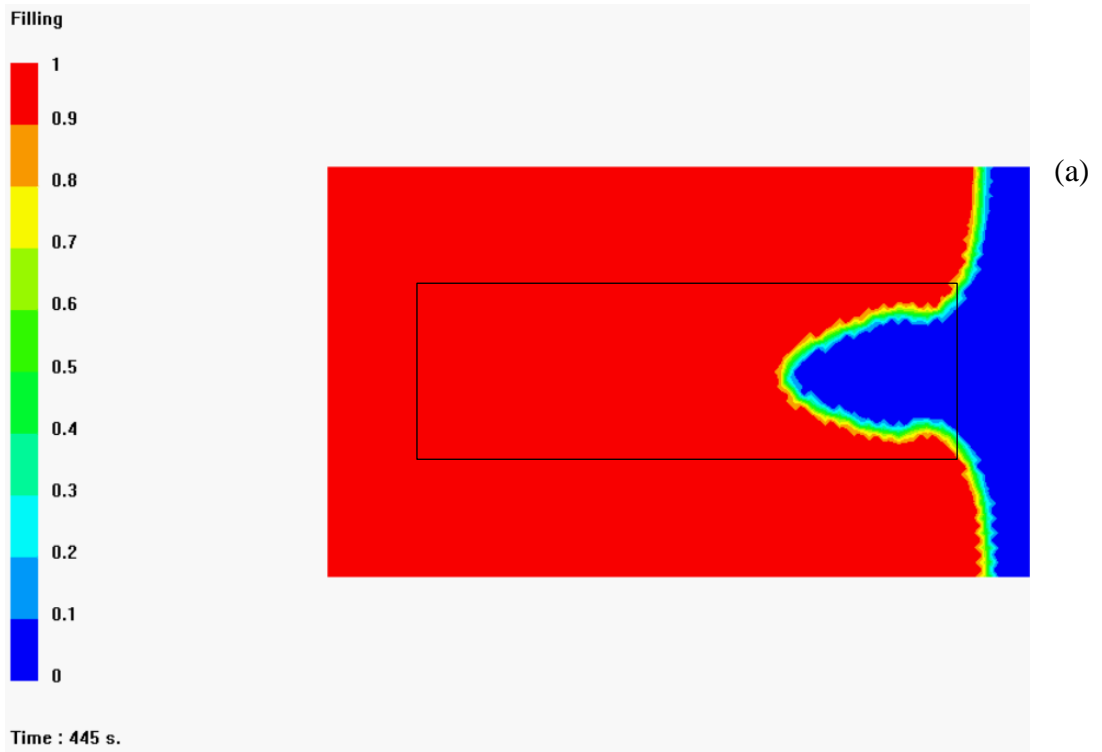


Figure 5.8. Filling pattern for case 1 (a) simulation, experiments at (b) 300s and (c) 550s



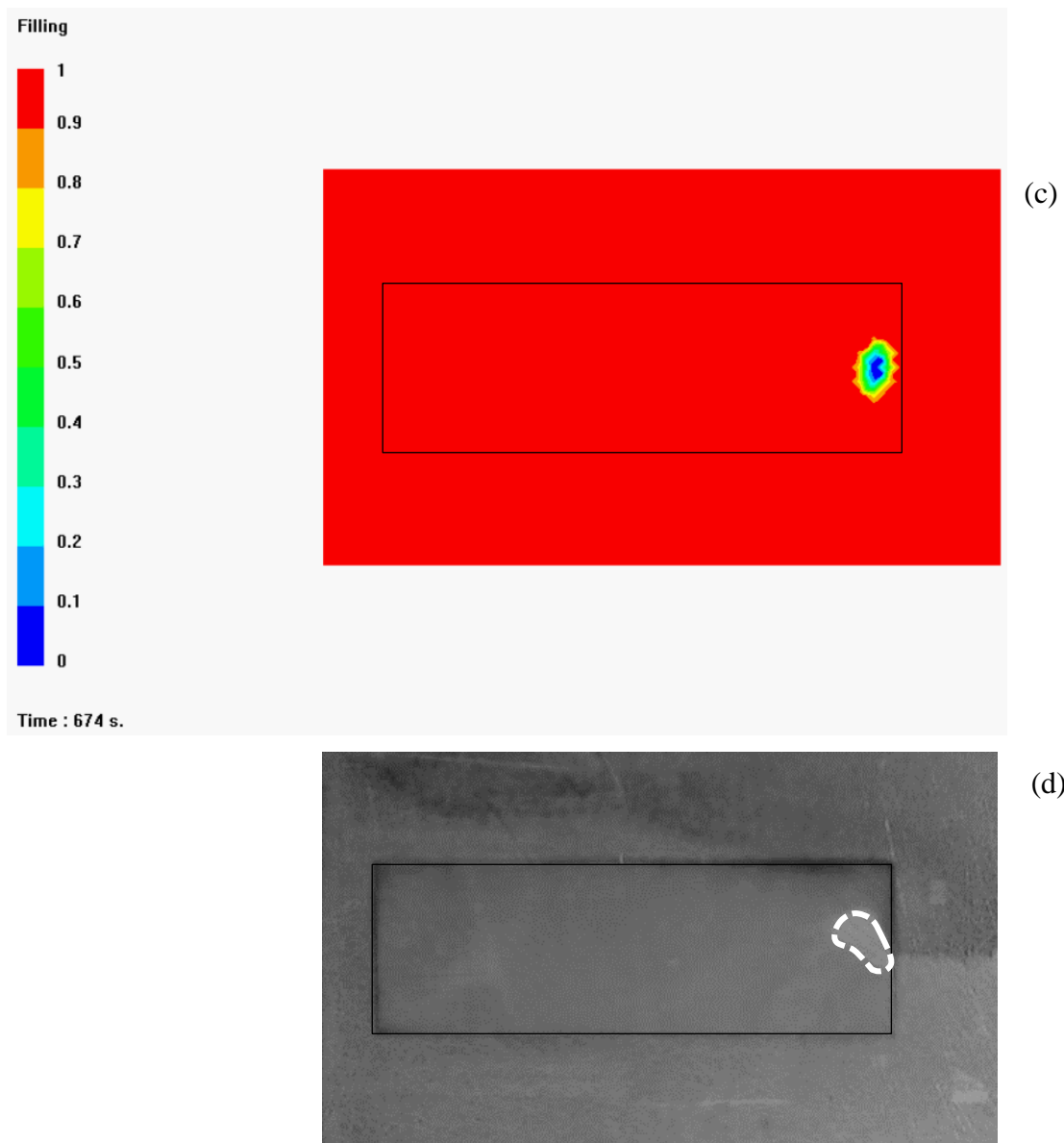


Figure 5.9. Flow front of case 1 (a) at 445s of VARTM process for simulation, (b) experiment, (c) dry spot in simulation and (d) dry spot in experiment

Figure 5.10 illustrates the filling pattern of case 2 in the EIPR process in comparison with the experimental images of flow front. Two frames of mold filling at times 357 and 459 seconds of process are selected to validate the simulation results. Flow front geometries are very like the simulation patterns corresponding to similar filling times. Figure 5.11 shows the simulation and experimental results for VARTM process. Similarly, reduction in the speed of flow in the low permeability section causes an air trap because of the fact that fluid flows faster in the high permeability sections surrounding this low permeability section.

Simulation of case 2 predicts the dry spot formation in VARTM process as well and the shape of dry spot zone reveals the good agreement between simulation and experiment.

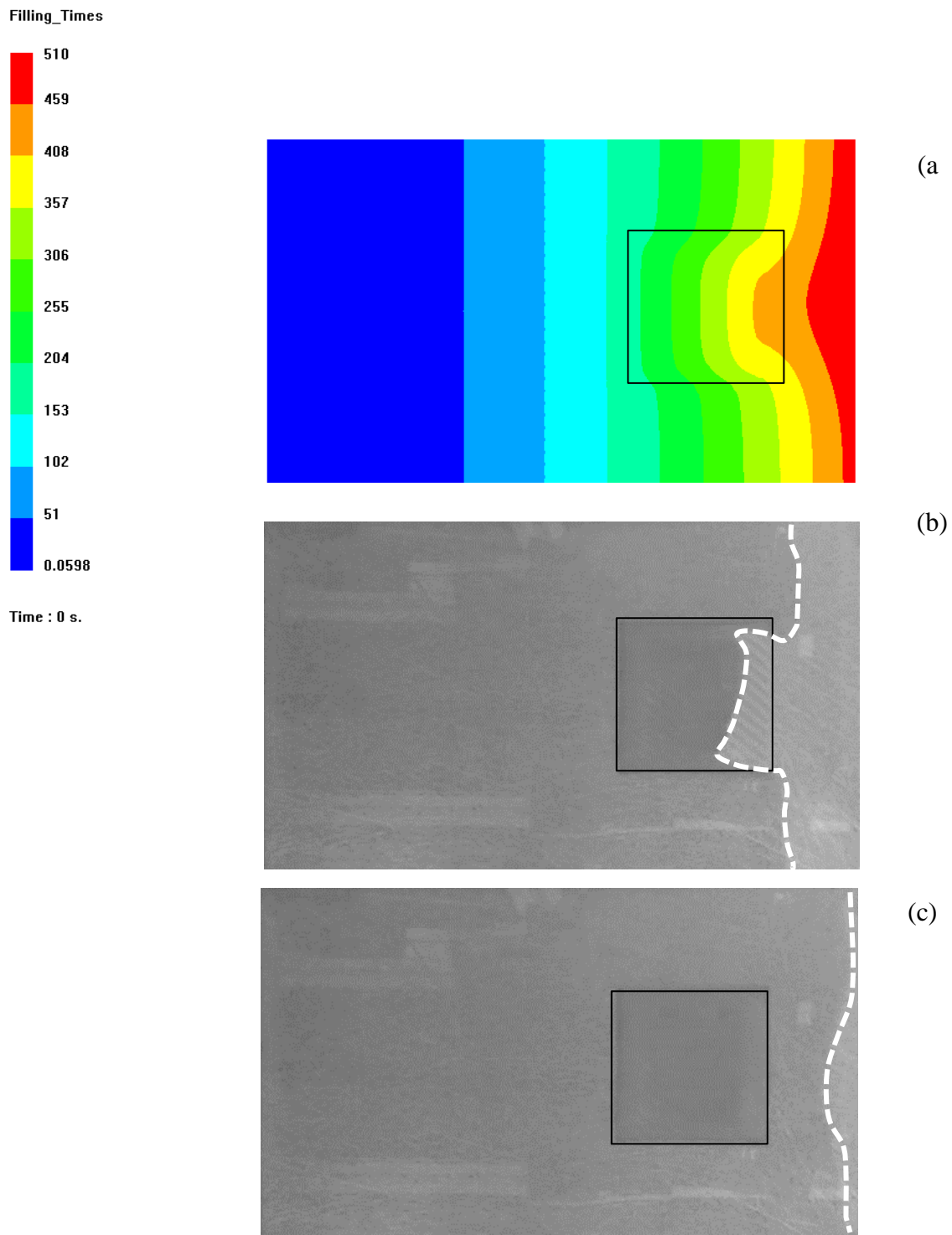
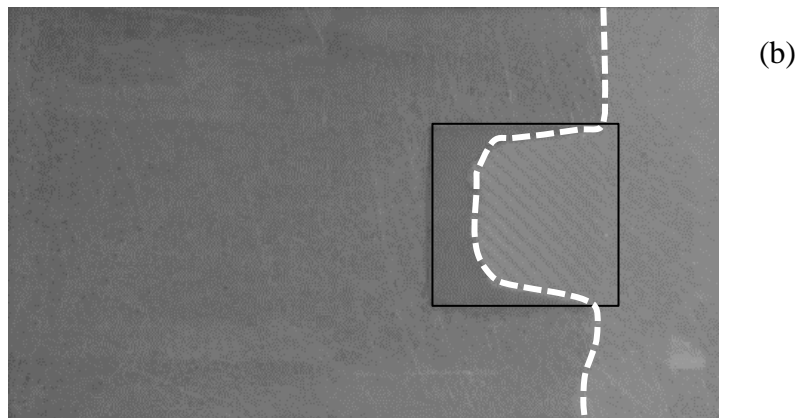
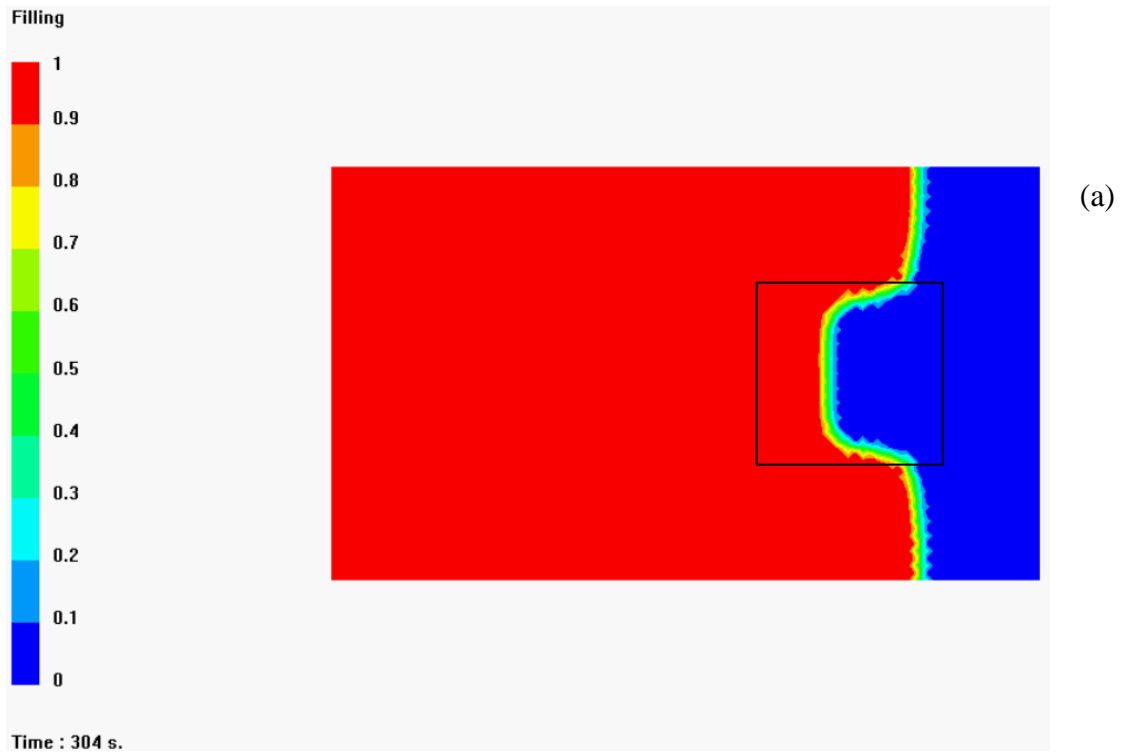


Figure 5.10. Filling pattern of case 2 for (a) simulation, experiments at (b) 357s and (c) 459s for EIPR process



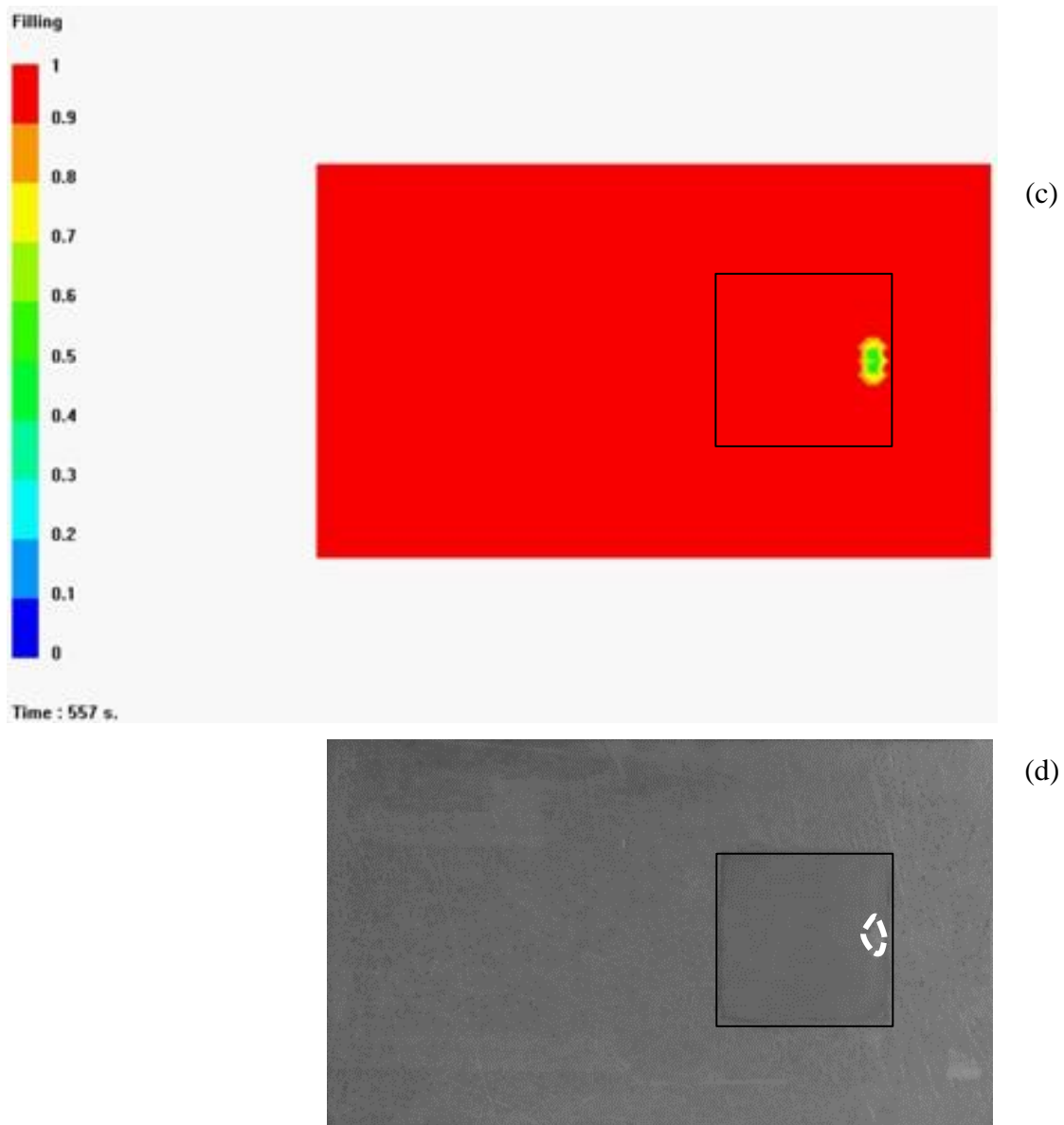


Figure 5.11. Flow front of case 2 (a) at 304s of VARTM process for simulation, (b) experiment, (c) predicted dry spot in simulation and (d) experiment

Mold filling time is one of the important parameters in the production of composite parts since the gel time of resins does not significantly vary. Thus, it can be used an index for comparison or evaluation purposes. Filling time values for the simulations and tests are given in Table 5.3. Filling time of case 1 in the EIPR and uncontrolled processes have approximately 5% and 3% difference, respectively. For case 2, corresponding values are 2 and 3%, respectively. Results show that the simulation predictions are quite satisfactory. Also, it can be observed that the EIPR process in both simulations and experiments reduces the filling time for each case.

Table 5.3 Filling time in simulations and experiments with/without the EIPR process

|        | Filling Time (s) |            |            |            |
|--------|------------------|------------|------------|------------|
|        | No-Control       |            | EIPR       |            |
|        | Simulation       | Experiment | Simulation | Experiment |
| Case 1 | 692              | 674        | 591        | 624        |
| Case 2 | 544              | 557        | 500        | 510        |

## 5.6 Summary

EIPR process can be considered as a sub-category of VARTM process which manipulates and corrects the flow front to eliminate dry spots. It is an active control process that detects the flow front. It devises a relaxation strategy if there is an unexpected development in the flow front and stimulates a ferro-magnetic element to rest the preform and pulsate it to increase the local permeability. In order to simulate this process, the permeability and compressibility of the preforms are obtained experimentally. For simulating the EIPR process an equivalent permeability of the preform under this controlling action is calculated and taken as the permeability of preform with low permeability. A simulation study is conducted for two case studies with/without EIPR process. The ability of the EIPR process to fill the mold completely without any dry spots is illustrated numerically. There is a good agreement between the simulation and experimental findings as the difference between results is below 5%.



## CHAPTER 6

### CONCLUSION AND FUTURE WORK

#### 6.1 Conclusions

In this study, the permeability measurement can be conducted with a single rectilinear infusion approach. The presented approach is not only to estimate the in-plane principle permeability values but it is also applicable to determine the permeability of several fabrics of different materials in a single test. The methodology consists of placing the preforms in a single VARTM infusion process one after the other with different orientations. An analytical approach to characterize the permeability of each zone is introduced. For the first zone, the method is same as the current method. For the second and third sections, Darcy's law is extended to calculate their permeability values, sequentially. The experimental validation of the presented approach is carried out for all possible permutations. The experimental results show the accuracy and reproducibility of the methodology in a more efficient way with just a single test. The permeability values are shown to be close to the reference values.

In order to prevent the formation of race-tracking and to have a repeatable and reliable process, a silicone vacuum bag is used in experiments. This study also shows the elastomer upper flexible mold in VARTM process is very useful and applicable. This type of flexible mold reduces the skilled labor and process preparations before the infusion. By using a self-sealing elastomer, there is no need for a seal tape and runner in each process. This process allows the formation of elastomer molds for various composite parts and these molds are reusable about 500 times to have a repeatable and reliable filling process.

Another contribution of this work can be considered as the development of the EIPR process to manipulate and redirect the resin flow front. The EIPR process is a smart and automated system that tracks the flow and redirect the flow front to fill the mold completely without any dry spot formation and defects. The presented approach provides an approach by which an electromagnet source moves over the problematic area to lift and pulsate the upper flexible mold which is made for this process specially to relax the preform and increase the permeability locally. For this purpose, ferro-magnetic elements are embedded in the upper flexible mold. The elements are invoked with an electromagnetic filed source. To have an effective vibration ‘thin non-oriented grades steel NO20’ with small amounts of residual magnetism is used. To automate the system and control the flow, a program is written in both MATLAB and Arduino. For this purpose, a workstation to mount the automated 2D gantry and transparent mold is built.

To evaluate the system, three case studies with two types of preforms in each case are studied. These preforms have a difference in their permeability values. Experimental results of the controlled processes in comparison with uncontrolled ones clearly unveil the efficiency of the EIPR process. Results show that the approach not only can manipulate and control the flow front but also assure the repeatability and reliability of the infusion process.

The preform permeability under the EIPR process is characterized where leading factors of the process are identified including frequency and amplitude of vibration. In order to evaluate this process and obtain a confident model, three preform types with permeabilities of high, medium and low values are selected. Central Composite Design (CCD) method is used for the design of experiment. For the EIPR process, a total of 39 experiments are conducted to study the effect of factors on the preform permeability. The filling time of preform infusion under the EIPR process shows a significant reduction from 20 to 60% depending on the material and factor levels. High reduction values relate to the low permeability preforms. The response surface methodology (RSM) approach is utilized to analyze and model the permeability response. A mathematical model is obtained as a function of frequency and amplitude for each material. It shows that the response defined in terms of permeability first increases with increasing frequency and then reduces. Meanwhile it

has an ever-increasing trend with increasing amplitude. The maximum preform permeability of the EIPR process is obtained at the optimum value of the process factors.

Finally, to simulate the EIPR process, an equivalent permeability of the preform under the controlling action is calculated and the value is taken as the permeability of the preform with low permeability which is under the controlling action. A simulation study for the process is conducted for two case studies with/without EIPR. The ability of the EIPR process to fill the mold perfectly without any dry spot is illustrated numerically. Results show the accuracy of the presented simplification in estimating filling time of process and dry spot formation. There is a close agreement between the simulation and experimental results as the difference between the results is shown to be less than 5%. The numerical study reveals the EIPR process to behave in a predictable manner with simplified preform properties.

According to the results obtained from this dissertation the following conclusions are achieved:

- 1- The single rectilinear infusion experiment for measuring the principle permeabilities provides the same test conditions to measure the permeability of the preforms at different directions to calculate the principle permeabilities of the preform. Results show there is not a significant scatter in the permeability values.
- 2- This permeability measurement approach can be extended to measure more components or it can be used to calculate the sheared preform permeabilities. The last one can be useful to define the preform properties in which the preforms are draped over a mold and characteristics of the preforms change as the fabrics shear to adapt the mold curvature. The shearing preform permeability is very useful to simulate the resin flow in a complex mold.
- 3- The presented measurement is applicable for RTM process and also it is applicable to estimate the permeability of preforms with different volume fraction in a single experiment.
- 4- Placement of the components one after the other must be done carefully to prevent gap formation among the components. Any gaps between the

components may change the permeability of them and principle permeability values.

- 5- The EIPR process dramatically and predictably changes the permeability temporarily of a selected region when vacuum bag actuated. This method increases the in-plane permeability by increasing the porosity of the preforms and it does not drive the resin through the thickness.
- 6- The presented method provides in-plane flow manipulation which does not create a gap between the vacuum bag and preform therefore it does not have permanent negative effect on the composite part.
- 7- To effectively use this process for manipulation in a predictable way, RSM is used to characterize the EIPR process. This analysis results show vibration and amplitude are the significant parameters. Regression model of each material shows that permeability of preform increases and then decreases with increasing frequency while it increases with increasing amplitude. According to the results, amplitude is more effective than the frequency to increase the permeability.
- 8- Shape of the element has an important role on the flow pattern. The circle one is useful to control the race tracking phenomena. Rectangular one is found more suitable for permeability measurement method and EIPR process characterization.
- 9- EIPR process reduces the filling time from 20% to 60% depend on the nature of the preforms. It is more effective for low permeability preforms than the high permeability ones.
- 10- The optimum values of frequency and amplitude depend on the preform are found 5.6-5.7 Hz and 0.5-0.7 mm for the selected ranges of these factors. Optimum values for the frequency may change by applying different materials for the element laminates and different electromagnetic forces. In this study, the optimum values show the best parameter values according to the conducted test results by this EIPR set-up.
- 11- Forecasted flow pattern and filling time of the simulations and the experiments are very close together. Simplified simulation of the EIPR process shows this method simulate the process with an error less than 5%.

## 6.2 Future works

This study establishes the EIPR process as a method for the real-time resin flow manipulation. This framework contains a 2D automated gantry system, an image processing unit and an upper flexible mold which is developed for this process for molding plate-like relatively simple structures. Each component of this system can be upgraded to a more complex for instance a curved structure. Such a modified system is suggested to include a 3D gantry system or a robot arm to access anywhere of the complex composite mold. For a proper flow front detection in a 3D mold, the development of a new image processing system is required. For the upper flexible mold, a new version can be fabricated from an elastomer with dispersed ferro-magnetic powder (Iron Oxide) instead of the current flexible upper mold with the embedded ferro-magnetic plates. Figure 6.1 shows this type of upper flexible mold with iron oxide powder. With such a vacuum bag, invoking would be possible anywhere on the mold.

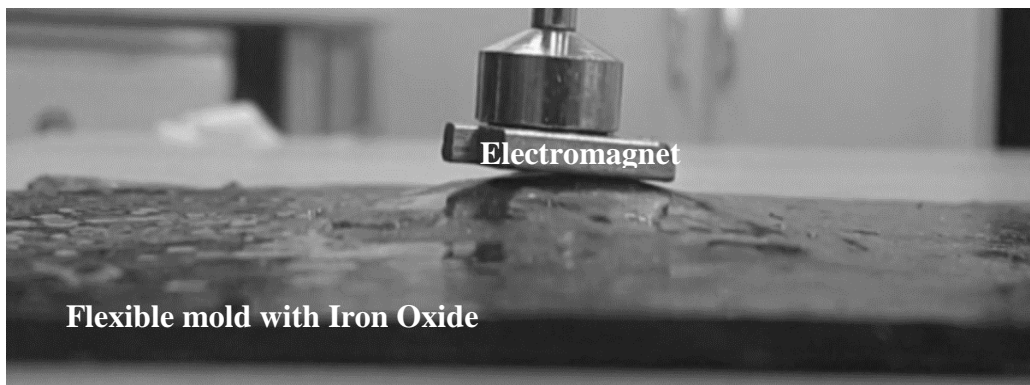


Figure 6.1. Suggested upper flexible elastomer mold with metal (Iron Oxide) powder

Finally, a further study for the fully simulation of the process i.e. resting the preform with an electromagnetic field source can be introduced as a field of research. It may include the simulation of lifting and vibrating the flexible mold and increasing the porosity of the preform locally.



## REFERENCES

- [1] Song YS, Youn JR. Numerical investigation on flow through porous media in the post-infusion process. *Polym Compos* 2009;30:1125–31. doi:10.1002/pc.20668.
- [2] Yang H, Lee LJ. A kinetic model for free-radical crosslinking copolymerization of styrene/vinylester resin. *Polym Compos* 2001;22:668–79. doi:10.1002/pc.10569.
- [3] Di Fratta C, Klunker F, Ermanni P. A methodology for flow-front estimation in LCM processes based on pressure sensors. *Compos Part A Appl Sci Manuf* 2013;47:1–11. doi:10.1016/j.compositesa.2012.11.008.
- [4] Johnson RJ, Pitchumani R. Enhancement of flow in VARTM using localized induction heating. *Compos Sci Technol* 2003;63:2201–15. doi:10.1016/S0266-3538(03)00179-9.
- [5] Lefevre D, Comas-Cardona S, Binetruy C, Krawczak P. Coupling filtration and flow during liquid composite molding: Experimental investigation and simulation. *Compos Sci Technol* 2009;69:2127–34. doi:10.1016/j.compscitech.2009.05.008.
- [6] Alms JB, Garnier L, Glancey JL, Advani SG. In-plane permeability characterization of the vacuum infusion processes with fiber relaxation. *Int J Mater Form* 2010;3:1267–75. doi:10.1007/s12289-010-0690-7.
- [7] Kruckenberg T, Ye L, Paton R. Static and vibration compaction and microstructure analysis on plain-woven textile fabrics. *Compos Part A Appl Sci Manuf* 2008;39:488–502. doi:10.1016/j.compositesa.2007.12.003.
- [8] Potluri P, Sagar T V. Compaction modelling of textile preforms for composite structures. *Compos Struct* 2008;86:177–85. doi:10.1016/j.compstruct.2008.03.019.
- [9] Carman PC. Fluid flow through granular beds. *Chem Eng Res Des* 1997;75:S32–48. doi:10.1016/S0263-8762(97)80003-2.
- [10] Lundström T. The permeability of non-crimp stitched fabrics. *Compos Part A Appl Sci Manuf* 2000;31:1345–53. doi:10.1016/S1359-835X(00)00037-3.
- [11] Papathanasiou T. Flow across structured fiber bundles: a dimensionless correlation. *Int J Multiph Flow* 2001;27:1451–61. doi:10.1016/S0301-9322(01)00013-1.
- [12] Belov EB, Lomov SV, Verpoest I, Peters T, Roose D, Parnas RS, et al. Modelling of permeability of textile reinforcements: lattice Boltzmann method. *Compos Sci Technol* 2004;64:1069–80. doi:10.1016/j.compscitech.2003.09.015.

- [13] Verleye B, Lomov SV, Long A, Verpoest I, Roose D. Permeability prediction for the meso–macro coupling in the simulation of the impregnation stage of Resin Transfer Moulding. *Compos Part A Appl Sci Manuf* 2010;41:29–35. doi:10.1016/j.compositesa.2009.06.011.
- [14] Verleye B, Croce R, Griebel M, Klitz M, Lomov SV, Morren G, et al. Permeability of textile reinforcements: Simulation, influence of shear and validation. *Compos Sci Technol* 2008;68:2804–10. doi:10.1016/j.compscitech.2008.06.010.
- [15] Sharma S, Siginer DA. Permeability measurement methods in porous media of fiber reinforced composites. *Appl Mech Rev* 2010;63:20802-1-19. doi:10.1115/1.4001047.
- [16] Fratta C Di. Improved anisotropic permeability characterization in unidirectional injections based on flow front angle measurements. *20th Int Conf Compos Mater (ICCM 20)* 2015:4106–4.
- [17] Vernet N, Ruiz E, Advani S, Alms JB, Aubert M, Barburski M, et al. Experimental determination of the permeability of engineering textiles: Benchmark II. *Compos Part A Appl Sci Manuf* 2014;61:172–84. doi:10.1016/j.compositesa.2014.02.010.
- [18] Arbter R, Beraud JM, Binetruy C, Bizet L, Bréard J, Comas-Cardona S, et al. Experimental determination of the permeability of textiles: A benchmark exercise. *Compos Part A Appl Sci Manuf* 2011;42:1157–68. doi:10.1016/j.compositesa.2011.04.021.
- [19] Bickerton S, Advani SG, Mohan R V., Shires DR. Experimental analysis and numerical modeling of flow channel effects in resin transfer molding. *Polym Compos* 2000;21:134–53. doi:10.1002/pc.10172.
- [20] Han K, Jiang S, Zhang C, Wang B. Flow modeling and simulation of SCRIMP for composites manufacturing. *Compos Part A Appl Sci Manuf* 2000;31:79–86. doi:10.1016/S1359-835X(99)00053-6.
- [21] Gokce A, Hsiao KT, Advani SG. Branch and bound search to optimize injection gate locations in liquid composite molding processes. *Compos Part A Appl Sci Manuf* 2002;33:1263–72. doi:10.1016/S1359-835X(02)00047-7.
- [22] Sánchez F, García JA, Chinesta F, Gascón L, Zhang C, Liang Z, et al. A process performance index based on gate-distance and incubation time for the optimization of gate locations in liquid composite molding processes. *Compos Part A Appl Sci Manuf* 2006;37:903–12. doi:10.1016/j.compositesa.2005.01.016.
- [23] Ratle F, Achim V, Trochu F. Evolutionary operators for optimal gate location in liquid composite moulding. *Appl Soft Comput* 2009;9:817–23. doi:10.1016/j.asoc.2008.05.008.
- [24] Young W-B. Gate Location Optimization in Liquid Composite Molding Using Genetic Algorithms. *J Compos Mater* 1994;28:1098–113. doi:10.1177/002199839402801202.
- [25] Mathur R, Advani SG, Fink BK. Use of genetic algorithms to optimize gate and vent locations for the resin transfer molding process. *Polym Compos*

- 1999;20:167–78. doi:10.1002/pc.10344.
- [26] Hsiao K. Intelligent RTM and VARTM for Polymer Composites Manufacturing n.d.:1–10.
- [27] Lawrence JM, Hsiao KT, Don RC, Simacek P, Estrada G, Sozer EM, et al. An approach to couple mold design and on-line control to manufacture complex composite parts by resin transfer molding. *Compos - Part A Appl Sci Manuf* 2002;33:981–90. doi:10.1016/S1359-835X(02)00043-X.
- [28] Modi D, Correia N, Johnson M, Long A, Rudd C, Robitaille F. Active control of the vacuum infusion process. *Compos Part A Appl Sci Manuf* 2007;38:1271–87. doi:10.1016/j.compositesa.2006.11.012.
- [29] Nalla AR, Fuqua M, Glancey J, Lelievre B. A multi-segment injection line and real-time adaptive, model-based controller for vacuum assisted resin transfer molding. *Compos Part A Appl Sci Manuf* 2007;38:1058–69. doi:10.1016/j.compositesa.2006.06.021.
- [30] Alms JB, Advani SG, Glancey JL. Liquid Composite Molding control methodologies using Vacuum Induced Preform Relaxation. *Compos Part A Appl Sci Manuf* 2011;42:57–65. doi:10.1016/j.compositesa.2010.10.002.
- [31] Alms J, Advani SG. Simulation and experimental validation of flow flooding chamber method of resin delivery in liquid composite molding. *Compos Part A Appl Sci Manuf* 2007;38:2131–41. doi:10.1016/j.compositesa.2007.06.011.
- [32] smooth on n.d. [www.smooth-on.com](http://www.smooth-on.com).
- [33] ESI Group International Ltd. n.d. <https://www.esi-group.com>.
- [34] P. Simacek, E.M. Sozer, S.G. Advani User manual for LIMS 4.0 Center for Composite Materials, University of Delaware (1998) n.d.
- [35] Polyworx inc. n.d. <http://www.polyworx.com/doc/>.
- [36] Darcy H. Les fontaines publiques de la ville de Dijon. Recherche 1856.
- [37] Woerdeman DL, Phelan FR, Parnas RS. Interpretation of 3-D permeability measurements for RTM modeling. *Polym Compos* 1995;16:470–80. doi:10.1002/pc.750160605.
- [38] Adams KL, Rebenfeld L. In-Plane Flow of Fluids in Fabrics: Structure/Flow Characterization. *Text Res J* 1987;57:647–54. doi:10.1177/004051758705701104.
- [39] Chan AW, Hwang S -T. Anisotropic in-plane permeability of fabric media. *Polym Eng Sci* 1991;31:1233–9. doi:10.1002/pen.760311613.
- [40] Adams KL, Russel WB, Rebenfeld L. Radial penetration of a viscous liquid into a planar anisotropic porous medium. *Int J Multiph Flow* 1988;14:203–15. doi:10.1016/0301-9322(88)90006-7.
- [41] Han K. Measurements of the permeability of fiber preforms and applications. *Compos Sci Technol* 2000;60:2435–41. doi:10.1016/S0266-3538(00)00037-3.
- [42] Parnas RS, Salem AJ. A comparison of the unidirectional and radial in-plane flow of fluids through woven composite reinforcements. *Polym Compos*

- 1993;14:383–94. doi:10.1002/pc.750140504.
- [43] Demaría C, Ruiz E, Trochu F. In-plane anisotropic permeability characterization of deformed woven fabrics by unidirectional injection. Part I: Experimental results. *Polym Compos* 2007;28:797–811. doi:10.1002/pc.20107.
- [44] Demaría C, Ruiz E, Trochu F. In-plane anisotropic permeability characterization of deformed woven fabrics by unidirectional injection. Part II: Prediction model and numerical simulations. *Polym Compos* 2007;28:812–27. doi:10.1002/pc.20108.
- [45] Weitzenböck JR, Sheno RA, Wilson PA. Radial flow permeability measurement. Part A: theory. *Compos Part A Appl Sci Manuf* 1999;30:781–96. doi:10.1016/S1359-835X(98)00183-3.
- [46] Gauvin R, Trochu F, Lemenn Y, Diallo L. Permeability Measurement and Flow Simulation. *Polym Compos* 1996;17:34–42.
- [47] Ferland P, Trochu F. *Resin Transfer Molding* 1996;17.
- [48] Hirt DE, Adams KL, Prud'homme RK, Rebenfeld L. In-Plane Radial Fluid Flow Characterization of Fibrous Materials. *J Therm Insul* 1987;10:153–72. doi:10.1177/109719638701000303.
- [49] Bickerton S, Advani SG, Mohan R V, Shires DR. Experimental analysis and numerical modeling of flow channel effects in resin transfer molding. *Polym Compos* 2000;21:134–53. doi:Doi 10.1002/Pc.10172.
- [50] Weitzenböck JR, Sheno RA, Wilson PA. Measurement of principal permeability with the channel flow experiment. *Polym Compos* 1999;20:321–35. doi:10.1002/pc.10359.
- [51] Fratta C Di. Angle analysis for the evaluation of in-plane anisotropic properties n.d.:5–7.
- [52] Endruweit A, Ermanni P. The in-plane permeability of sheared textiles. Experimental observations and a predictive conversion model. *Compos Part A Appl Sci Manuf* 2004;35:439–51. doi:10.1016/j.compositesa.2003.11.002.
- [53] Parnas RS, Howard JG, Luce TL, Advani SG. Permeability characterization. Part 1: A proposed standard reference fabric for permeability. *Polym Compos* 1995;16:429–45. doi:10.1002/pc.750160602.
- [54] Lugo J, Simacek P, Advani SG. Analytic method to estimate multiple equivalent permeability components from a single rectilinear experiment in liquid composite molding processes. *Compos Part A Appl Sci Manuf* 2014;67:157–70. doi:10.1016/j.compositesa.2014.08.031.
- [55] Di Fratta C, Klunker F, Trochu F, Ermanni P. Characterization of textile permeability as a function of fiber volume content with a single unidirectional injection experiment. *Compos Part A Appl Sci Manuf* 2015;77:238–47. doi:10.1016/j.compositesa.2015.05.021.
- [56] Di Fratta C, Koutsoukis G, Klunker F, Trochu F, Ermanni P. Characterization of anisotropic permeability from flow front angle measurements. *Polym Compos* 2016;37:2037–52. doi:10.1002/pc.23382.

- [57] Brouwer WD, Van Herpt ECFC, Labordus M. Vacuum injection moulding for large structural applications. *Compos Part A Appl Sci Manuf* 2003;34:551–8. doi:10.1016/S1359-835X(03)00060-5.
- [58] Williams CD, Grove SM, Summerscales J. The compression response of fibre-reinforced plastic plates during manufacture by the resin infusion under flexible tooling method. *Compos Part A Appl Sci Manuf* 1998;29:111–4. doi:10.1016/S1359-835X(97)00038-9.
- [59] Poorzeinolabedin M, Parnas L, Dashatan SH. Resin infusion under flexible tooling process and structural design optimization of the complex composite part. *Mater Des* 2014;64:450–5. doi:10.1016/j.matdes.2014.08.008.
- [60] Bayldon JM, Daniel IM. Flow modeling of the VARTM process including progressive saturation effects. *Compos Part A Appl Sci Manuf* 2009;40:1044–52. doi:10.1016/j.compositesa.2009.04.008.
- [61] Hsiao K-T, Heider D. 10 - Vacuum assisted resin transfer molding (VARTM) in polymer matrix composites. Woodhead Publishing Limited; 2012. doi:10.1533/9780857096258.3.310.
- [62] Hancox NL. The effects of flaws and voids on the shear properties of CFRP. *J Mater Sci* 1977;12:884–92. doi:10.1007/BF00540969.
- [63] LIU X, CHEN F. A review of void formation and its effects on the mechanical performance of carbon fiber reinforced plastic. *Eng Trans* 2016;64:33–51.
- [64] Johnson RJ, Pitchumani R. Active control of reactive resin flow in a vacuum assisted resin transfer molding (VARTM) process. *J Compos Mater* 2008;42:1205–29. doi:Doi 10.1177/0021998308091264.
- [65] Matsuzaki R, Kobayashi S, Todoroki A, Mizutani Y. Control of resin flow/temperature using multifunctional interdigital electrode array film during a VaRTM process. *Compos Part A Appl Sci Manuf* 2011;42:782–93. doi:10.1016/j.compositesa.2011.03.004.
- [66] Alms JB, Glancey JL, Advani SG. Mechanical properties of composite structures fabricated with the vacuum induced preform relaxation process. *Compos Struct* 2010;92:2811–6. doi:10.1016/j.compstruct.2010.04.007.
- [67] Nielsen DR, Pitchumani R. Control of flow in resin transfer molding with real-time preform permeability estimation. *Polym Compos* 2002;23:1087–110. doi:10.1002/pc.10504.
- [68] Nielsen DR, Pitchumani R. Closed-loop flow control in resin transfer molding using real-time numerical process simulations. *Compos Sci Technol* 2002;62:283–98. doi:10.1016/S0266-3538(01)00213-5.
- [69] Matsuzaki R, Kobayashi S, Todoroki A, Mizutani Y. Flow control by progressive forecasting using numerical simulation during vacuum-assisted resin transfer molding. *Compos Part A Appl Sci Manuf* 2013;45:79–87. doi:10.1016/j.compositesa.2012.09.014.
- [70] Goldman A. *Handbook of Modern Ferromagnetic Materials*. Boston, MA: Springer US; 1999. doi:10.1007/978-1-4615-4917-8.
- [71] Domínguez JC, Oliet M, Alonso M V., Rojo E, Rodríguez F. Structural,

- thermal and rheological behavior of a bio-based phenolic resin in relation to a commercial resol resin. *Ind Crops Prod* 2013;42:308–14. doi:10.1016/j.indcrop.2012.06.004.
- [72] Teoh KJ, Hsiao KT. Improved dimensional infidelity of curve-shaped VARTM composite laminates using a multi-stage curing technique - Experiments and modeling. *Compos Part A Appl Sci Manuf* 2011;42:762–71. doi:10.1016/j.compositesa.2011.03.003.
- [73] Khan LA, Mehmood AH. *Cost-Effective Composites Manufacturing Processes for Automotive Applications*. Elsevier Ltd; 2016. doi:10.1016/B978-1-78242-325-6.00005-0.
- [74] Fan J, Njuguna J. *An Introduction to Lightweight Composite Materials and Their Use in Transport Structures*. Elsevier Ltd; 2016. doi:10.1016/B978-1-78242-325-6.00001-3.
- [75] Ortiz de Mendibil I, Aretxabaleta L, Sarrionandia M, Mateos M, Aurrekoetxea J. Impact behaviour of glass fibre-reinforced epoxy/aluminium fibre metal laminate manufactured by Vacuum Assisted Resin Transfer Moulding. *Compos Struct* 2016;140:118–24. doi:10.1016/j.compstruct.2015.12.026.
- [76] Menta VK. *Advanced Composites Using Non-Autoclave Proceeded: Manufacturing and Characterization* 2011.
- [77] Advani SG. Role of Process Models in Composites Manufacturing. *Ref. Modul. Mater. Sci. Mater. Eng.*, Elsevier; 2017. doi:10.1016/B978-0-12-803581-8.09898-2.
- [78] Holmes M. Aerospace looks to composites for solutions. *Reinf Plast* 2017;61:237–41. doi:10.1016/j.repl.2017.06.079.
- [79] Varna J, Joffe R, Berglund LA, Lundström TS. Effect of voids on failure mechanisms in RTM laminates. *Compos Sci Technol* 1995;53:241–9. doi:10.1016/0266-3538(95)00024-0.
- [80] Arbter R. Contribution to Robust Resin Transfer Molding 2008:1–287. doi:10.3929/ethz-a-005730612.
- [81] Grunenfelder LK, Nutt SR. Void formation in composite prepregs - Effect of dissolved moisture. *Compos Sci Technol* 2010;70:2304–9. doi:10.1016/j.compscitech.2010.09.009.
- [82] *Optimization of Resin Infusion Processing for Composite Materials: Simulation and Characterization Strategies*. 2011.
- [83] Sayre JR. Vacuum-Assisted Resin Transfer Molding (VARTM) Model Development, Verification, and Process Analysis. *Analysis* 2000:179.
- [84] Devillard M, Hsiao KT, Advani SG. Flow sensing and control strategies to address race-tracking disturbances in resin transfer molding - Part II: Automation and validation. *Compos Part A Appl Sci Manuf* 2005;36:1581–9. doi:10.1016/j.compositesa.2004.04.009.
- [85] Lawrence JM, Advani SG. Dependence Map-Based Flow Control to Reduce Void Content in Liquid Composite Molding. *Mater Manuf Process* 2005;20:933–60. doi:10.1081/AMP-200060419.

- [86] Hsiao KT, Advani SG. Flow sensing and control strategies to address race-tracking disturbances in resin transfer molding. Part I: Design and algorithm development. *Compos Part A Appl Sci Manuf* 2004;35:1149–59. doi:10.1016/j.compositesa.2004.03.010.
- [87] Lawrence JM, Fried P, Advani SG. Automated manufacturing environment to address bulk permeability variations and race tracking in resin transfer molding by redirecting flow with auxiliary gates. *Compos Part A Appl Sci Manuf* 2005;36:1128–41. doi:10.1016/j.compositesa.2005.01.024.
- [88] Rostamiyan Y, Fereidoon A, Rezaeiashtiyani M, Mashhadzadeh AH, Salmankhani A. Experimental and optimizing flexural strength of epoxy-based nanocomposite: Effect of using nano silica and nano clay by using response surface design methodology. *Mater Des* 2015;69:96–104. doi:10.1016/j.matdes.2014.11.062.
- [89] Johnson RJ, Pitchumani R. Simulation of active flow control based on localized preform heating in a VARTM process. *Compos Part A Appl Sci Manuf* 2006;37:1815–30. doi:10.1016/j.compositesa.2005.09.007.
- [90] Rostamiyan Y, Fereidoon A, Mashhadzadeh AH, Ashtiyani MR, Salmankhani A. Using response surface methodology for modeling and optimizing tensile and impact strength properties of fiber orientated quaternary hybrid nano composite. *Compos Part B Eng* 2015;69:304–16. doi:10.1016/j.compositesb.2014.09.031.
- [91] Box AGE, Wilson KB, Journal S, Statistical R, Series S. On the Experimental Attainment of Optimum Conditions Published by : Wiley for the Royal Statistical Society Stable URL : <http://www.jstor.org/stable/2983966> 2017;13:1–45.
- [92] Matsuzaki R, Shiota M. Composites : Part A Data assimilation through integration of stochastic resin flow simulation with visual observation during vacuum-assisted resin transfer molding : A numerical study. *Compos PART A* 2016;84:43–52. doi:10.1016/j.compositesa.2016.01.006.
- [93] Sreekumar PA, Joseph K, Unnikrishnan G, Thomas S. SCIENCE AND A comparative study on mechanical properties of sisal-leaf fibre-reinforced polyester composites prepared by resin transfer and compression moulding techniques 2007;67:453–61. doi:10.1016/j.compscitech.2006.08.025.
- [94] Fink BK, Mathur R. On the Application of Genetic Algorithms for Optimization of RTM Process Parameters 2000.
- [95] Trochu F, Ruiz E, Achim V, Soukane S. Advanced numerical simulation of liquid composite molding for process analysis and optimization. *Compos Part A Appl Sci Manuf* 2006;37:890–902. doi:10.1016/j.compositesa.2005.06.003.
- [96] Liu B, Bickerton S, Advani SG. Modelling and simulation of resin transfer moulding (RTM) - Gate control, venting and dry spot prediction. *Compos Part A Appl Sci Manuf* 1996;27:135–41. doi:10.1016/1359-835X(95)00012-Q.
- [97] Chen YF, Stelson KA, Vollert VR. Prediction of Filling Time and Vent Locations for Resin Transfer Molds. *J Compos Mater* 1997;31:1141–61. doi:10.1177/002199839703101104.

- [98] Gokce A, Advani SG. Simultaneous gate and vent location optimization in liquid composite molding processes. *Compos Part A Appl Sci Manuf* 2004;35:1419–32. doi:10.1016/j.compositesa.2004.05.001.
- [99] Allende M, Mohan R V., Walsh SM. Experimental and numerical analysis of flow behavior in the FASTRAC liquid composite manufacturing process. *Polym Compos* 2004;25:384–96. doi:10.1002/pc.20032.
- [100] Song X. Vacuum Assisted Resin Transfer Molding ( VARTM ): Model Development and Verification. Dr Thesis 2003:161.
- [101] de Oliveira IR, Amico SC, Souza JÁ, de Lima AGB. Resin transfer molding process: a numerical and experimental investigation. *Int J Multiphys* 2013;7:125–36. doi:10.1260/1750-9548.7.2.125.
- [102] Koziół M. Simplified Simulation of Vari Process Using Pam - Rtm Software 2016.
- [103] Isoldi LA, Oliveira CP, Rocha LAO, Souza JA, Amico SC. Three-Dimensional Numerical Modeling of RTM and LRTM Processes. *J Brazilian Soc Mech Sci Eng* 2012;XXXIV:105–11. doi:10.1590/S1678-58782012000200001.
- [104] Letzow M, Amico SC, Souza JA, Isoldi LA. Computational Modeling of Rtm and Lrtm 2012;11:93–9.
- [105] Trevino L, Rupel K, Young WB, Liou MJ, Lee LJ. Analysis of Resin Injection Molding in Molds With Paepplaced Fiber Mats. I: Permeability and Compressibility Measurements. *Polym Compos* 1991;12:20–9. doi:10.1002/pc.750120105.
- [106] No Title n.d. <http://www.electronics-tutorials.ws/electromagnetism/magnetic-hysteresis.html>.

## VITA

### PERSONL INFORMATION

Surname, Name: POORZEINOLABEDIN Mohsen

Nationality: IRAN

Date and Place of Birth: 1 Augustus 1983, Sharafkhane-Tabriz

Marital Status: Married

Email: poorzeinolabedin\_m@yahoo.com

### EDUCATION

| <i>Degree</i> | <i>Institution</i>          | <i>Year of Graduation</i> |
|---------------|-----------------------------|---------------------------|
| MS            | Tarbiat Modares Uni. Tehran | 2009                      |
| BS            | Islamic Azad Uni. Tabriz    | 2006                      |
| High School   | Nomune Dolati, Shabestar    | 2001                      |

### WORK EXPERIENCE

| <i>Year</i>  | <i>Place</i>                | <i>Enrollment</i> |
|--------------|-----------------------------|-------------------|
| 2014-present | Leopar Composite, Ankara    | R&D Specialist    |
| 2009-2011    | Islamic Azad Uni. Shabestar | Lecturer          |

### PUBLICATIONS

M. Poorzeinolabedin, L. Parnas, (2017), “Analytical and Experimental Approach to Obtain Principal Permeability of Fabric from a Single Rectilinear Experiment in Liquid Composite Modeling“, In Preparation.

M. Poorzeinolabedin, L. Parnas, (2017), “Electromagnetically Induced Preform Resting Process for Resin Flow Correcting“, In Preparation.

M. Poorzeinolabedin, L. Parnas, (2017), “Permeability Characterization of Vacuum Infusion Process by Electromagnetically Induced Preform Resting Method“, In Preparation.

M. Poorzeinolabedin, L. Parnas, (2017), “Numerical and Experimental Investigation of Electromagnetically Induced Preform Resting Process in Comparison with Vacuum Assisted Resin Transfer Molding“, In Preparation.

M. Poorzeinolabedin, L. Parnas, S. Hosseinpour, (2014), "Resin infusion under flexible tooling process and structural design optimization of the complex composite part", *Materials & Design*, Volume 64, Pages 450–455

M. Poorzeinolabedin, and M. Golzar, (2011), “Improving the Woven Glass/Epoxy Composite for Automobile Exterior Body Cover”, *International Journal of Materials and Manufacturing Processes*, 1532-2475, Volume 26, Issue 4, 2011, Pages 562 – 566.

M. Golzar and, M. Poorzeinolabedin, (2010), “Prototype fabrication of a composite automobile body based on integrated structure”, *International Journal of Advanced Manufacturing Technology*, Volume 49, Numbers 9-12, Pages 1037-1045.

M. Poorzeinolabedin, and M. Golzar, “Effect of number and orientation of lamina in energy absorption of automobile composite designed body”, *The 10th Iranian Conference of Manufacturing Engineering in Babol University (ICME 2010)*.

M. Poorzeinolabedin, and M. Golzar, “Optimization and fabrication of automobile body with E-glass/epoxy composite”, *The 10th Iranian Conference of Manufacturing Engineering in Babol University (ICME 2010)*.

M. Poorzeinolabedin, M. Golzar and Ehsan Soury (2009). “Design and Manufacture of Woven Reinforced E-glass/Epoxy Composites for Car Outer Side Body”, *Seventh International Conference on Composite Science & Technology (ICCST/7)*.